Innovative Lignin Nanoparticle Manufacturing and Applications in Sustainable Packaging Solutions

A Dissertation Presented for the

Doctor of Philosophy

Degree

The University of Tennessee, Knoxville

Zhongjin Zhou

May 2025

DEDICATION

I dedicate this work to my beloved mother, Xiugen Lu.

Your unwavering love and encouragement have always inspired me to pursue my dreams and find fulfillment in my work. You taught me that true success is measured not just by achievements, but by the happiness we find along the way.

I know that if you could, you would be here celebrating this milestone with me.

ACKNOWLEDGEMENTS

My time as a graduate student and the journey of completing this dissertation have been among the most enlightening, educational, and challenging experiences of my life. I am deeply grateful to all those who have supported me throughout this endeavor.

First and foremost, I would like to express my sincere gratitude to my advisor, Dr. Siqun Wang, for giving me the opportunity to join your research group and for making me feel like a valued colleague from day one. Working under your guidance has been an incredible learning experience. I am grateful for your mentorship, which has shaped my ability to think across disciplines—balancing science and engineering, fundamentals and applications, and bridging laboratory research with industrial impact.

To my committee members, Drs. Niki Labbé, Mi Li, and Tong Wang, thank you for your invaluable mentorship, insights, and guidance as I navigated an entirely new field of materials science. Coming into graduate school with a background in chemical engineering, I had much to learn about biomass and sustainable materials, and your support was instrumental in that journey. Your feedback has been invaluable in shaping both this dissertation and my broader scientific perspective.

To my lab mates, Kalavathy Rajan, Shahaboddin Saedi, Kailong Zhang, Di Xie, and Anna Kim, I am grateful for your camaraderie, knowledge, and the countless scientific conversations and otherwise—that made long lab days more enjoyable. Whether in formal lab meetings or over a beer after work, your insights and encouragement have meant the world to me.

I am also deeply appreciative of Mr. Chris Helton, Mr. Thomas Patterson, Mrs. Candy Anderson, and the entire staff at the Center for Renewable Carbon. The environment you have fostered has been one of unwavering support, providing a sense of community that carried me through even the most challenging moments of this journey.

I would also like to extend my gratitude to all the educators who have shaped my academic journey. A special thanks to Dr. Nannan Sun, my master's advisor and mentor, for introducing me to the principles of Green Chemistry and encouraging me to think critically about solutions to climate challenges. Your guidance has had a lasting impact on my research and scientific approach.

Finally, I owe everything to my family. To my mother, whom I miss dearly, thank you for all the sacrifices you made to ensure I had not only what I needed but also what I dreamed of. Your love and dedication continue to inspire me. And to my partner, Lirui Cong, my other half and greatest support, I am incredibly fortunate to have found you in Shanghai and even prouder to call you, my wife. Your unwavering belief in me has meant more than words can express. I love you—forever, my Lirui.

ABSTRACT

The extensive use of synthetic materials, particularly plastics and per- and polyfluoroalkyl substances (PFAS), has led to severe environmental issues, including microplastic contamination, and elevated PFAS levels in water resources. Additionally, plastic waste, such as sheets, ropes, and nets, poses significant threats to wildlife. These challenges underscore the urgent need for sustainable, degradable alternatives. Lignin, which is biodegradable, inherently hydrophobic due to its low hydroxyl content, and UV-resistant owing to its polyaromatic structure, presents a promising solution. However, the complex and non-uniform composition of industrial lignin limits its practical applications. Reducing lignin to the nanoscale through mechanical processes eliminates the need for solvent chemicals, facilitating scalable and sustainable production.

This study investigated the manufacturing of lignin micro- and nanoparticles (LMNP), focusing on the effects of temperature and solid content during ultrafine grinding (UFG), as well as the associated electricity consumption producing 1 kg LMNP. Additionally, the use of LMNP as functional agents in biomass-based food packaging and tableware applications was explored. The impact of processing temperature on nanoparticle formation was systematically examined. Results revealed that elevated temperatures (~70°C) accelerated particle size reduction, whereas lower temperatures (~0°C) resulted in smaller final particle sizes. Increasing the solid content significantly reduced energy consumption during processing.

The LMNP suspension was then applied to paper and hot-pressed to form a dense, smooth film. Under optimized conditions (160°C, 3 MPa, and 3 minutes), the lignin film exhibited water resistance for over an hour and oil resistance for 25 minutes. To address aesthetic concerns, a sandwich structure was introduced, embedding the lignin composite between two paper sheets. This design enhanced tensile strength by 50% while maintaining water- and oil-resistant properties. Furthermore, a dry processing method was developed by blending LMNP with dry fibers, followed by direct hot pressing. This approach demonstrated energy and water efficiency compared to wet molding method, offering a viable pathway for sustainable, high-performance applications in green packaging.

TABLE OF CONTENTS

LIST OF TABLES

LIST OF FIGURES

LIST OF ABBREVIATIONS

3D	Three-dimensional
AKD	Alkyl ketene dimer
CF	Cellulose fiber
CNF	Cellulose nanofibril
DI	Deionized
DLS	Dynamic laser scattering
$Đ_M$	Molar-mass dispersity
DMSO	Dimethyl sulfoxide
DMSO-d_6	Deuterated DMSO
DSC	Differential scanning calorimetric analysis
DTG	Differential thermal gravimetric analysis
EDX	Energy dispersive X-ray spectroscopy
EtOH	Ethanol
EVD	Extreme vertices design
FP	Filter paper
FTIR	Fourier transform infrared
EPA	Environmental Protection Agency
G	Guaiacyl
GVL	γ-valerolactone
GPC	Gel permeation chromatographic
H	p-Hydroxyphenyl
HCl	Hydrochloric acid
HSQC	1H-13C heteronuclear single quantum coherence
KL	Kraft lignin
LMNP	Lignin micro-nanoparticles
MWL	Milled wood lignin
MW	Molecular weight
M_w	Weight-average molecular weight

M_n	Number-average molecular weight
NMR	Nuclear Magnetic Resonance
NOP	Natural oil polyols
OH	Hydroxyls
PA	Polyamide
PBS	Polybutylene Succinate
PE	Polyethylene
PLA	Polylactic acid
PVA	Poly(vinyl alcohol)
PCL	Poly(ε-caprolactone)
PFAS	Per- and polyfluoroalkyl substances
PHA	Polyhydroxyalkanoates
PHB	Polyhydroxybutyrate
PUF	Polyurethane Foam
RT	Room temperature
R^2	Coefficient of determination
SEM	Scanning electron microscopy
S	Syringyl
SW	Softwood
T_m	Melting temperature
T_{max}	Temperature at the maximum mass loss
T_{onset}	Onset temperature of thermal degradation
T_g	Glass transition temperature
TGA	Thermal gravimetric analysis
UFG	Ultrafine grinding
UV	Ultraviolet
UV-vis	Ultraviolet-visible spectroscopy
WCA	Water contact angle
XG	Xyloglucan

CHAPTER ONE : INTRODUCTION AND GENERAL INFORMATION

The rapid development of the petrochemical industry in the 20th century marked a transformative era in material science, giving rise to petroleum-based plastics that quickly replaced traditional materials. Plastics, praised for their excellent processability, low cost, and lightweight properties, became ubiquitous in industrial applications and daily life.[1] According to the US Environmental Protection Agency (EPA), global plastic production reached 368 million tons in 2019, with 40% of this total comprising single-use products such as disposable cups, lunch boxes, and take-out bags. While many plastics are theoretically recyclable, the actual recycling rate remains alarmingly low—approximately 8% globally—with over 80% of single-use plastics ending up in landfills or the natural environment.[2,3] These persistent materials do not decompose easily; instead, they fragment into smaller pieces over time, ultimately forming microplastics. These fragments can persist for hundreds of years, creating long-term environmental issues.

Plastic waste poses a dual threat to ecosystems and human health. Large plastic debris, such as fishing nets and bags, entangle marine and terrestrial wildlife, causing injury or death. Additionally, microplastics enter aquatic ecosystems, where they infiltrate the food chain, accumulate in drinking water sources, and pose risks to human health.[4] These environmental and health concerns have driven a growing interest in sustainable and biodegradable materials to replace traditional plastics.

Degradable materials have received increasing attention as viable alternatives to non-biodegradable plastics. Significant advancements have been made in wood-based products, bioplastics, and pulp fiber-based materials to meet growing demand for eco-friendly solutions. Among these, cellulose, the most abundant renewable biomaterial, plays a pivotal role in the production of disposable fiber products.[5-7] These products account for nearly half of the disposable market in the United States, with an annual production of USD 1.25 billion in 2022.[8] Despite their prominence, cellulose-based materials face inherent limitations. Their hydrophilic nature leads to high moisture absorption, which significantly compromises mechanical properties in

wet conditions.[9] This limitation hinders the application of cellulose-based products in sectors requiring water- and oil-resistant materials.

Various strategies have been developed to address the shortcomings of cellulose-based materials. Physical methods include constructing multi-layered structures, applying plastic films to enhance air tightness, and laminating with aluminum foil to improve UV resistance and waterproofing.[10] While effective, these approaches often rely on non-biodegradable synthetic materials, thereby undermining their environmental benefits. Furthermore, such methods can be cost-prohibitive, particularly for disposable applications. Chemical treatments have also been explored, with hydrophobic agents such as alkyl ketene dimer and other low-surface-energy additives used to enhance waterproofing.[11] However, these solutions often fall short in addressing oil resistance, a critical requirement for many applications. The primary solution for oil resistance in the industry has been the use of per- and polyfluoroalkyl substances (PFAS), which have unique properties but significant environmental drawbacks.[12]

PFAS were first developed and commercialized by DuPont and 3M.[13] Initially celebrated for their chemical stability and versatility, PFAS has since become synonymous with environmental pollution and health risks. These compounds, characterized by strong carbon-fluorine bonds, are highly resistant to degradation, making them persistent in the environment. PFAS exhibit excellent resistance to chemicals, acids, and bases, and their ultra-low surface energy makes them unparalleled as oil-proof additives. However, these same properties render PFAS virtually non-biodegradable.[12, 14, 15]

The environmental impact of PFAS became evident when residents near Solvay Specialty Polymers plant suffered from water contamination linked to these chemicals.[16] Studies revealed that prolonged exposure to PFAS in drinking water was associated with severe health issues, including cancer.[15, 17] The realization of PFAS' persistence and toxicity has spurred regulatory actions and public demand for safer,

biodegradable alternatives.[2, 18] As the search for replacements continues, natural polymers such as lignin have emerged as promising candidates.

Lignin, a natural polymer, holds significant promise as a renewable and biodegradable material, as it can be broken down in nature by specialized microorganisms, primarily white-rot and brown-rot fungi, through enzymatic action involving lignin peroxidases, manganese peroxidases, and laccases. It is the second most abundant biopolymer on Earth, surpassed only by cellulose, and is derived from trees and grasses.[19, 20] Unlike cellulose, lignin is hydrophobic due to its low hydroxyl content and is naturally UV-resistant because of its polyaromatic structure.[21-24] These properties make lignin an attractive material for applications requiring moisture resistance and durability. Furthermore, lignin is a byproduct of the pulp and paper industry, making it both abundant and cost-effective. However, despite its potential, lignin's industrial applications remain limited due to its complex and non-uniform chemical structure.[25, 26]

One of the most promising approaches to overcoming lignin's limitations is nano-sizing, which enhances its properties and expands its application potential.[27] Mechanical methods for producing lignin micro- and nano- particles (LMNPs) are particularly appealing because they avoid the solvent-intensive processes associated with chemical methods, making them more environmentally friendly and scalable.[26] However, mechanical production methods are not without challenges. Energy consumption during the grinding process remains a significant barrier to cost-effective production.[28, 29] Optimizing the process to reduce energy requirements while maintaining product quality is crucial for enabling large-scale, high-value applications of LMNPs. Despite these challenges, the unique properties of LMNPs, such as their film-forming ability, make them highly suitable for creating composite materials with enhanced water and oil resistance.

Numerous studies have demonstrated the potential of lignin-based composite materials in disposable tableware and packaging. These composites often exhibit

competitive advantages over traditional plastics and pulp materials, particularly in strength and barrier properties. However, several challenges remain. The dark coloration of lignin-derived products poses aesthetic concerns, while the complexity and multi-step nature of manufacturing processes hinder scalability.[30] Moreover, while lignin composites generally perform well in waterproofing, their oil-resistant properties are often underexplored or insufficient.[10] This limitation arises from the intrinsic challenges of achieving oil resistance, given the lower surface energy of oils compared to water. Although lignin's aromatic structure and hydrophobic nature provide some advantages, these properties alone are insufficient to meet the demands of oil-resistant applications.

This dissertation addresses key challenges in the development and application of lignin-based materials by pursuing five interrelated research objectives:

1. **To identify processing parameters that govern the particle size and morphology of LMNPs** produced via UFG. It is hypothesized that particle size can be effectively controlled by adjusting temperature, solid content, and grinding cycles.
2. **To reduce energy and water consumption in LMNP production**, thereby improving its cost-efficiency. The central hypothesis is that high-solids-content grinding significantly decreases resource usage without compromising nanoparticle quality.
3. **To evaluate the film-forming capability and barrier performance of LMNPs** in water- and oil-resistant applications. It is hypothesized that LMNPs form continuous coatings capable of enhancing surface protection in cellulose-based substrates.
4. **To enhance the aesthetic and mechanical properties of LMNP-cellulose composites** through structural innovations. The hypothesis is that composite performance can be improved by optimizing the distribution and integration of LMNPs within the fiber network.

5. **To explore the scalability and environmental potential of LMNP-based molded products** using a dry-forming approach. It is hypothesized that thermally assisted molding with LMNPs as binders yields composites suitable for sustainable packaging, eliminating the need for water and synthetic additives.

This dissertation is organized into several chapters. Following this introduction, Chapter 2 provides a comprehensive review of the literature, encompassing the environmental challenges posed by synthetic materials, advancements in sustainable materials for packaging, nano-sizing methods for LMNP manufacturing, and their diverse applications. Subsections delve into specific topics such as the environmental impact of microplastics and PFAS, the properties of cellulose and lignin, bottom-up and top-down manufacturing approaches for LMNP, and the integration of lignin-based composites in packaging solutions. This structured review underscores the critical role of lignin and its nano-sized derivatives in driving the transition towards greener and more sustainable material systems. Chapter 3 outlines the experimental methodologies for producing and characterizing LMNP, as well as the fabrication of LMNP paper composites, sandwich-structured paper composites, and molded fiber products. It also details the performance, mechanical, and chemical characterizations of these composites. Chapter 4 examines the effect of grinding temperature on LMNP size. Chapter 5 focuses on optimizing energy consumption in LMNP manufacturing by increasing solid content. Chapter 6 explores the application of LMNP suspensions in water- and oil-resistant films for sustainable packaging. Chapter 7 introduces the innovative sandwich-structured paper composite for packaging and disposable tableware, addressing lignin's aesthetic concerns. Chapter 8 discusses the application of lignin and its derivatives in dry-formed molded fiber products for packaging and tableware. Finally, Chapter 9 summarizes key contributions and offers recommendations for advancing LMNP-based materials research.

A schematic representation of the overall process for manufacturing LMNP and applying them to water- and oil-resistant packaging is shown in **Figure 1.1**. By addressing the challenges outlined, this research aims to contribute to the development of sustainable materials that can effectively replace conventional plastics in packaging and other applications, aligning with global efforts to reduce environmental pollution and promote a circular economy.

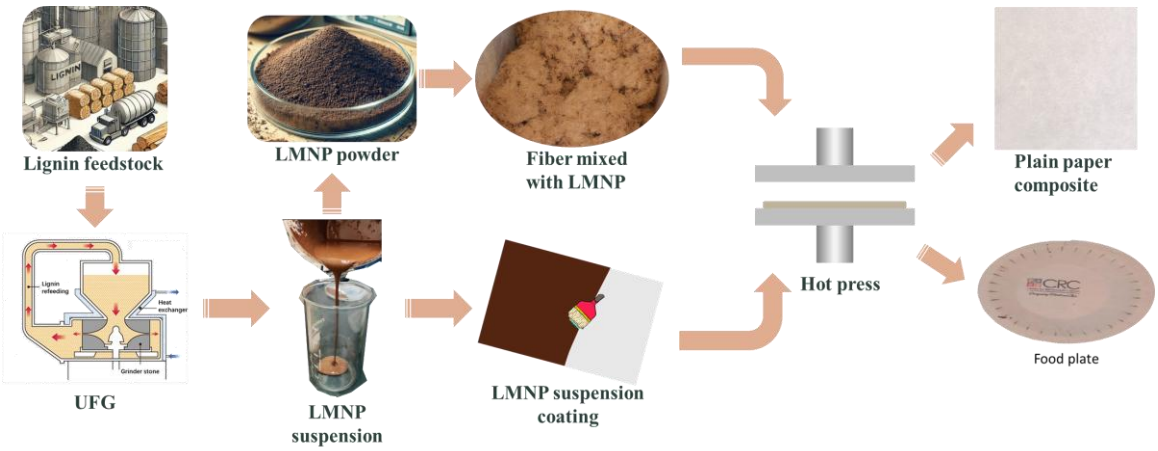

Figure 1.1 Scheme of LMNP manufacturing and its application in biodegradable packaging and tableware

CHAPTER TWO : LITERATURE REVIEW

2.1 Environment concerns of synthetic materials

The rapid development of the petrochemical industry in the 20th century marked a transformative era in material science, giving rise to petroleum-based plastics that quickly replaced traditional materials. Praised for their excellent processability, low cost, and lightweight properties, plastics became ubiquitous in industrial applications and daily life. However, the environmental issues associated with plastic waste, commonly referred to as white pollution, have been a longstanding concern. Additionally, synthetic substances such as PFAS, often deemed the most stable artificial compounds, present even more significant challenges due to their resistance to degradation.[14]

2.1.1 Plastics

According to the U.S. Environmental Protection Agency (EPA), global plastic production reached 368 million tons in 2019, with 40% of this total comprising single-use products such as disposable cups, lunch boxes, and take-out bags.[31] While many plastics are theoretically recyclable, the actual recycling rate remains alarmingly low—approximately 8% globally—with over 80% of single-use plastics ending up in landfills or the natural environment.[31] These persistent materials do not decompose easily; instead, they fragment into smaller pieces over time, ultimately forming microplastics that can persist for hundreds of years, creating long-term environmental issues.

Plastic waste poses a dual threat to ecosystems and human health. Large plastic debris, such as fishing nets and bags, entangle marine and terrestrial wildlife, causing injury or death.[32] Additionally, microplastics infiltrate aquatic ecosystems, where they enter the food chain, accumulate in drinking water sources, and pose risks to human health.[33] These environmental and health concerns have driven a growing interest in sustainable and biodegradable materials to replace conventional plastics.

2.1.2 PFAS

PFAS were first discovered and commercialized by Dupond Chemical.[13] Initially celebrated for their chemical stability and versatility, PFAS have since become synonymous with environmental pollution and health risks. Characterized by strong carbon-fluorine bonds, these compounds are highly resistant to degradation, making them persistent in the environment.[14] PFAS exhibit excellent resistance to chemicals, acids, and bases, and their ultra-low surface energy makes them unparalleled as oil-proof additives. However, these same properties render PFAS virtually non-biodegradable.

The environmental impact of PFAS became evident when residents near Solvay Specialty Polymers' New Jersey plant suffered from water contamination linked to these chemicals.[16] Studies revealed that prolonged exposure to PFAS in drinking water was associated with severe health issues, including cancer.[15] This realization of PFAS' persistence and toxicity has spurred regulatory actions and public demand for safer, biodegradable alternatives. As the search for replacements continues, natural polymers such as lignin have emerged as promising candidates for addressing the dual challenges of functionality and environmental safety.

2.2 Sustainable materials in package

The increasing demand for sustainable materials has brought attention to biomass as a renewable and versatile resource. Biomass-derived materials are increasingly used to produce biocomposites with reduced environmental footprints, aligning with global efforts toward a circular economy.

2.2.1 Bioplastics

Biopolymers such as polylactic acid (PLA), polyhydroxyalkanoates (PHA), polyhydroxybutyrate (PHB), and polybutylene succinate (PBS) are synthesized from renewable feedstocks, offering excellent biodegradability and mechanical properties comparable to conventional petroleum-based plastics.[34, 35] These polymers are

increasingly vital in developing biocomposites, addressing the growing demand for sustainable and environmentally friendly materials.

PLA:

PLA, derived from renewable resources like corn starch, sugarcane, and other carbohydrate-rich biomass, is widely recognized for its biodegradability, processability, and transparency.[36] Synthesized through biomass fermentation into lactic acid followed by polymerization, PLA serves as a thermoplastic matrix with favorable properties for biocomposite applications.[37] These properties include moderate tensile strength, good processability, and high transparency. However, its brittleness, limited thermal stability, and low barrier properties pose challenges for broader applications.[38, 39] Researchers have addressed these limitations through blending, copolymerization, and reinforcement with fillers such as cellulose, lignin, or nanoclays.

Bio-Polyurethane Foam (PUF):

The substitution of natural oil polyols (NOPs) for conventional polyol content during manufacturing distinguishes bio-polyurethane foam from regular PUF.[39] By incorporating NOPs, the health hazards associated with PUF production—such as risks of lung damage, asthma, and other respiratory problems—can be significantly reduced.[40] NOPs are primarily derived from fatty acids or triacylglycerols in agricultural feedstocks, including palm oil, soybean oil, and castor oil.[41] While castor oil naturally contains hydroxyl groups, other NOPs undergo chemical modification to introduce hydroxyl groups, enabling them to react with Poly isocyanate. Bio-PUF is used in packaging for protective cushioning of electronics, thermal insulation in food containers, custom inserts for retail products, cold-chain logistics for perishables, and as a sustainable alternative to expanded polystyrene.[42]

PHA and PHB:

PHAs, a diverse class of naturally occurring biopolymers synthesized by microorganisms as intracellular carbon and energy storage, exhibit remarkable

environmental compatibility.[43] Derived from renewable biomass sources such as agricultural residues and industrial byproducts, PHAs are known for their biodegradability and biocompatibility. A prominent subclass, PHB, offers high crystallinity, good tensile strength, and excellent environmental biodegradability.[44] However, its brittleness, low impact resistance, and high production costs have hindered widespread adoption. Blending PHB with other biopolymers or reinforcing it with fibers like cellulose and lignin has proven effective in enhancing its mechanical and thermal properties.[45] PHA and PHB are used in packaging as biodegradable films, trays, and containers for food products, replacing conventional plastics with compostable, bio-based alternatives.[46]

Bio-Based Polyethylene (PE):

PE is derived from ethylene, which can be obtained through ethanol produced from the fermentation of agricultural raw materials such as sugarcane or corn. While its production utilizes renewable resources, bio-based PE is physically identical to conventional PE and does not degrade biologically.[47]

Polybutylene Succinate (PBS):

PBS, a biodegradable aliphatic polyester synthesized from succinic acid and 1,4-butanediol derived from renewable sources, has emerged as a versatile biocomposite matrix.[48] Known for its balanced properties—excellent processability, thermal stability, flexibility, and biodegradability—PBS is suitable for applications in packaging, agriculture, and consumer goods.[48] Its relatively low stiffness and mechanical strength, however, limit its use in demanding applications.[49] Reinforcing PBS with natural fibers like cellulose or bio-based nanoparticles such as lignin or nanoclays has improved its mechanical properties while maintaining biodegradability.[49] Advances in chemical synthesis have reduced PBS's production cost and environmental footprint, increasing its accessibility for large-scale applications. PBS aligns with circular economic principles, enabling the development of bio-based, compostable materials that replace petroleum-based plastics.

2.2.2 Cellulose

Cellulose, a versatile and sustainable material derived from renewable biomass sources such as wood, agricultural residues, and grasses, serves as a key component of these fibers. Composed of linear chains of β-1,4-linked glucose units, cellulose fibers have a hierarchical structure, ranging from micro- to nanoscale, making them suitable for advanced biocomposites.[50] Their intrinsic properties—high tensile strength, low density, biodegradability, and excellent thermal stability—enhance their attractiveness as eco-friendly reinforcements in composite materials. By modifying their surface or blending them with other biopolymers (e.g., lignin, starch) or synthetic polymers, cellulose fibers can be tailored for specific applications, from packaging to construction materials.[50, 51] These innovations improve interfacial compatibility, reduce manufacturing energy consumption, and enhance sustainability, aligning with global efforts to reduce petroleum dependency, minimize environmental impacts, and foster circular economies. The structural diversity of biomass fibers further supports the creation of functional composites with customized performance characteristics.

2.2.3 Lignin and LMNPs

Approximately 150 billion tons of lignin is produced by plants annually, with nearly 50 million tons isolated during pulp and paper manufacturing.[52-54] Lignin represents the primary underutilized co-product in the pulp and paper industry.[55, 56] Due to its complex structure and heterogeneous chemical composition, only about 5% of lignin is currently utilized in value-added applications. The vast majority is burned in recovery boilers, not only to generate steam and electricity, but also to facilitate the recovery of pulping chemicals in industrial processes such as kraft pulping.[57] Valorizing lignin as a feedstock for materials production would enhance the economic prospects of the bioeconomy and promote net carbon neutrality.

In recent years, converting lignin into value-added products, such as nanomaterials, has been considered an essential strategy to improve the sustainability of lignocellulosic biomass processing. Nanosizing lignin enhances its antibacterial,

antioxidant, and UV light absorption properties.[58, 59] LMNPs improve the flame retardancy of thermally conductive laminates and the mechanical strength of films used in fireproofing.[60] Additionally, LMNPs can produce graphene and nanodiamonds under ambient conditions using a pulsed femtosecond laser.[61] They also have potential applications as adhesives, replacing phenyl formaldehyde resins in various commercial applications.[62] LMNPs' smaller size, nucleating capability, and hydrogen bond formation increase cross-linking within polymer matrices, enhancing mechanical strength. The development of nanocomposite networks with LMNPs forms the basis for future biomaterials exhibiting superior functions and represents a viable strategy to valorize lignin.

2.3 LMNPs' manufacturing

There are still technical barriers to developing high-value products from lignin, and its application has not yet reached the commercialization stage. Therefore, it is essential to develop feasible technologies for lignin processing. In the case of LMNPs, two manufacturing methods are usually employed: a bottom-up approach using self-assembly[63] and a top-down approach using mechanical force.[64]

2.3.1 Bottom-up method

Bottom-up means, from molecular level to LMNP. As the most popular method in bottom-up, self-assembly refers to the spontaneous organization of lignin molecules into nanoscale structures driven by non-covalent interactions such as hydrogen bonding, hydrophobic effects, and π-π stacking [65]. This process is typically induced by altering environmental conditions like solvent composition, pH, or temperature, causing lignin to aggregate into stable nanoparticles. The self-assembly method is efficient, and enabling precise control over nanoparticle size and surface properties without the need for complex chemical reactions.[58, 66] LMNPs formed through this process have diverse applications in biodegradable coatings, drug delivery, and water- and oil-resistant materials, highlighting the importance of optimizing self-assembly conditions for tailored functionality.[67] However, the self-

assembly method consumes large quantities of organic solvents, such as methanol, ethanol, tetrahydrofuran, toluene, ethylene glycol, and dimethylformamide.[26,68] While some of these solvents can be recovered, others volatilize in the environment cause health hazards to humans.

2.3.2 Top-down method

The top-down approach is advantageous as it employs mechanical means, such as sonication[69], high-shear homogenization[70], and UFG [71], which partially or completely avoid the use of toxic and corrosive solvents.

The UFG method has been previously used to manufacture 100% cellulose and lignin-containing cellulose nanofibers.[72,73] During UFG, biological materials are comminuted under the compression of grinding stones and collision with abrasive grains to generate ultrafine particles. Commonly, the sample slurries are passed several times through the grinding chamber to achieve the desired particle size.[74-76] This technique has also been used to produce LMNPs from softwood kraft lignin, requiring a duration of 4 h to achieve a particle size reduction from 500 nm to 22 nm.[70] However, the energy consumption and time required for LMNP production by UFG can be high, with as many as 40 passes needed to achieve a reasonably small particle size.[74,77] While UFG is eco-friendly, addressing its energy and efficiency drawbacks remains essential.

2.3.3 Energy and water consumption sensitivity in UFG

Whether employing a top-down or bottom-up approach, both entail substantial water consumption, typically amounting to 50 times the net lignin weight during LMNP production[78]. Reducing water usage often leads to less wastewater generation during the preparation process. By optimizing water usage, manufacturers can lower operational costs associated with water procurement, treatment, and disposal. Lower water consumption helps maintain ecological balance, protecting aquatic habitats and overall biodiversity. Among existing low-water-consuming techniques, ultrasonication and microwave treatments are highly energy-sensitive, often resulting

in significant temperature increases detrimental to the LMNP manufacturing process.[79]

Conversely, grinding, which can continuously process materials, offers advantages in terms of energy consumption and large-scale processing compared to the aforementioned methods. Hence, reducing water usage in techniques like grinding would pave the way for sustainable LMNP production. To industrially scale up mechanical manufacturing of LMNPs, energy consumption must be low enough to be competitive with other nanomaterials. Although LMNP yield has greatly improved, there is still room for reducing unit energy consumption. **Table 2.1** summarizes state-of-the-art mechanical manufacturing methods for LMNPs, their production parameters, and energy use efficiency. Many mechanical methods, such as gas-driven shearing and high-pressure homogenization, use high-shear delamination to break down plant material into small particles. These methods are suitable for scaling up LMNP production but have yet to achieve optimal energy efficiency. Except for the twin-screw extrusion process, which employs ≤ 30% solids concentration[80], most mechanical methods typically use a low solids concentration of ≤ 5%.[28, 64, 81-83] This leads to higher energy consumption per unit weight of dry lignin and adversely affects water usage, as well as the subsequent transport, drying, storage, separation, and utilization of LMNPs.

2.4 Lignin composite in package

Cellulose nanofibers (CNF) possess excellent mechanical strength and oxygen barrier properties, making them a premier functional additive for food packaging materials.[84, 85] However, their inherent hydrophilicity limits compatibility with hydrophobic additives, complicating the formation of strong, uniform, and hydrophobic films on paper surfaces without adhesives.[86] To date, no studies have demonstrated the successful formation of pure lignin-based continuous films as an effective barrier layer for paper composites. This limitation is likely due to lignin's inherent brittleness, processing challenges, and potential concerns about residual

Table 2.1 State-of-the-art methods and parameters for lignin nanoparticle manufacturing

Methods	Processing conditions		Efficiency parameters		Reference
	Lignin feedstock	Concentration (wt. %)	Energy related information	Duration	
Aerosol flow drying	Kraft, alkali lignin	0.5 – 2.0	153ºC	N/A	[28]
	Hydrothermally treated birch wood	5.0	No heating	N/A	[87]
Ultrafine friction grinding	Kraft lignin	1.0	12 cycles	1.0 h	[88]
	Poplar wood	1.3	10-30 cycles	N/A	[89]
	Softwood biomass	3.0	N/A	1.5 h - 3.0 h	[72]
	Lignin-coated cellulose from switchgrass	1.0	19 cycles	N/A	[90]
	Lignin from soda black liquor	2.0	100 cycles	N/A	[71]
Gas-driven shearing	Alkali lignin	0.1	0.5 MPa, 600 L/h driven air	N/A	[91]
Ultrasonication	Alkali lignin	0.1	6 kW	1.0 h	[92]
	Softwood kraft lignin	0.1	130 W	6.0 h	[69]

Table 2.1 continued

Ultrasonication	Wheat straw lignin and Sarkanda grass lignin	0.7	600 W	1.0 h	[79]
High shear homogenization	Organosolv lignin	1.0	750 bar	0.25 h	[93]
	Soda lignin	1.0	12,400 RPM	1.0 h	[94]
	Softwood kraft lignin	0.5	15,000 RPM	4.0 h	[70]

impurities or extractives in technical lignins that may affect food safety compliance.[95] The size of commercial lignin particles ranges from tens to hundreds of microns[19], making integration into cellulose or nanocellulose fibrils challenging. When combined with cellulose in paper composites, lignin often agglomerates and distributes unevenly. During thermoforming, uneven heat can induce partial decomposition, hindering the production of smooth and uniform films.

LMNPs, with sizes ranging from 100 to 1000 nm, present a promising alternative as they can theoretically fill the cavities between cellulose fibers. The application of heat and enhanced hydrogen bonding can improve the compatibility between cellulose fibers and lignin layers.[96-99] This approach facilitates the formation of composite or layered films with improved structural and barrier properties. Bhagia et al.[89] demonstrated that hot-pressed lignocellulose-based paper produced at temperatures between 150 °C and 180 °C exhibited doubled mechanical strength compared to air-dried paper.

Building on this, it is hypothesized that under hot-pressing conditions, LMNPs can melt and fill voids in cellulosic paper, forming a continuous dense layer on the surface. This layer would effectively block oil droplet penetration, enhancing the paper's suitability for food packaging applications. Further research is needed to optimize LMNP integration and evaluate the performance of these composites in real-world conditions.

2.5 Development of molded products

Molded fiber products are at the forefront of green packaging solutions, offering an eco-friendly alternative to conventional plastic-based materials. These products have gained significant attention as a sustainable approach to mass-produced packaging due to their biodegradability and reliance on renewable resources. Conventional manufacturing techniques for molded fiber products include casting, laminated paper methods, paper cutting, and roll-to-shape molding. However, these methods often involve multiple processing steps and long production times, resulting

in inefficiencies. Moreover, scaling up these traditional methods often requires extensive space, large-scale equipment, and considerable operational costs, which can hinder the broader adoption of molded fiber packaging.

The introduction of modern molding techniques, particularly those employing multiple molds on a single template, has significantly enhanced production efficiency. Among the available methods, the wet molded process is the most established one due to its ability to produce strong and durable products. However, a relatively new approach, known as dry forming, has emerged as a superior alternative. This method addresses some of the critical limitations of wet molding, such as high water and energy consumption, while also improving production speed and resource utilization.

2.5.1 Wet molding method

The wet molded fiber process has been widely used for decades and involves several distinct stages to produce molded fiber products. The process typically proceeds as follows: 1. Pulp regeneration: Dry pulp is rehydrated to achieve slurry with the desired solid concentration. 2. Addition of additives: Waterproofing agents, oil-proofing agents, and other functional additives are mixed into the slurry to enhance the product's performance and meet specific requirements. 3. Wet molding: The pulp slurry is poured into a mold equipped with pores. Excess liquid is removed by vacuum suction, and the remaining pulp forms an initial layer on the mold surface. 4. Initial molding: Further water removal is achieved through compression, solidifying the structure. 5. Hot pressing: High temperature and pressure are applied to finalize the product, resulting in its desired strength, shape and moisture content.[100]

This method leverages the inherent hydrogen bonding between cellulose fibers to produce strong products without the need for additional binders or adhesives. However, products created using this technique are sensitive to moisture. When exposed to humid environments, they tend to absorb water, leading to a reduction in mechanical strength. Additionally, the wet molding process requires significant water

usage and energy input, particularly during the drying stage, making it less sustainable and cost-effective for large-scale production.

2.5.2 Dry forming method

In very recent years, dry molded fiber technology, developed by PulPac®, has emerged as a transformative approach to molded fiber manufacturing. This innovative process addresses several critical drawbacks associated with the wet molding method, offering substantial improvements in water and energy efficiency, production speed, and scalability. Dry forming eliminates the need for pulp suspension regeneration, which is a water-intensive step in traditional wet molding.

The key advantages of dry forming include: 1) Water conservation: Unlike wet molding, the dry forming process does not require water to rehydrate pulp fibers. This significantly reduces overall water consumption and eliminates the generation of wastewater, making the process more environmentally sustainable. 2) Energy efficiency: Dry forming avoids the drying stage, which is one of the most energy-intensive steps in wet molding. By eliminating this step, the production cycle is shortened, and energy consumption is significantly reduced. 3) High production speed: The absence of a drying stage enables dry forming to achieve much faster production times. For instance, hot-pressing molding can be completed in an average of three seconds, compared to at least fifteen seconds for wet molding. This efficiency allows manufacturers to meet high-volume demands with fewer resources.

PulPac's collaboration with JOA® led to the development of a highly automated dry forming machine that is versatile and adaptable to a wide range of pulp fibers. The process shown in **Figure 2.1**, begins with raw fibers undergoing a milling process to create dispersed fibers. These fibers are compressed and formed into loose cardboard on a web. As the web progresses along a conveyor belt, waterproofing agents, oil-proofing agents, and adhesives can be applied as needed to enhance the material's properties. The treated cardboard is then fed into a hot-pressing unit, where it is molded into the desired shape within just three seconds. Finally, the product is cut

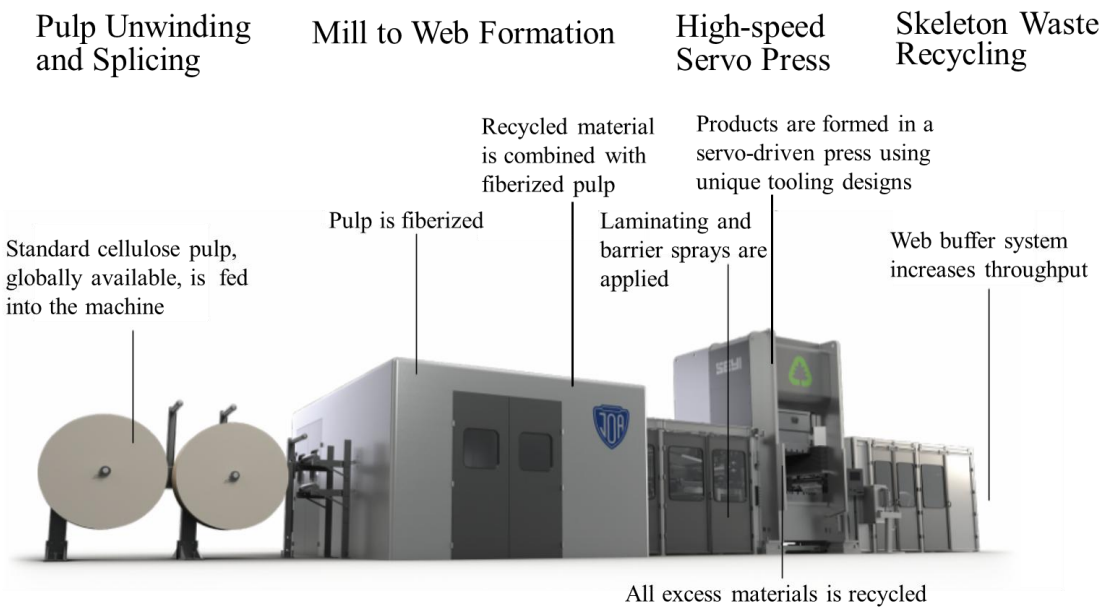

Figure 2.1 Overall view of JOA inc.'s dry forming machine. Reprinted with permission from reference.[101] Copyright 2025 PulPac. Further permissions related to the material excerpted should be directed at PulPac.

and deburred to meet precise specifications. Any leftover scraps from the cutting process are recycled back into the milling stage, resulting in a material utilization rate of 99%.

The dry forming method not only conserves resources but also offers significant economic advantages. By eliminating the need for extensive water treatment and energy-intensive drying equipment, manufacturers can reduce operational costs. Additionally, the high production efficiency of dry forming makes it an attractive option for large-scale packaging operations.

2.5.3 Implications for the future of molded fiber products

The development of dry forming technology marks a significant advancement in the field of molded fiber packaging. By addressing the limitations of traditional wet molding methods, dry forming paves the way for scalable and sustainable production. The combination of water and energy conservation, high material utilization, and rapid production times positions dry forming as a key driver of innovation in the green packaging industry. As demand for eco-friendly packaging continues to grow, further optimization of dry forming processes and machinery will likely enhance its adoption across various sectors.

In conclusion, while wet molding remains an established method with its own strengths, the emergence of dry forming offers a promising alternative for the mass production of molded fiber products. By prioritizing sustainability and efficiency, dry forming represents the future of green packaging technology.

CHAPTER THREE : MATERIALS AND METHODS

3.1 Materials and chemicals

The kraft softwood lignin used in this study was provided by WestRock Co. (East Dublin, Georgia). Pulp was obtained from WestRock® (Atlanta, GA, USA). The substrate paper, a xerographic paper with a grammage of 75 g/m², was purchased from Corporate Express (Broomfield, Colorado) and used without further treatment.

Various chemicals were employed in this research. Toluene (99.9% purity) was obtained from Fisher Chemical. Castor oil and n-heptane (99% purity) were sourced from Thermo Scientific, while soybean oil was purchased from a local Walmart store. Additional specialty chemicals, including lithium bromide, hydrobromic acid, and acetic anhydride, were also obtained from Thermo Scientific. Acetone, dimethyl sulfoxide (DMSO), pyridine, deuterated chloroform, sulfuric acid, and sugars (glucose, xylose, galactose, arabinose, and mannose) were purchased from Sigma-Aldrich. All reagents were used as received, without further purification.

Deionized water (18.2 MΩ·cm resistivity) was prepared using a Milli-Q® EQ 7000 ultrapure water purification system (Millipore Sigma) to ensure high purity and eliminate potential contaminants.

3.2 Experimental procedure

3.2.1 Preparation of LMNPs

The UFG method was employed using a small-scale MKCA6-5 Supermasscollider, equipped with a pair of GA 6-80 standard grinding disks, from Masuko Sangyo Company Ltd. (Kawaguchi, Japan). The grinding stones had a diameter of 150 mm, with a wet grinding capacity of ≤120 kg/h. The stone clearance and grinding speed were maintained at –200 μm and 1500 rpm, respectively. The grinder setup is shown in **Figure 3.1**.

For LMNP production, lignin/water suspensions were prepared at a total volume of 2 L and subjected to UFG at designed temperature. The pH of these

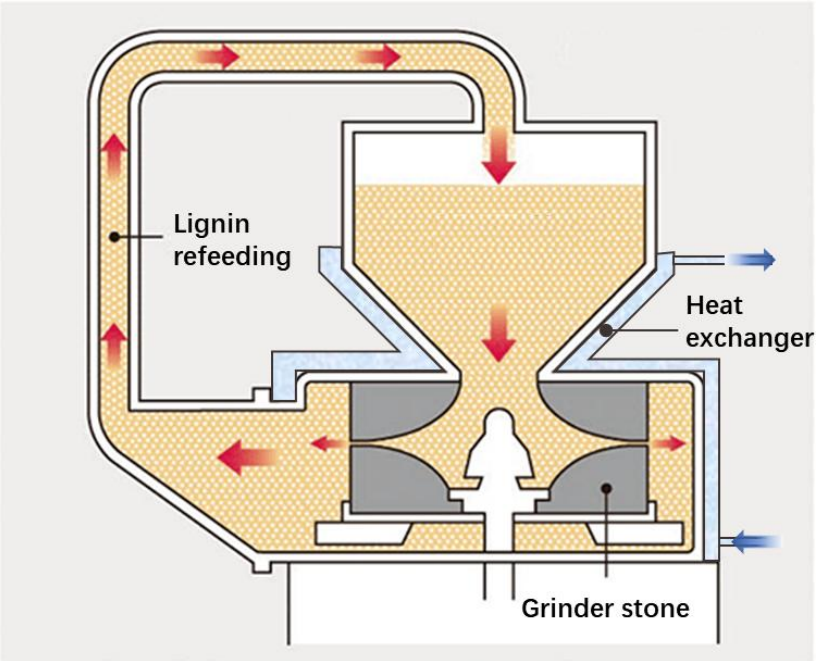

Figure 3.1 Schematic diagram of ultrafine friction grinding under temperature-controlled condition for lignin micro- and nano- particles (LMNPs) production.[88] Copyright Industrial Crop and Products 2023

suspensions were found to be neutral. To achieve the target processing temperatures, all lignin suspensions were pre-cooled or pre-heated accordingly. For grinding at 0°C, lignin was first dispersed in ice-cold water, and an external heat exchanger (VWR®, Radnor, PA) set to –5°C was used to maintain the grinding chamber temperature (**Figure 3.1**). The suspension temperature at the sample outlet was monitored using a standard mercury thermometer for reference.

For grinding treatments at 25°C and 70°C, lignin suspensions were heated on a hot plate with constant stirring for approximately 1 hour before UFG. The external heat exchanger was set at 15°C and 80°C to maintain the sample outlet temperature at 25°C and 70°C, respectively. The heat exchanger settings for each treatment group were determined through preliminary experiments, which established the relationship between the external jacket temperature and the sample outlet temperature.

Each treatment group underwent a maximum of 12 grinding passes, based on preliminary optimizations. A 100-mL sample was collected every fourth pass for characterization. A portion of the collected LMNP samples were freeze-dried using a FreeZone 4.5 L system (Labconco, Kansas City, MO) under reduced pressure (0.15 Torr) for subsequent thermal and spectroscopic analyses. The entire UFG process was conducted in triplicate for each treatment group.

3.2.2 Preparation of LMNP-paper composites

A 50 wt.% suspension was prepared by dispersing 50 g of LMNPs in 50 g of deionized water using a mixer. The grammage of the LMNP layer was controlled by adjusting the amount of LMNP suspension applied to the paper surface. For instance, a 10 g/m² lignin layer was formed by applying 0.2 g of the 50 wt.% LMNP suspension onto a square piece of paper with a side length of 100 mm. Similarly, 20, 30, and 40 g/m² lignin layers were formed by adjusting the corresponding amount of LMNPs. The entire paper with the wet LMNP coating was then hot-pressed at 3 MPa, 160 °C for 3 mins to form an LMNP-paper composite. These samples were labeled as C10-P3-T160-M30, C20-P3-T160-M30, C30-P3-T160-M30, and C40-P3-T160-M30,

as shown in **Table 3.1**. The manufacturing process of the LMNP-paper composite is depicted in **Figure 3.2**, with images of the raw materials and equipment provided in **Figure 3.3**. Three replicate samples were prepared for each treatment.

3.2.3 Preparation of polymer blend

To develop a multifunctional polymer blend suitable for coating and packaging applications, LMNPs, PVA, PLA, and $Zn(NO_3)_2$ were selected based on their complementary properties. LMNPs provide hydrophobicity and antioxidative capacity; PVA contributes film-forming ability and mechanical flexibility; PLA offers biodegradability and structural integrity; and $Zn(NO_3)_2$ serves as a crosslinking agent and potential antimicrobial additive. The composition of the polymer blend was optimized using a mixture model extreme vertices design (EVD) in JMP. The EVD is a constrained mixture design used when component proportions are limited within specified upper and lower bounds. In total, 20 different formulations were prepared, each with 3 replicates, resulting in 60 experiments seen in **Table 3.2**.

For the preparation of the polymer blend, the solid components were sequentially dispersed in deionized water in the following order: $Zn(NO_3)_2$, PVA, PLA powder, and LMNP. To facilitate dissolution of PVA, water was heated to 70 °C. Each component was thoroughly mixed to ensure homogeneous dispersion before the addition of the next. The resulting suspension had a total solids content of 50 wt%.

3.2.4 Preparation of sandwich structure paper composites

Figure 3.4 illustrates the procedure for preparing the sandwich-structured paper composite. A polymer blend film, with a thickness of 120 microns, was applied to the surface of parchment using a bar coating technique. Another piece of parchment was then placed over the film to form a sandwich structure. This structure was subsequently subjected to hot pressing with a flat pressing plate at 3 MPa and 180 °C for 3 minutes. After pressing, the heat was turned off, and the resulting flat, sandwich-

Table 3.1 Manufacturing parameters and the corresponding abbreviations of LMNP-paper composites

Abbreviations	LMNP coating weight (g/m^2)	Hot-pressing pressure (MPa)	Hot-pressing temperature (°C)	Moisture of LMNP suspension (wt.%)
Variations in coating weight				
C10-P3-T160-M30	10	3	160	30
C20-P3-T160-M30	20	3	160	30
C30-P3-T160-M30	30	3	160	30
C40-P3-T160-M30	40	3	160	30
Variations in hot-press pressure				
C40-P1-T160-M30	40	1	160	30
C40-P3-T160-M30	40	3	160	30
C40-P5-T160-M30	40	5	160	30
Variations in hot-press temperature				
C80-P3-T120-M30	80	3	120	30
C80-P3-T140-M30	80	3	140	30
C80-P3-T160-M30	80	3	160	30
C80-P3-T180-M30	80	3	180	30
Variations in moisture of LMNP				
C40-P3-T160-M10	40	3	160	10
C40-P3-T160-M30	40	3	160	30
C40-P3-T160-M50	40	3	160	50

Note: LMNP – Lignin micro- and nanoparticle

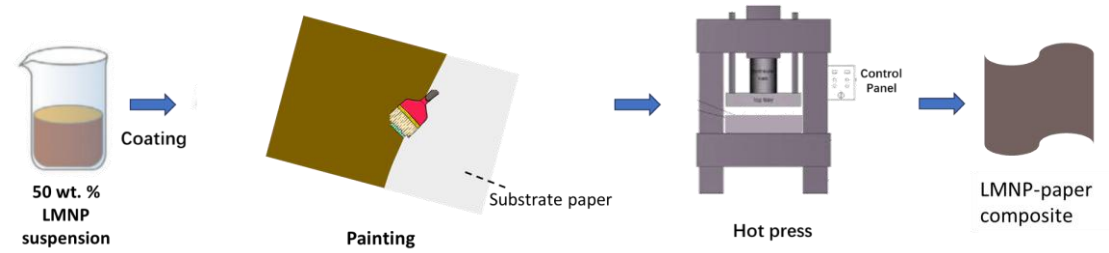

Figure 3.2. Scheme for coating the substrate (xerographic paper) with lignin micro- and nanoparticle (LMNP) suspension to form a multilayered LMNP-paper composite.

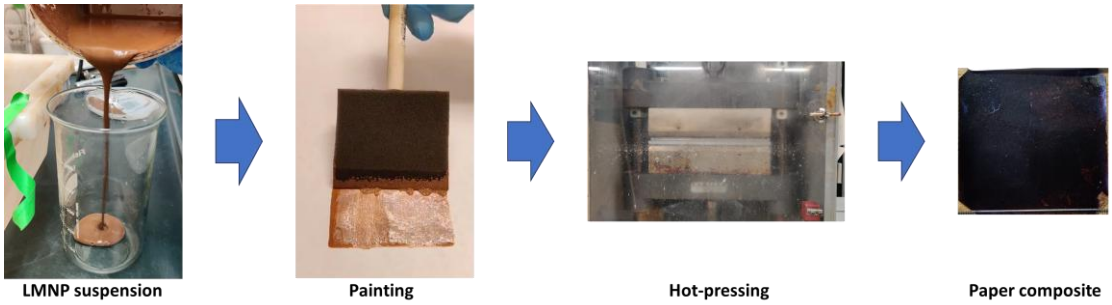

Figure 3.3. Step-by-step fabrication process of the LMNP paper composite: preparing LMNP suspension, applying a coating, hot pressing, and the final composite paper.

Table 3.2 Composition and experimental design of the interlayer polymer blend in sandwich-structured paper composites, based on an Extreme Vertices Mixture Design (EVMD)

Species Order	Percentage of each component (wt.%)			
	LMNP	PLA	PVA	$ZnNO_3$
1	50	0	40	10
2	50	0	45	5
3	50	0	50	0
4	50	20	20	10
5	50	23	23	4
6	50	25	25	0
7	50	40	0	10
8	50	45	0	5
9	50	50	0	0
10	63	13	13	10
11	67	17	17	0
12	70	0	20	10
13	70	20	0	10
14	73	0	23	5
15	73	23	0	5
16	75	0	25	0
17	75	25	0	0
18	90	0	0	10
19	95	0	0	5
20	100	0	0	0

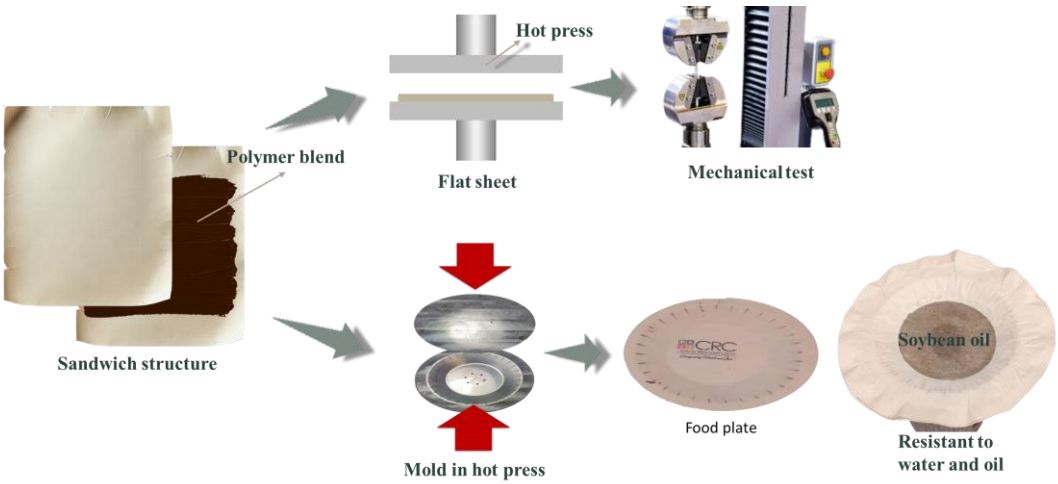

Figure 3.4 Schematic representation of sandwich-structured paper composite making and its potential applications

structured paper composite was retrieved. To demonstrate its potential application in tableware, a food plate mold was used in the hot press to fabricate a molded paper plate.

3.2.5 Preparation of molded fiber products – dry forming method

Dry pulp sheets were disintegrated into individual fibers using a Ninja® blender (Madison, TN, USA) with a peak power of 1700 W, operating in Max-Crush mode for 2 minutes. The resulting fibers were then mixed with LMNPs at predetermined weight percentages under dry conditions. Three LMNP loading (10, 30, and 50 wt.%) were selected to examine the effect of LMNP loading on composite properties. The mixtures were subsequently hot-pressed at 200°C under 5 MPa for 3 minutes to form composites, designated as L1-PF9, L3-PF7, and L5-PF5 according to their LMNP content. Additionally, pure pulp fibers were used to produce molded samples (L0-PF10) as control sample, where 30% water was added during hot pressing to facilitate hydrogen bonding.

3.3 Electricity consumption calculation

The electricity consumption for producing 1 kg of LMNP was determined based on the power usage of the grinder during operation, measured in accordance with our previous methodology.[90] Briefly, the power (P) of the grinder was assessed by using a power meter (Model No. 380976, Extech Instrument, Rochester, NY) and measure the current in A and the voltage in V. The energy consumption (in kWh) was then obtained by multiplying the residence time of the lignin suspension in the grinder and the calculated power (in kW) as shown in Equation 1. To study the energy consumed per kg of lignin, all energy consumption was finally divided by the mass of corresponding lignin, as detailed in Equation 2. To determine the accumulated energy consumption at the end of each cycle through the grinder, the total energy consumption was obtained by adding up the energy for all completed cycles, as shown in Equation 3. Energy usage for chilling lignin suspension was not included for

energy comparison. In commercial production, heating may not be necessary as processing will generate enough heat.

Equation 1

$$E = \int_{t0}^{t'} pdt, \quad (1)$$

$E - energy, in\ kWh; p - power, in\ kW; t - time, in\ s$

Equation 2

$$E' = \frac{\mathrm{E}}{\mathrm{M}}, \quad (2)$$

$\mathrm{E}' -$ energy consumption per kg lignin; $\mathrm{M} -$ mass of lignin (in kg)

Equation 3

$$Accumulatd\ energy, E_{ac} = \sum_{1}^{x} E', \quad (3)$$

$\sum_{1}^{x} E' - subtotal\ from\ the\ first\ cycle\ to\ the\ present\ x^{th}\ cycle\ (in\ kW).$

3.4 Analytical instrumentation

3.4.1 Characterization of biomass samples

3.4.1.1 Chemical composition of lignin

The structural carbohydrate, ash, and lignin content of the original softwood kraft lignin (**Table 3.3**) was determined according to the standard analytical protocols developed by the National Renewable Energy Laboratory (NREL), Golden, CO (Sluiter et al., 2012). The analysis was conducted in triplicate and for each replicate, 300 mg of lignin were weighed and transferred into a pressure tube and then hydrolyzed with 3 mL of 72% (w/w) sulfuric acid at 30°C for 60 min. Upon completion, the acid concentration was diluted to 4% (w/v) using deionized water and then the sample was autoclaved for 1 h at 121°C. To measure the acid insoluble lignin content, the solid residues recovered from the autoclaved hydrolysis solution were

Table 3.3 The average chemical composition (% w/w on oven dry basis) of the starting lignin material.

Sample name	**Lignin**			**Carbohydrates**				**Ash**	**Total mass balance**
	ASL	AIL	TL	Glucan	XMG	Arabinan	TC		
Softwood kraft lignin	2.6 ± 0.1	87.7 ± 1.1	90.3 ± 1.1	N.D.[a]	2.8± 0.0	N.D.[a]	2.8 ± 0.0	3.8 ± 0.0	96.9 ± 1.1

ASL: Acid Soluble Lignin, AIL: Acid Insoluble Lignin, TL: Total Lignin, XMG: Xylan-Mannan-Galactan, TC: Total Carbohydrates, [a]Not detected. All means and standard deviations are provided for $N = 3$.

dried at 105°C and then weighed and adjusted by accounting for the ash content, which was determined by combusting the dried solid residues at 575°C for 4 h in a muffle furnace (Sluiter et al., 2008). To measure the acid soluble lignin, the filtrate was subjected to UV-Vis spectrophotometry where the absorbance at 214 nm was used to calculate the dissolved lignin quantity as per the NREL protocol (Sluiter et al., 2012). For the structural carbohydrate determination, the same filtrate was neutralized using calcium carbonate, passed through a 0.22 μm membrane, and then analyzed for monosugars using a Flexar high-performance liquid chromatography (HPLC) system fitted with a Bio-Rad Aminex HPX-87P analytical columns and a refractive index detector (PerkinElmer, Shelton, CT). The concentration of glucose, xylose, galactose, arabinose, and mannose was determined using in-house calibration curves.

3.4.1.2 FT-IR analysis

FTIR was employed to investigate chemical bonds shift of lignin and its integration in composites. FTIR spectra in the range of 4000 to 600 cm-1 were collected in absorbance mode with 64 scans per sample and a resolution of 4 cm-1 using a Spectrum Two spectrometer (PerkinElmer, Shelton, CT) fitted with a diamond universal attenuated total reflectance (UATR) accessory. The UATR assembly has a pressure arm which ensures good surface contact between the sample and the diamond crystal. All FTIR spectra were processed via detrending and standard normal variate normalization and then subjected to principal component analysis (PCA) using the Unscrambler X v10.4 software (Aspen Technology, Inc.). PCA scores differentiate or group the treatments according to their chemical signature, whereas the PCA loadings identify the spectral peaks that were responsible for the sample grouping.[88]

3.4.1.3 Gel permeation chromatography (GPC)

GPC was employed to investigate molecular weight change of lignin in UFG processing. The molecular weight of original lignin and LMNPs was determined after derivatization via acetobromination using a Tosoh EcoSEC GPC instrument (Tosoh

Bioscience LLC, Grove City, OH) fitted with two Tosoh TSKgel SuperMultiporeHZ-M analytical columns and a refractive index detector following Nair's method.[70] The column oven temperature was set to 40°C and THF was used as the mobile phase at a flow rate of 0.35 mL/min. The total run time was 15 min, and the resulting chromatograms were calibrated using polystyrene standards in the molecular weight range of 600 to 7,500,000 Da. For derivatization, 10 mg of lignin samples were mixed with 9.2 mL of glacial (anhydrous) acetic acid and 0.8 mL of acetyl bromide and then incubated at 50 °C for 2 h with constant stirring. Afterwards, the derivatization reagents were removed under reduced pressure using a rotary evaporator. The acetobrominated lignin residues were dissolved in 10 mL THF, passed through 0.45 μm membrane filter, and analyzed using the GPC.

3.4.1.4 Thermal analysis

The freeze dried LMNPs were used for all thermal analyses. The thermal degradation profile of original lignin and LMNPs was obtained using a Q500 thermogravimetric analyzer (TGA) from TA Instruments (Waters LLC, New Castle, DE, USA). Approximately 10 mg of sample were heated in the range of 25 – 600°C, at 10°C /min, with a nitrogen flow rate of 40 mL/min.

The glass transition temperature (Tg) of the original lignin and LMNPs was determined using a Q2000 differential scanning calorimeter (DSC) from TA Instruments. For DSC analysis, 6 to 7 mg samples were weighed carefully and sealed hermetically in aluminum pans and then heated from 0 to 250°C at 20°C/min. Each DSC experiment consisted of three heating and cooling cycles in a nitrogen atmosphere and the heat flow curve from the final heating cycle was used to calculate the T_g.

3.4.1.5 Nuclear magnetic resonance (NMR) spectroscopy

The original lignin and LMNPs obtained after 12 grinding passes were dissolved in DMSO-d6 at a concentration of 100 mg/mL, filtered through a 0.22 μm membrane to remove any undissolved particles, and then subjected to NMR analysis.

The proton and two-dimensional (1H-13C) heteronuclear single quantum coherence (HSQC) NMR spectra were collected using a solution state Varian VNMRS 500 MHz system (Varian, Inc., Palo Alto, CA). A phase-sensitive gradient-edited HSQC program (gHSQCAD) was used, and the default acquisition parameters were followed except for using 128 t1 increments, at 4 scans per t1 increment, and a scan range of 0 to 190 ppm in the F1 (13C) dimension. The acquired spectra were processed using MestReNova 14.2 (Mestrelab Research S. L., Spain) software where first they were subjected to a 3rd order polynomial baseline correction in all dimensions, then automatic phase correction, Gaussian (90 in F1 and 10 in F2) and exponential (-10 in F1 and -0.5 in F2) apodization, t1 noise reduction, and finally adjusted to a spectrum size of 1024 (in both dimensions). The DMSO peak at δC/ δH – 39.5/2.52 ppm was used as internal reference. The cross peaks were integrated, normalized to the intensity of DMSO peak, and identified according to previous literature (De Menezes et al., 2017; Nishimura et al., 2018; Miyagawa et al., 2020; Smink et al., 2020). The relative quantity of inter-unit linkages and terminal substructures are expressed as a number per 100 aromatic (guaiacyl) units (Constant et al., 2016).

3.4.2 Characterization of particles' morphology

3.4.2.1 Scanning electron microscopy (SEM)

The micromorphology of the LMNPs and starting lignin was characterized using a Zeiss Auriga (Oberkochen, Germany) scanning electron microscope (SEM), operating at 1 kV. The LMNP suspensions were diluted to 0.05% (w/v), dispersed on polished aluminum sample platforms, air dried, and then sputter coated with gold prior to analysis.

3.4.2.2 Dynamic light scattering analysis

Samples collected at the 4th, 8th, and 12th UFG passes, for all three treatments (0, 25 and 70°C), were equilibrated to room temperature and then subjected to dynamic light scattering (DLS) analysis. The original lignin and LMNP aqueous suspensions were diluted to a concentration of 0.2 mg/mL and then analyzed using a

Zetasizer Nano series instrument (Malvern Panalytical, Malvern, UK), at 25°C, to determine their average size, particle size distribution, and zeta-potential. To measure LMNP stability, the zeta-potential of samples stored at 4°C for 90 days were also tested. All measurements were performed at least in triplicate.

3.4.3. Characterization of morphology of paper composites

3.4.3.1 Scanning electron microscopy (SEM)

Both top-view and cross-sectional images of the LMNP-paper composites were characterized utilizing a Zeiss Auriga scanning electron microscope (Oberkochen, Germany), operating at 2 kV. The coated paper was fractured in liquid nitrogen to acquire the film cross-section. Additionally, Forced Ion Beam (FIB) technique was employed for obtaining the film cross-section. Initially, a coarse section was generated under a Xe ion beam at 30 kV and 60 nA, followed by polishing the section under 30 kV and 2 nA conditions to achieve a smoother surface. Prior to imaging, all samples underwent gold coating.

3.4.3.2 Thickness, grammage, and density measurement

The thickness of the LMNP-paper composite was measured using a micrometer at five different points, and the average value was taken as the thickness. The grammage of the lignin layer was calculated by subtracting the weight of the paper base from the total weight of the LMNP-paper composite. The density of the paper composite was determined by dividing the weight of the LMNP-paper composite by its volume, which was calculated from its area and thickness.

3.4.3.3 Surface elemental Analysis

The surface elemental composition and distribution of the interlayer polymer blend in samples $10^{\#}$ (63 wt.% LMNP, 13 wt.% PLA, 13 wt.% PVA, and 10 wt.% Zn $(NO_3)_2$) and $20^{\#}$ (100% LMNP) were analyzed using an Escalab 250Xi X-ray photoelectron spectrometer (XPS, Thermo Scientific K-Alpha, USA) and energy-dispersive X-ray (EDX) spectroscopy, integrated with a scanning electron microscope (SEM; EVO10, Carl Zeiss, Germany). For XPS Analysis**,** a full-spectrum scan was

performed, followed by the collection of high-resolution spectra for C 1s, O 1s and Zn 2p peaks to provide detailed insight into the chemical states of the elements present in the composite. For EDX Mapping**,** a SEM image of the polymer blend surface was obtained, and elemental distribution maps for carbon (C), oxygen (O), and zinc (Zn) were generated to visualize the spatial dispersion of these elements within the polymer blend.

3.4.4. Performance of paper composites

3.4.4.1 Mechanical Property

The tensile properties of all LMNP-paper composites were measured using a universal testing machine (Instron 5567) in accordance with the ASTM D828-22 standard36. A 30 kN load cell was used, with a gauge length of 60 mm and an extension speed of 5 mm/min. Tests were conducted at 25 °C and 50% relative humidity. Each test specimen had a length of 100 mm and an average width of 20 mm, with thickness measured individually for each sample. An average of three repeated measurements per sample was taken. The average values of tensile properties, including Young's modulus and ultimate strain, along with their standard deviations, were reported.

3.4.4.2 Oil and grease resistance (OGR) testing

The oil kit test (TAPPI T 559 cm-22) was used to test the oil and grease resistance of all LMNP-paper composite and uncoated paper [37]. This method uses 12 liquids with varying surface tensions (**Table 3.4**). To initiate the test, a drop of oil is placed onto the paper using a glass dropper from a height of 1.3 cm (0.5 inch). The oil is allowed to permeate the paper for a duration of 15 seconds. Subsequently, the oil droplet present on the paper is gently wiped off using a clean sponge. If the color of the contact area between the oil droplet and the paper remains unaltered, this indicates that the paper complies with the grease resistance standard. Conversely, the presence of a darkened contact area signifies that the oil has successfully penetrated the paper,

Table 3.4. Components of the OGR test kit and their properties

Grease resistance value	Castor oil (g)	Toluene (mL)	*n*-Heptane (mL)	Surface tension ($N \cdot m^{-1}$)
1	969.0	0	0	0.0345
2	872.1	50	5	0.0327
3	775.2	100	100	0.0293
4	678.3	150	150	0.0254
5	581.4	200	200	0.0250
6	484.5	250	250	0.0241
7	387.6	300	300	0.0232
8	290.7	350	350	0.0228
9	193.8	400	400	0.0225
10	96.9	450	450	0.0225
11	0	500	500	0.0224
12	0	450	550	0.0220

leading to a failure in the test. To ensure accuracy, five independent experiments were conducted, with a maximum variation of less than 0.5 in KIT values across replicates.

3.4.4.3 Water and oil penetration assessment

The water and oil resistance capacity of all LMNP-paper composites and uncoated paper samples was tested using an in-house instrument seen in **Figure 3.5**. A height gauge is affixed to a transparent glass jar and the test liquid is generally filled to a height of 3 cm. When conducting the water/oil penetration test, the paper composite sample is initially positioned with its coated surface facing inward. Subsequently, the glass jar is positioned on an elevated platform, featuring a grid, to enable clear observation of the uncoated (underside) paper surface. Following this setup, the test liquid is applied, and a timer is started to track water or oil penetration over time, as illustrated in **Figure 3.5**. Soybean oil and DI water were used as test liquids.

3.4.4.4 Water and oil retention assessment (ASTM F119-82 method)

The water and oil resistance of the paper composite were evaluated following ASTM F119-82 method [102]. To assess these properties, six drops of the test liquid were applied to a cotton patch with a diameter of 4 cm, placed on top of the paper composite. A 100 g weight was then placed on the cotton patch, with ground glass positioned beneath the composite to detect any potential leakage, as shown in **Figure 3.6**The test was considered a failure if infiltration was observed on the frosted glass, and the time until the first sign of leakage was recorded. The maximum recorded time for this test was set at 100 minutes; any specimen that exceeded this threshold was reported as 100 minutes.

3.4.4.5 Contact angle analysis

Water contact angle (WCA) were performed using a Ramé-hart contact angle goniometer (Model No. 100-25-M, Ramé-hart Instruments Corp., USA) at room temperature. A 4 μL droplet of deionized water was dispensed onto the surface of each specimen, and the dynamic contact angle was recorded over a period of 60

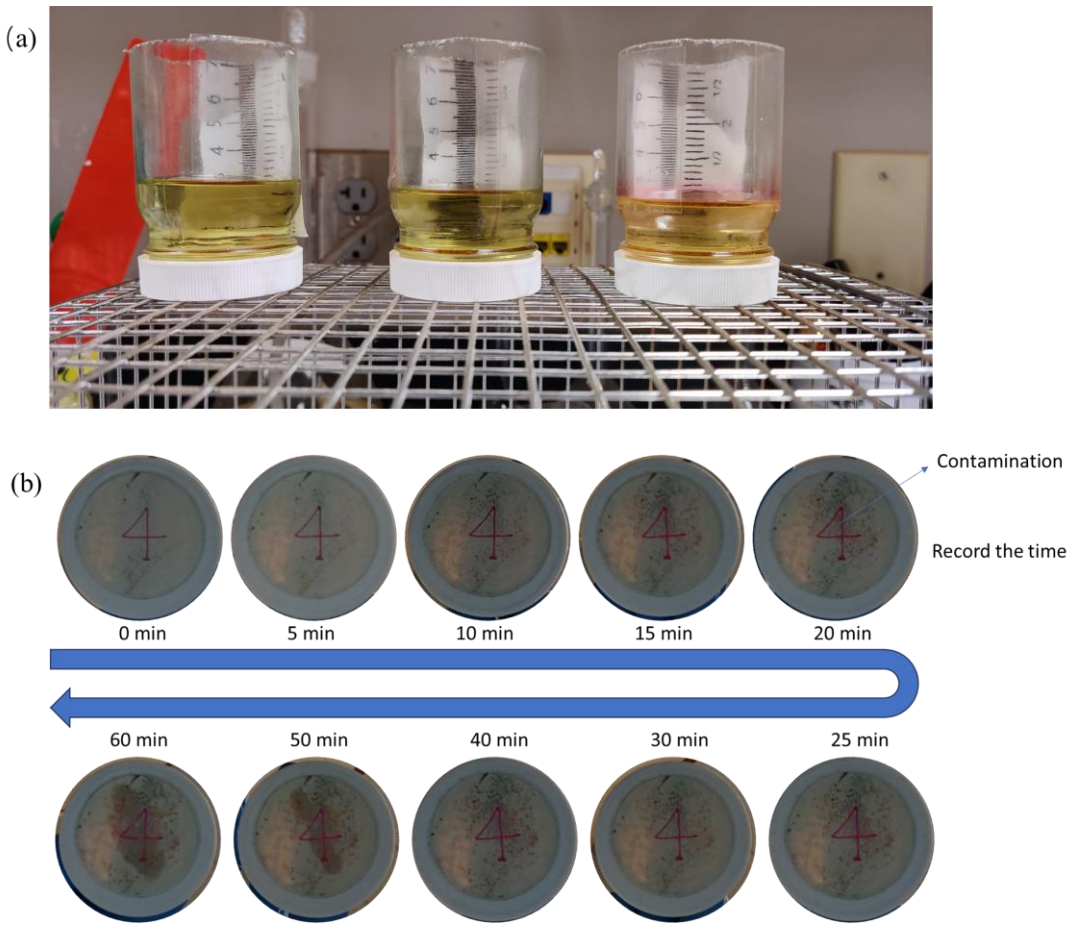

Figure 3.5 (a) Experimental setup for oil and water retention tests, (b) demonstration of sequential assessment of leakage and time monitoring.

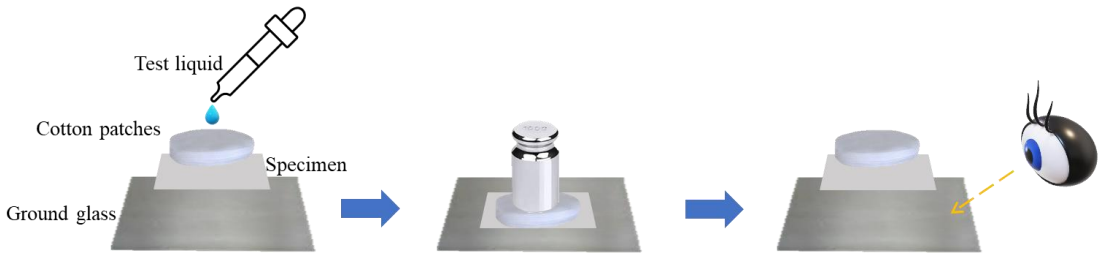

Figure 3.6 Experimental setup for assessing water and oil resistance

seconds. The average WCA values were calculated from measurements taken at five distinct positions on each sample.

3.5 Aerobic soil biodegradation test

Simulated soil degradation experiments were conducted at room temperature following the published methods.[103-105] The LMNP-paper composite C40-P3-T160-M30, was buried 15 cm beneath the soil surface, with soil moisture maintained at 25 wt.% by adding measured amounts of water every 7 days. The condition of the paper composites was visually inspected and documented with photographs at 7-day intervals.

3. 6 Error analysis

Error analysis was conducted by evaluating the physical, chemical, and mechanical properties using three or more replicate measurements. The reported results represent the average values obtained from independent tests. Error bars shown in tables or figures indicate the standard deviation, reflecting the variability of the data relative to the mean.

CHAPTER FOUR : EFFECT OF PROCESSING TEMPERATURE ON NANOLIGNIN QUALITY DURING ULTRAFINE FRICTION GRINDING

A version of this chapter was originally published as:
Zhongjin Zhou, Kalavathy Rajan, Tim Young, Nicole Labbé, Siqun Wang. (2023). Effect of processing temperature on nanolignin quality during ultrafine friction grinding. *Industrial Crops and Products*, 198, 116685.
Author contributions are listed as follows. **Zhongjin Zhou**: Conceptualization, Methodology, Formal analysis, Investigation, Writing-original draft, Writing - Review & Editing. **Siqun Wang**: Conceptualization, Methodology, Formal analysis, Investigation, Writing - Review & Editing, Supervision, Project administration, Funding acquisition. **Kalavathy Rajan**: Investigation, Validation, Review & Editing, Funding acquisition. **Tim Young**: Writing - Review & Editing, Supervision, Funding acquisition. **Nicole Labbé**: Conceptualization, Resources, Writing - Review & Editing, Supervision, Project administration, Funding acquisition.

4.1 Abstract

Nanoparticles are a new frontier to valorize underutilized and abundant lignin generated by biorefineries. Typical chemical processes to synthesize LMNPs use large quantity of organic solvents and therefore, could adversely impact the environment. Hence, we have employed an eco-friendly mechanical approach, *i.e.*, UFG, to produce "green" LMNPs with controlled size and micromorphology. Specifically, we investigated the effect of processing temperature, at 0, 25 and 70 °C, on lignin nanosizing. Our results showed that low temperature (0°C) significantly favored the size reduction of lignin where we achieved a median particle size of ~100 nm after 12 grinding passes. At 70°C, LMNPs reached a size equilibrium of ~160 nm within four passes but did not decrease in size upon subsequent grinding. Moreover, analysis of the LMNPs by SEM showed that samples produced at 0°C mostly had irregular flat shapes with sharp angles, such as stars and polyhedron, with a glabrous surface, whereas samples produced at 25 and 70°C featured spheres and rods with nanoscopic pores on the surface. Physico-chemical properties of LMNPs, such as molecular weight and thermal degradation, did not change significantly compared to the original lignin, however, samples generated at 0°C exhibited significantly fewer inter-unit linkages than those generated at 70°C. Our study thus shows that varying the grinding temperature facilitates the customization of LMNP micromorphology. Furthermore, the proposed method for LMNP manufacturing is simple and eco-friendly and presents a viable approach for lignin valorization.

4.2 Introduction

As the world's most abundant renewable resource, lignocellulosic biomass offers an incredible opportunity to exploit their polymeric constituents, i.e., cellulose, hemicellulose and lignin, for the production of biofuels, biochemicals, and biomaterials [106, 107]. About 150 billion tons of lignin is produced by plants per year on a global scale, and nearly 60 million tons of this lignin is isolated during pulp and paper manufacturing [54, 108]. Lignin represents the main underutilized co-product in the

pulp and paper industry. Due to its complex structure and chemical composition, only about 5% of lignin is currently used to produce value-added products, whereas the rest is combusted for heat generation [109]. Hence using lignin as a feedstock for materials production would valorize a low-value co-product and subsequently improve the economic prospects of the nascent bioeconomy. Ultimately, the development of biomaterials using a renewable resource like lignin would reduce the dependence on fossil fuel feedstocks and promote net-carbon neutrality.

In recent years, converting lignin into value-added products, such as nanomaterials, has been considered an essential strategy to improve the sustainability of lignocellulosic biomass processing [20]. Nanosizing lignin has been reported to enhance its antibacterial [110], antioxidant [107], and UV light absorption properties [111, 112]. Lignin micro- and nano-particles (LMNPs) have been reported to improve the flame retardancy of thermally conductive laminates [26] and the mechanical strength of films used in fireproofing [113]. They could also be used to produce graphene and nanodiamonds under ambient conditions using a pulsed femtosecond laser [61, 114]. Moreover, LMNPs have the potential to form versatile adhesives that could replace phenyl formaldehyde resins in various commercial applications [115]. They are good mechanical strength enhancers due to their significantly smaller size, nucleating capability, and intermolecular hydrogen bond formation, that increases cross linking between polymer matrices [22, 116]. In the near future, lignin may replace traditional, usually petroleum-derived, materials like polyurethane foams [109] because of its renewability and the above-mentioned functional advantages. The synergistic improvement of nanocomposite network structure in the presence of LMNPs forms the basis for developing future biomaterials that exhibit superior functions [117] and a viable strategy to valorize lignin.

There are still technical barriers for developing high-value products from lignin, and so its application has not yet reached the commercialization stage. Therefore, it is essential to develop feasible technologies for lignin processing. In the

case of LMNPs, two manufacturing methods are usually employed [64]; a bottom-up approach using self-assembly [118,119] and a top-down approach using mechanical force. The self-assembly method consumes large quantities of organic solvents, such as methanol, ethanol, tetrahydrofuran, toluene, ethylene glycol, and dimethylformamide [26,68]. While some of these solvents can be recovered, others volatilize in the environment and/or cause health hazards to humans [26]. The top-down approach is advantageous as its employ mechanical means, such as sonication [79], high shear homogenization [70], and ultrafine friction grinding [120,121], which partially or completely avoid the use of toxic and corrosive solvents.

UFG method has been previously used to manufacture 100% cellulose and lignin-containing cellulose nanofibers [74,90]. During UFG, biological materials are comminuted under the compression of grinding stones and collision with abrasive grains to generate ultrafine particles and commonly, the sample slurries are passed several times through the grinding chamber to achieve a desired particle size [74,90]. This technique has also been used to produce LMNP from softwood kraft lignin, but a duration of 4 h was required to achieve a particle size reduction from 500 nm to 22 nm [70]. The energy consumption and time required for LMNP production by UFG could be high and, in some cases, as many as 40 passes may be required to achieve a reasonably small particle size [74,77,122]. Hence, even though it is eco-friendly, these drawbacks of UFG need to be addressed.

One of the main parameters that has been overlooked so far is the temperature of UFG, which could potentially reduce the number of grinding cycles. Temperature affects the transition of a polymer from glassy to rubbery state. At the glass transition temperature (T_g) the aromatic chains of lignin begin to move and create free volume between the molecular chains. The T_g of lignin has been reported to range from 50 to 160 °C depending on the plant species and isolation method [70,123-125]. Because of its heterogenous nature, lignin usually exhibits a broad glass transition domain whose onset may occur as low as 50°C [125]. This means that, without having to reach the T_g,

we could still manipulate the structure of lignin at about 70°C. We also propose that, at low temperatures (0°C) lignin is brittle and will break easily compared to a rubbery state at higher temperatures [126], thus allowing for the particle size to decrease significantly. Overall, we hypothesize that by altering the processing temperature we could affect the glassy and rubbery state of lignin and thus modulate the efficiency of LMNP generation using UFG.

The main goal of this study is to elucidate the effect of three different processing temperatures (0, 25 and 70°C) on the number of grinding passes and the resulting particle size of LMNPs. Physico-chemical characterizations of the lignins samples, before and after UFG, were carried out to determine the impact of processing temperature on LMNP structure and micromorphology. To the best of our knowledge, this is the first study that investigates the impact of UFG temperature on LMNP production. Ultimately, our study provides a critical approach for improving the efficiency of UFG and enhancing the overall sustainability of LMNP production via mechanical means

4.3 Experimental methods

4.3.1 Materials and sample preparation

The kraft softwood lignin and other chemicals used in this chapter such as acetone, dimethyl sulfoxide (DMSO), pyridine, deuterated chloroform, sulfuric acid, and sugars (glucose, xylose, galactose, arabinose, and mannose) used in this study was described in section 3.1, and the preparation of LMNPs is detailed in section 3.2.1.

4.3.2 Characterizations

The chemical composition of lignin is presented in section 3.4.1.1. Fourier-transform infrared (FTIR) spectroscopy analysis is described in Section 3.4.1.2. The gel permeation chromatography (GPC) analysis is provided in section 3.4.1.3, while thermal analysis is discussed in section 3.4.1.4. and morphological analysis is detailed in section 3.4.2.

4.4 Results and discussion

4.4.1 Effect of grinding temperature on LMNPs size

UFG has been previously employed to reduce the size of lignin and other phenolic suspensions [127], which is achieved by massive compression, shearing, and rolling friction forces that cause disintegration of polyaromatic molecules. During UFG, it is a common phenomenon for the feedstock temperature to inherently increase up to 70°C, regardless of the starting temperature, when the mill is not equipped with a heat exchanging system [71]. However, the impact of UFG temperature fluctuations on particle size has not yet been investigated. Therefore, we selected three grinding temperatures, i.e., 0, 25 and 70°C, which were maintained using an external heat exchanger system, and determined their impact on the particle size and morphology of LMNPs.

Since the LMNPs produced by grinding are irregular solids and not typical one- or two- dimensional structures, their size was approximated to a sphere during the dynamic light scattering measurements [91]. The particle size distribution of original lignin is shown in **Figure 4.1 a, b and c**. It should be noted that, because the original lignin's particles were large and settled quickly, the measured particle size distribution was an underestimation of the actual values. The vast majority of particles were larger than 500 nm in size, and there were almost no particles below 300 nm. When verified using SEM, particles with a diameter greater than 20 μm were also detected, as shown in the later sections.

The particle size distributions of LMNPs at different UFG passes when processed at 0°C, 25°C and 70°C are shown in **Figure 4.1**, respectively. Each experiment was repeated three times and the error in particle size estimation was within acceptable limits, as indicated by the shading in **Figure 4.1**. At 0°C, the particle size distribution migrated steadily towards smaller sizes as the number of grinding passes increased. However, this trend did not apply for the processing temperatures of 25°C and 70°C. At 25°C, the initial lignin suspensions displayed a

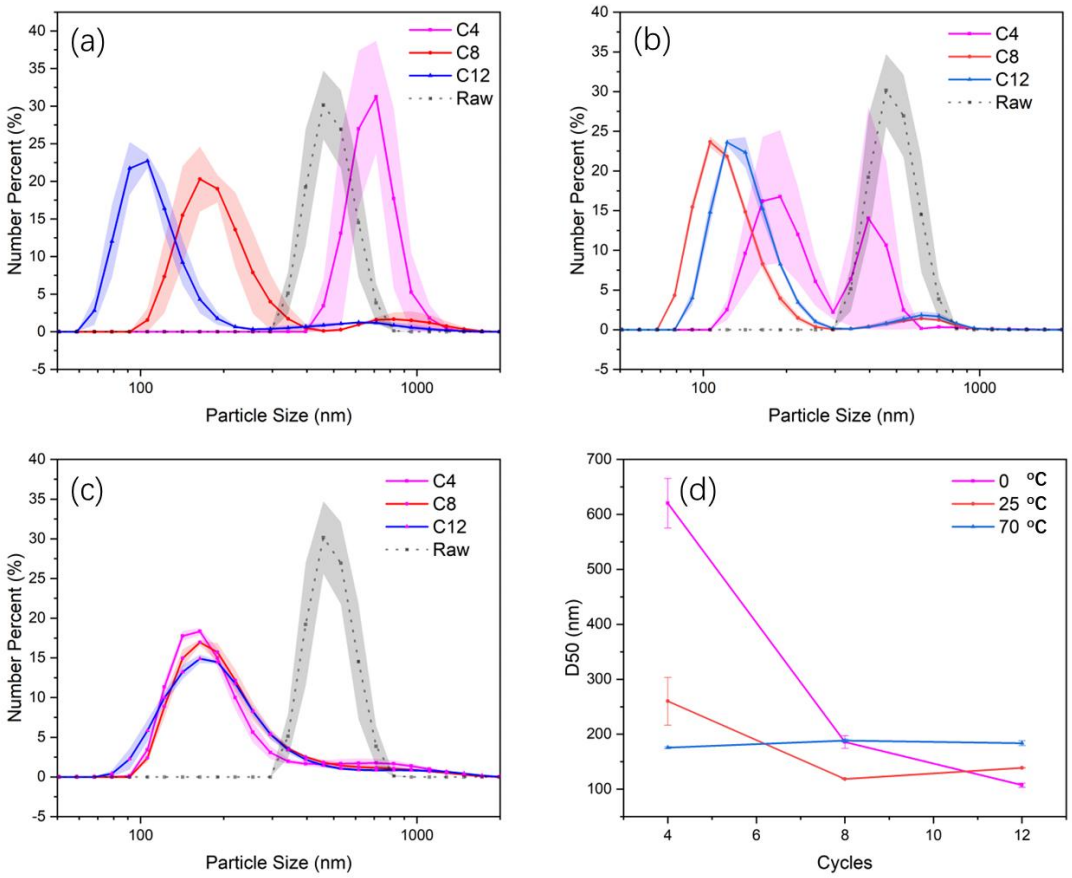

Figure 4.1 Average particle size distribution of the original (raw) lignin and LMNPs (lignin micro- and nanoparticles) obtained at the 4th, 8th, and 12th grinding passes (represented as C4, C8, and C12, respectively) at a processing temperature of (a) 0°C, (b) 25°C and (c) 70°C. Standard deviations for size distribution are represented as shaded regions; (d) relationship between D50 and the number of grinding passes at different processing temperatures.

bimodal distribution which converged to become unimodal during the 8th and 12th UFG passes and displayed only a minor decrease in particle size distribution. At 70°C, there was no significant difference between the particle size distribution of LMNPs at the 4th, 8th, and 12th UFG passes.

Two clear and highly valuable patterns emerge as we analyze the LMNP properties. At a processing temperature of 0°C, the D50 value (diameter of particles at 50% of number accumulation) decreases as the number of grinding passes increases (**Figure 4.1d**). Since the other processing conditions, namely disk gap and lignin concentration, were kept constant we can conclude that low temperature favored a significant and continuous reduction in lignin particle size. This could be explained by the mechanism of particle crushing [128, 129], which propounds that polymers are rigid at low temperatures and are therefore easily broken into tiny particles with sharp angles under pressure and friction. The second observation is that, at 25°C and above, fewer grinding passes are sufficient for the end particle size to reach an equilibrium. Moreover, at high processing temperature of 70°C, only four cycles are needed to reach size equilibrium. This is due to the increase in elasticity of lignin with increasing temperature [130], which in turn decreases the strength of particle fracture and allows for a fewer grinding cycles to achieve nanosizing. Moreover, when processing at 70°C, we did not observe a decrease in particle size at the 8th or 12th passes when compared to the 4th pass (**Figure 4.1d**). This could be because of a combination of re-agglomeration of finer particles as well as the conservation of lignin inter-unit linkages, as discussed in the following SEM and NMR analysis sections.

4.4.2 Stability of LMNP suspensions

Zeta-potential is used to characterize the surface charge carried by particles which determined the interaction between the particles and subsequent stability of the colloidal system. A high absolute value of zeta-potential means that Coulombic repulsion will prevent particle aggregation, and a colloidal system having greater than

30 mV absolute zeta-potential is considered to be stable [68, 131]. Since lignin naturally has many hydroxyl groups as well as displays the potential to adsorb negative hydroxide ions on its hydrophobic surface, it generally carries a negative charge [93]. In this study, the zeta-potential values of all lignin samples (original lignin and LMNPs) were negative, and the absolute values were greater than 20 mv, which is similar to previous reports about LMNPs produced using anti-solvent precipitation techniques [132]. As seen in **Figure 4.2a**, amongst the LMNPs, samples produced at 0°C possessed the highest absolute zeta-potential of 37.5 mV whereas those produced at 70°C possessed the lowest absolute zeta-potential of 27.4 mV. A Pearson correlation analysis showed that the particle size and zeta-potential had a correlation coefficient of 0.98, at a confidence interval of 95%, demonstrating that the particle size had a significant effect on LMNP's zeta-potential. In case of LMNPs produced at 70°C, the D50 value was high even after 12 grinding passes (**Figure 4.2d**), and as shown in the following section, there was also a minor aggregation of nanoparticles. Thus, an increase in particle size could explain the decrease in absolute zeta-potential of LMNPs produced at room or higher temperatures. In case of the original lignin, the high absolute zeta-potential (35.8 mV) was not a true representation of the system since larger particles precipitated during measurement and were unaccounted for. Despite having a seemingly lower absolute zeta-potential, the LMNPs produced at 25 and 70°C were still stable after 90 days of storage (**Figure 4.3**). Their absolute zeta-potential also did not change significantly over time (**Figure 4.2b**). Previous studies have shown that lignin nanoparticles produced via anti-solvent precipitation, and having an average particle size of 200 to 340 nm, were stable for 30 to 60 days [133, 134]. Based on our study results, it could be concluded that, significantly decreasing the particle size of lignin ($\leq$ 200 nm) using UFG will increase the negative potential and stability of the resulting LMNP suspensions.

4.4.3 Effect of grinding temperature on LMNPs' micromorphology

SEM imaging (**Figure 4.4**) confirmed the size reduction of lignin from dozens

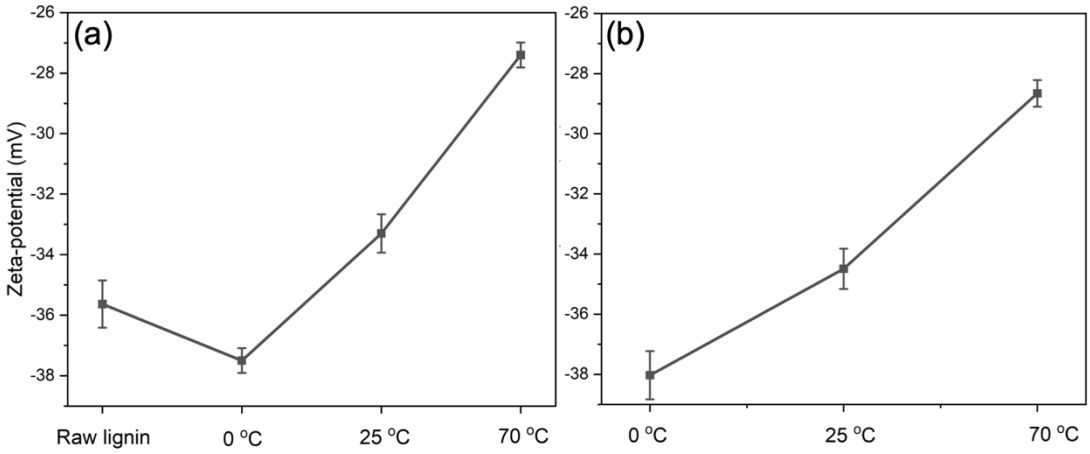

Figure 4.2 (a) Zeta-potential of the original (raw) lignin and that of the LMNPs produced after 12 grinding passes at the temperatures of 0, 25 and 70°C; (b) Zeta-potential of the same LMNPs after 90 days of storage at 4°C.

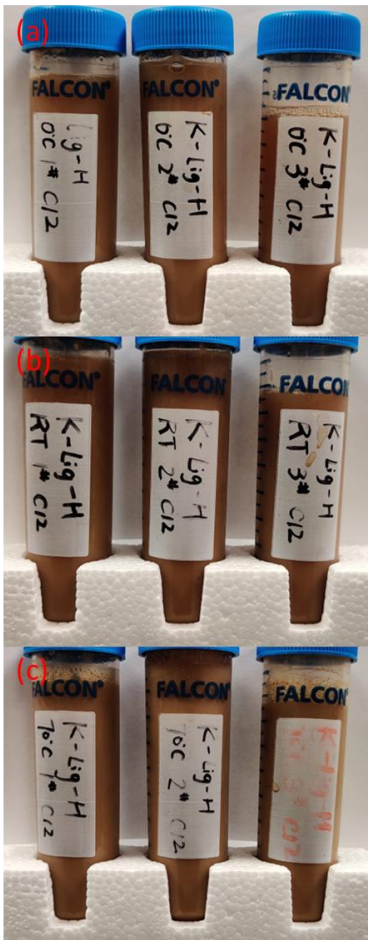

Figure 4.3. Photographs of LMNP suspensions after 90 days of incubation at 4°C, prepared by 12 UFG (ultrafine friction grinding) passes at (a) 0°C, (b) 25°C and (c) 70°C.

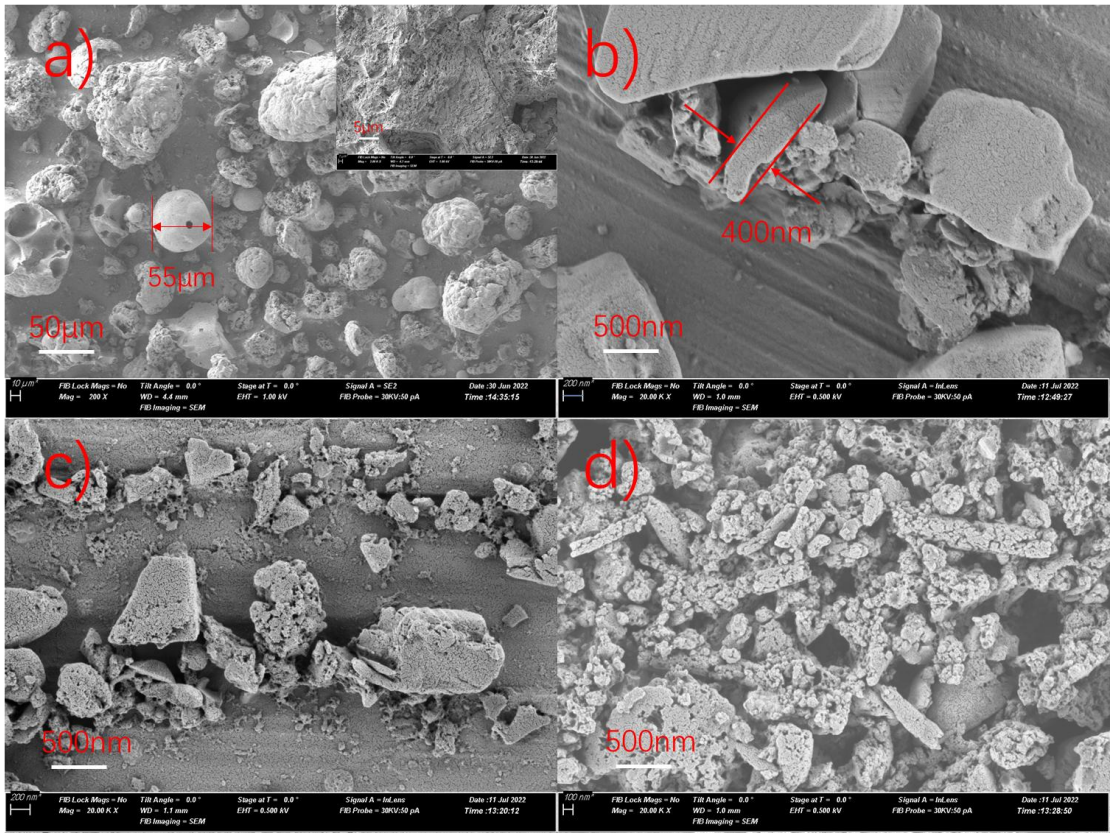

Figure 4.4 SEM images at 20K magnification of (a) original lignin and LMNPs (lignin micro- and nanoparticles) produced after 12 grinding passes at (b) 0℃, (c) 25℃, and (d) 70℃.

of micrometers to hundreds of nanometers after 12 UFG passes. Although the size of lignin decreased at all processing temperatures, the micromorphology of LMNPs was significantly different. Samples processed at 0℃ were dominated by irregular shapes such as polyhedrons and plates with sharp angles and smooth surfaces. On the other hand, the 25℃-treatment group had both cubic and spherical particles, with some pores occurring on the surface. Finally, the 70℃-treatment group was dominated by highly porous spheres and rods. A closer look revealed that several small particles aggregated into bigger structures at 70℃, which is in accordance with the corresponding zeta-potential characterization.

Surface changes may occur due to the interaction of lignin particles with the grinding disks in the local thermal environment. In previous studies it was shown that lignin's micromorphology changed under high temperature conditions and that it could become soft and flowable [135, 136]. It is therefore reasonable to postulate that at lower temperatures the lignin is more brittle leading to the formation of sharply angled LMNPs. As the temperature approached the onset of T_g the newly formed interfaces of LMNPs became softer and after natural cooling these LMNPs formed a low surface free energy structure such as spheres. Surface features of lignin particles are important for many applications, like for example in the formation of films on the surface of other materials [137, 138]. Fortunately, a simple method for controlling the surface morphology of LMNPs has been devised in this study.

4.4.4 Changes in thermal properties of LMNPs

To compare the properties of lignin before and after UFG, we analyzed physicochemical properties such as molecular weight, thermal degradation, T_g, and chemical bonding. **Figure 4.5a** shows the results of TGA where a small mass loss can be observed in the shaded region for all the samples at temperatures below 105ºC, which can be attributed to the evaporation of moisture. The UFG temperatures did not lead to a shift in the derivative thermogram peaks, as seen in **Figure 4.5b**. The maximum thermal decomposition temperature (T_{max}) of the original lignin was 338℃,

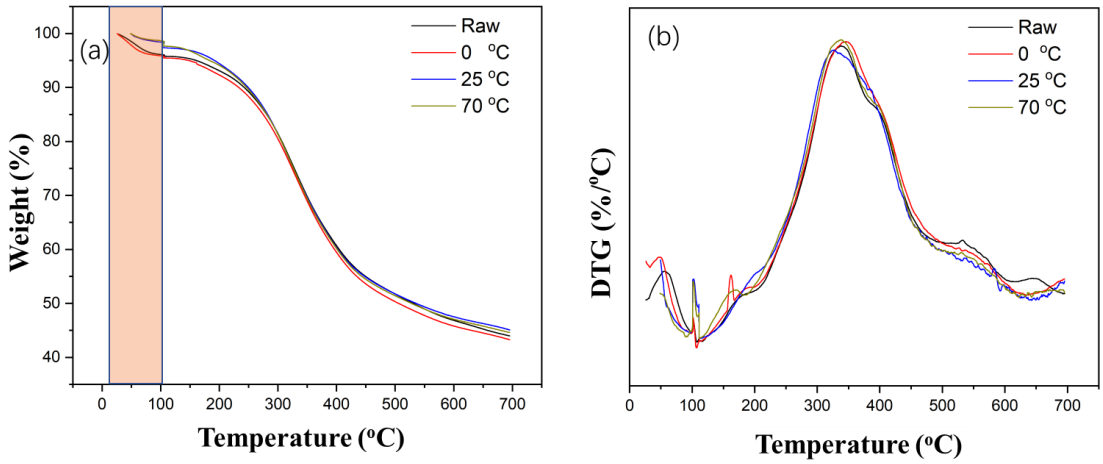

Figure 4.5 (a) TGA curves and (b) first derivative thermograms (DTG) of the original (raw) lignin and LMNPs (lignin micro- and nanoparticles) generated after 12 grinding passes at different processing temperatures (i.e., 0, 25 and 70°C).

whereas for the LMNPs it ranged from 327 to 345°C (**Table 4.1**). This indicates that the processing temperature also did not affect the thermal stability of resulting LMNPs. The heat flow curves of the original lignin and LMNPs are provided in **Figure 4.6**, and the T_g of all samples occurred between 155 and 160°C (**Table 4.1**). The T_g of LMNPs were also not affected by the processing temperature. Interestingly, the T_g of original lignin was marginally (2-3%) lower than the LMNPs, which could be because the LMNPs underwent some chemical changes that decreased their mobile structural linkages (C-O, C-O-C) as explained in the FTIR and NMR sections below. lignin and LMNPs were measured by GPC and provided in **Table 4.1**. All LMNP treatments presented lower M_w values compared to the original lignin and followed a trend of 70°C ~ 25°C < 0°C < unprocessed lignin. Although these results suggest that kraft lignin may undergo depolymerization at room or higher processing temperatures, these differences are minor when compared to a previous publication where ultrasonic irradiation was shown to cause almost 3-fold decrease in molecular weight of wheat straw lignin [79]. Moreover, the polydispersity values of the LMNP samples were lower than the original lignin, indicating a narrowing of molecular weight distribution. These observations support the dynamic light scattering results where 12 grinding passes imparted particle size reduction and an increase in uniformity. The average molecular weight (M_w) and polydispersity index (M_w/M_n) of original

4.4.5 Changes in chemical properties of LMNPs

The FTIR spectra (**Figure 4.7**) of original lignin and different LMNP treatments were processed using principal component analysis (PCA) [139] to probe changes in chemical structure. The PCA scores plot (**Figure 4.8a**) shows a clear separation between the starting material and the LMNPs by PC1 which accounts for 97% of the total variance. Additionally, the LMNPs separate along PC2 with accounts for 2% of the variance. The loadings of PC1 (**Figure 4.8b**), which documents the major FTIR bands responsible for the separation between original lignin and LMNPs,

Table 4.1 Physico-chemical properties of softwood kraft lignin before and after ultrafine friction grinding

	Original lignin	LMNPs* Processing Temperature		
		0°C	**25°C**	**70°C**
T_{max}† (°C)	338	345	327	339
T_g‡ (°C)	155	161	159	160
M_w[f] (g/mol)	2888	2340	2067	2046
M_w/M_n[f]	1.4	1.2	1.2	1.2

*LMNPs – Lignin micro- and nano-particles produced from 12 grinding passes;
†Maximum degradation temperature obtained from first derivative thermograms;
‡Glass transition temperature obtained from differential scanning calorimetry;
[f]Weight average molecular weight and molar mass dispersity measured using gel permeation chromatography.

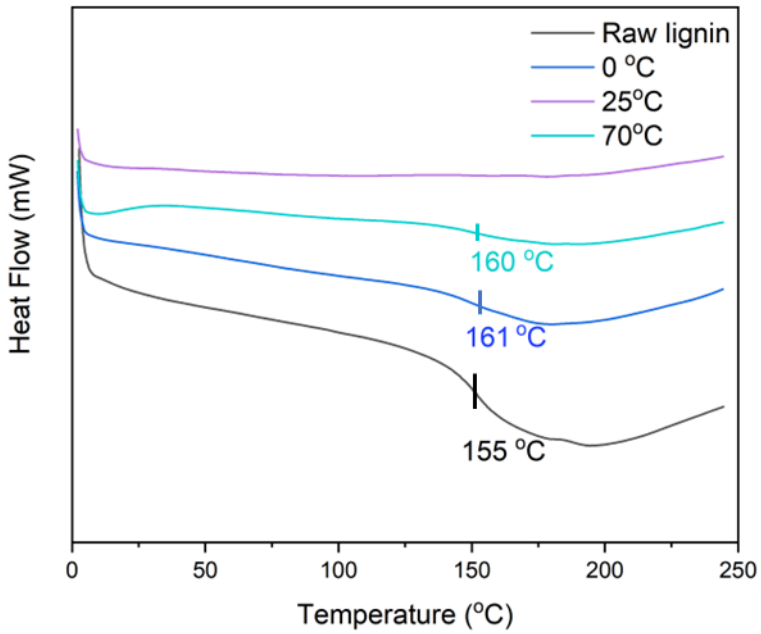

Figure 4.6 Heat flow curves of original kraft lignin and LMNPs obtained under N_2 atmosphere at 20°C/min using differential scanning calorimeter.

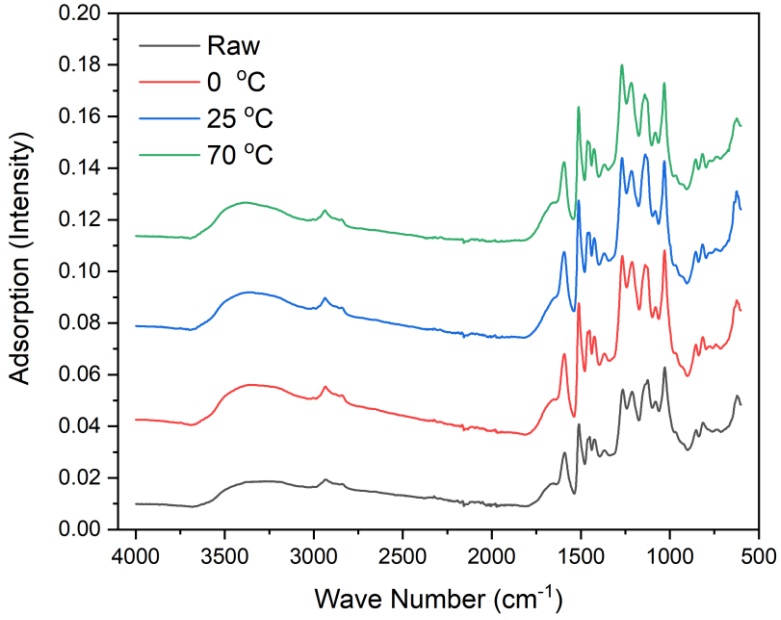

Figure 4.7. Complete FTIR spectra of original kraft lignin and LMNPs manufactured at different UFG temperatures.

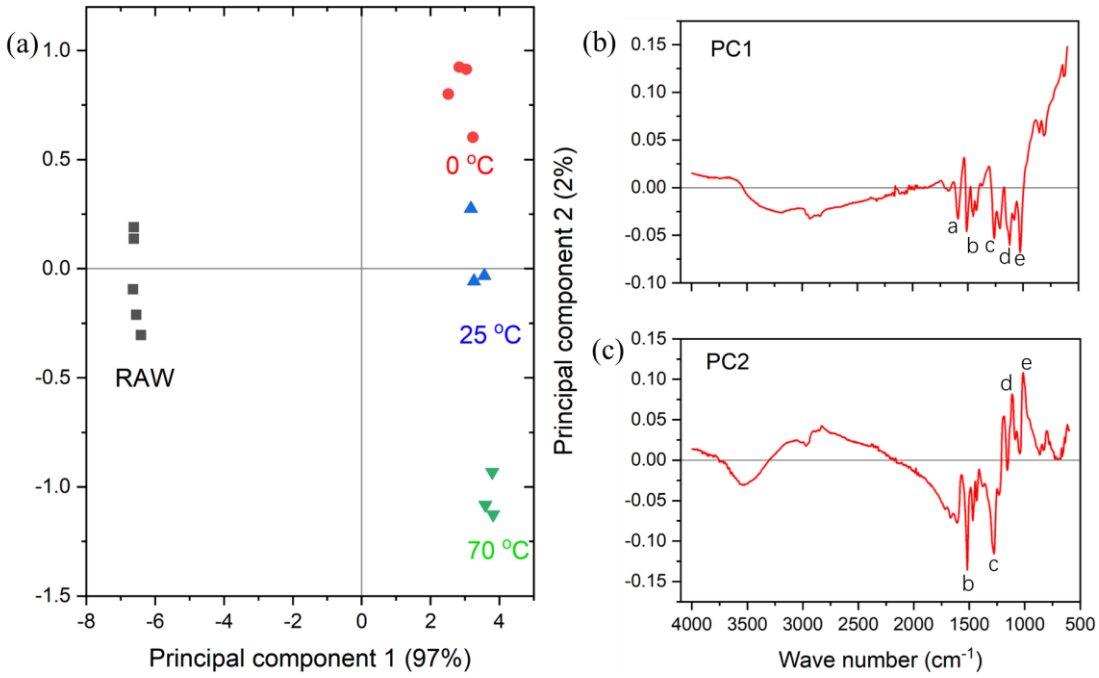

Figure 4.8 (a) Scores plot of the principal component analysis (PCA) of the FTIR spectra of original (raw) lignin and LMNPs produced via ultrafine friction grinding at 0°C, 25°C and 70°C; (b) Loadings plot of principal component 1 (PC1), which accounts for 97% of the data variance; (c) Loadings plot of PC2, which accounts for 2% of the data variance (Peak legend: a – 1591 cm^{-1}; b – 1511 cm^{-1}; c – 1263 cm^{-1}; d – 1123 cm^{-1}; c – 1027 cm^{-1}).

shows that the LMNPs have a significantly lower number of aromatic skeletal vibrations (at 1591 cm^{-1} and 1511 cm^{-1}), C–O in phenolic OH groups (1263 cm^{-1}), deformation of aryl C–H bonds (1123 cm^{-1}), and unconjugated C–O vibrations in guaiacyl groups (1027 cm^{-1}), when compared to the starting lignin [140]. These can be attributed to the breakage of lignin framework during UFG, which is also substantiated by NMR results as discussed below. Additionally, the PC2 loadings plot (**Figure 4.8c**) indicates that the LMNPs obtained at 70°C displayed higher skeletal vibrations of aromatic ring (1511 cm^{-1}) and C–O vibrations in phenolic OH groups (1263 cm^{-1}) than those produced at 0°C. As illustrated by the low contribution to the variance of the data (2%), this difference between the LMNPs is relatively minor.

Analysis using 2D-HSQC NMR showed that the original lignin's spectrum is typical to that of softwood kraft lignin with enrichment in guaiacyl groups and presence of other condensed and oxidized substructures as a result of the kraft pulping process. The cross-peak ($^{13}C/^{1}H$) assignments, and the side chain and aromatic regions of the 2D-HSQC NMR spectra are provided in **Table 4.2** and **Figure 4.9**, respectively. Semi-quantitative estimation of the inter-unit and terminal linkages, as well as aromatic substructures, showed that the processing temperature had significant effects on kraft lignin's chemical structure. As seen in **Table 4.3**, UFG caused a significant decrease in kraft lignin's inter-unit (ether) linkages, especially at 0°C. Loss of β–5 and β–β linkages, as a result of the lignin fractionation method, was reported to cause a significant decrease in the corresponding nanolignin's z-average particle size [141]. These losses were also proposed to cause an increase in aromatic density and loss of mobility [119], which in turn may explain the brittle behavior of lignin at 0°C and the significant reduction in LMNP particle size after 12 grinding passes. On the other hand, the inter-unit linkages and γ-esterified cinnamyl alcohol type lignin carbohydrate complexes (LCCs) were mostly preserved in LMNPs produced at 70°C. In previous reports[119], higher amounts of β-O-4 linkages were proposed to increase intramolecular π-π stacking and subsequently cause a significant reduction in

Table 4.2. Cross-peak assignments for 2D-HSQC NMR spectra of original kraft lignin and lignin micro- and nanoparticles (LMNPs)

Substructures	Chemical shift δC/δH (ppm)*	
	Original lignin	**LMNPs**
Side-chain region		
C_β-H_β in phenylcoumaran (B_β)	53.5/3.5	-
C_β-H_β in resinol (C_β)	53.6/3.05	53.5/3.06
C-H in methoxyl	55.4/3.74	55.6/3.76
C_γ-H_γ in β-O-4 (A_γ)	59.8-60.1/3.25-3.59	59.8-60.1/3.4 and 3.7
Cγ–Hγ in cinnamyl alcohol end-groups (Iγ)	61.48/4.08	-
Cγ −Hγ in γ-acylated β−O−4′ (Aγ′)	62.8/3.77-4.26	62.8/3.77-4.26
Cγ–Hγ in phenylcoumaran (Bγ)	62.4-63.4/3.3-3.46	-
γ-esterified cinnamyl alcohol groups in lignin carbohydrate complex (LCCγ)	-	66.6/4.2 and 67.5/4.5
α-ether-type lignin carbohydrate complex (LCCα)	-	67.9/3.6
Cα −Hα in β−O−4 (Aα)	71/4.75	-
Cγ-Hγ in resinol (Cγ)	71.65/3.91 and 4.19	-
C_β–H_β in β–O–4′ (A_β) linked to a G unit	84.3/4.28	-
Cα–Hα in resinol (Cα)	84.8/4.65	-
Aromatic region		
C_2–H_2 in guaiacyl (G_2)	109.5-110.5/6.97-7.13	
C_2–H_2 in α-oxidized guaiacyl units (G_2')	110.6/7.38	110.6/7.38
$C_{3,5}$–$H_{3,5}$ in *p*-hydroxyphenyl ($H_{3,5}$)	112.2/6.7	112.2/6.7
C_5–H_5 in guaiacyl (G_5)	115.4/6.74	115.4/6.74
C_6–H_6 in guaiacyl (G_6)	118.6-119.6/6.7-6.9	
γ-esterified cinnamyl alcohol in LCC (Iγ)	119.9-121.1/6.5-6.6	119.9-121.1/6.5-6.6 and 118.0/5.2
Stilbene in β-5 (SB_β)	119.9/7.2	-
$C_{2,6}$–$H_{2,6}$ in *p*-hydroxyphenyl ($H_{2,6}$)	126.0/7.4	-
Stilbene in β-1 (SBα)	125.6/6.97 or 7.6	-

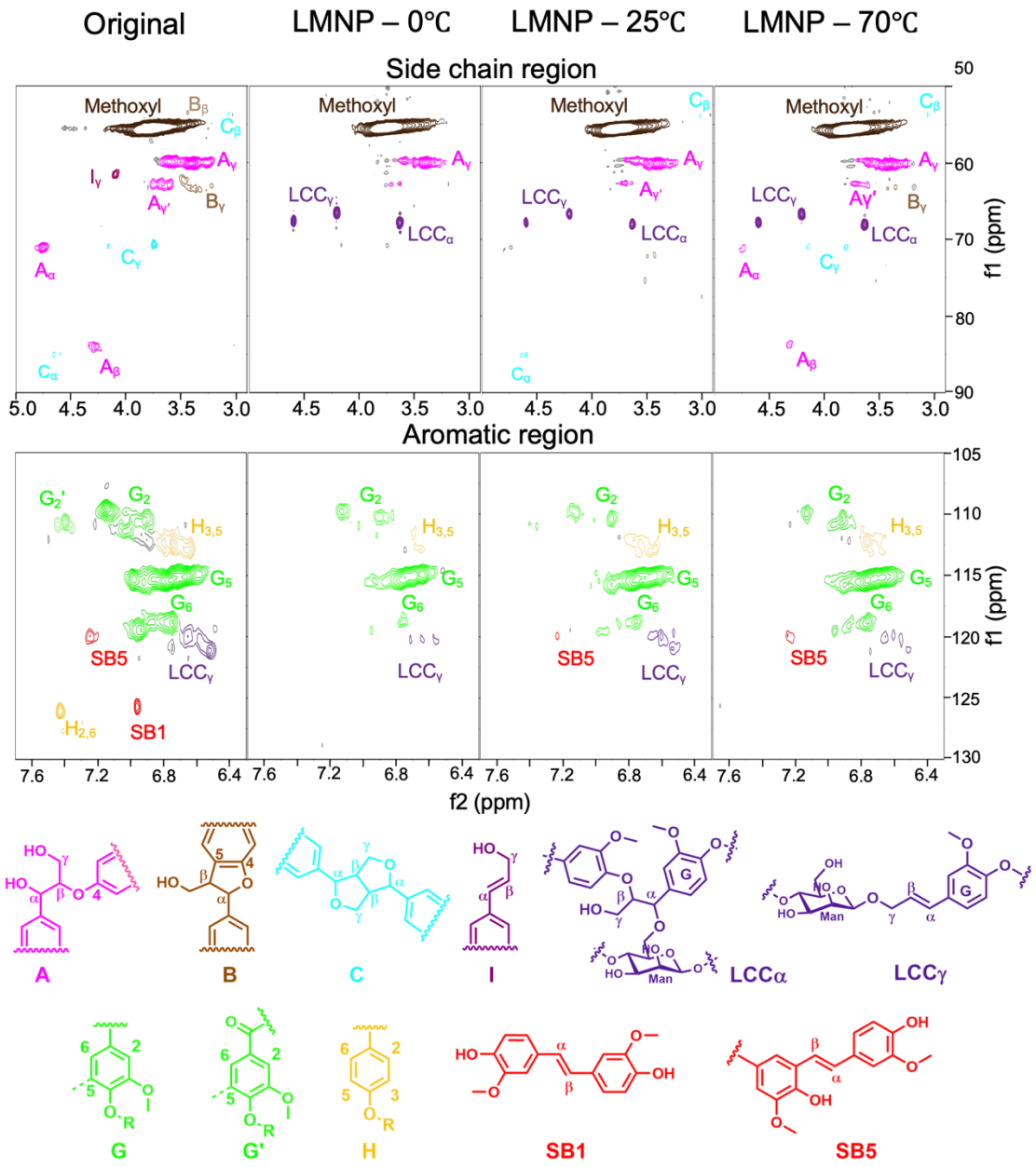

Figure 4.9. 2D-HSQC NMR spectra of original kraft lignin and LMNPs manufactured at different UFG temperatures.

Table 4.3 Semi-quantitative estimation of inter-unit and aromatic substructures in original lignin and LMNPs (lignin micro- and nanoparticle) using 2D-HSQC NMR analysis.

Substructure	Original lignin	LMNP*		
		0°C	25°C	70°C
Aryl ether (β-O-4) †	1.82	1.41	1.70	1.98
Phenylcoumaran (β-5) †	0.39	0.00	0.06	0.38
Resinol (β-β') †	0.13	0.00	0.09	0.28
Total ether side chains†	2.34	1.41	1.85	2.64
γ-esterified cinnamyl alcohol type lignin carbohydrate complexes (LCCγ)	0.37	0.25	0.33	0.46
α-ether type lignin carbohydrate complexes (LCCα)†	0.00	1.12	0.81	0.53
Guaiacyl (G)	2.93	1.40	2.11	2.41
p-hydroxyphenyl (H)	0.30	0.06	0.19	0.20
Stilbenes ($SB_{1,5}$)	0.05	0.00	0.01	0.04

†The number of inter-unit linkages are expressed as $\frac{\int X}{\int G_2} \times 100$; The H and SB integral values are obtained by dividing the cross-peak intensities by 2; *LMNPs generated after 12 ultrafine friction grinding passes were tested.

nanolignin particle size. In this study, during UFG at 70°C, conservation of β-O-4 and cinnamyl alcohol-type ester linkages may have led to a similar intramolecular π-π stacking phenomenon and facilitated a rapid decrease in lignin particle size within 4 grinding passes. However, preservation of inter-unit linkages may also have prevented further particle size reduction of LMNPs between 4 and 12 grinding passes.

Other than these processing temperature-dependent changes, all LMNPs exhibited new α-ether type LCC units (**Table 4.3**, **Figure 4.9**). They also displayed decreases in the *p*-hydroxyphenyl units (33 to 80%) and guaiacyl units (18 to 53%), which commonly denotes depolymerization due to harsh processing conditions [142, 143]. This decrease in aromatic substructures and appearance of new α-ether type linkages indicates that UFG, under higher pressure and friction, causes minor depolymerization and recondensation in softwood kraft lignin. In future, computational chemistry tools could be used to predict the changes in LMNP shape as a result of changes in terminal and inter-unit linkages [144].

4.5 Conclusion

This research demonstrated that controlled processing temperature could be used to tune the size and micromorphology of LMNPs during UFG. At low temperatures lignin underwent significant reduction in particle size with increasing number of grinding passes. This could be because there was a significant reduction in inter-unit linkages and aromatic substructures. After 12 grinding passes, at 0°C, a median particle size of ~100 nm was achievable and the corresponding LMNP suspensions were less likely to agglomerate (based on a zeta-potential of -37.5 mV). At higher temperatures (70°C) we obtained comparatively larger LMNPs (~160 nm), however, significantly fewer grinding cycles (4) were needed to reach an equilibrium particle size. Moreover, the micromorphology of the lignin particles was affected by the processing temperature. At 0°C, irregular plate-like structures with sharp angles were predominant, whereas at 70°C, spherical and rod-like structures were predominant. Since this is a mechanical treatment, we did not observe significant

changes in the molecular weight, Tg, or thermal degradation properties of lignin. Thus, our study shows that it is possible to obtain nano-sized lignin particles (150 to 200 nm) with controlled micromorphology, even within 4 UFG cycles, by increasing the processing temperature (25-70°C). Future research will investigate the energy consumption and technoeconomic requirements of LMNP production using high- and low-temperature UFG, such that a sustainable and eco-friendly method can be developed for valorizing lignin.

CHAPTER FIVE : SIGNIFICANTLY REDUCING ENERGY CONSUMPTION DURING NANOLIGNIN PRODUCTION VIA HIGH-SOLID CONTENT GRINDING

A version of this chapter was originally published as:
Zhongjin Zhou, Kalavathy Rajan, Nicole Labbé, Siqun Wang. (2024). Significantly reducing energy consumption during nanolignin production via high-solid content grinding. *Industrial Crops and Products*, 211, 118209.
Author contributions are listed as follows. **Zhongjin Zhou**: Conceptualization, Methodology, Formal analysis, Investigation, Writing-original draft, Writing - Review & Editing. **Siqun Wang**: Conceptualization, Methodology, Formal analysis, Investigation, Review & Editing, Supervision, Project administration, Funding acquisition. **Kalavathy Rajan**: Investigation, Validation, Review & Editing. **Nicole Labbé**: Conceptualization, Resources, Review & Editing, Funding acquisition.

5.1 Abstract

The production of LMNP has garnered significant attention in recent decades, particularly due to its emerging industrial applications. In the context of particle size reduction during UFG, energy consumption refers to the amount of energy required to break down or reduce the size of particles to a desired level. This energy is an important parameter to consider in industrial processes, as it can have significant economic and environmental implications. High energy consumption can lead to increased operating costs and may also contribute to environmental concerns, especially if the energy source is non-renewable. However, traditional UFG, used for the production of nanolignin production, usually performs at low solid concentrations of 1-2 wt. %, resulting in high energy consumption and water usage. Achieving such fine particle sizes often requires high-energy input, and the efficiency of the grinding process is closely related to the energy consumption. In this study, we investigated the energy efficiency and particle size reduction of lignin at four different concentrations (1, 20, 30 and 40 wt. %) during UFG. Our results show that the 20 wt. % solid loading has the best energy efficiency for achieving the same lignin particle size (~150 nm) as the 1wt. % loading; total energy consumption was reduced from ~30 kWh per kg LMNPs at 1wt.% solid loading to 3.1 kWh per kg of LMNPs at 20 wt.% loading. Despite the increased number of grinding cycles, higher concentrations required lower amount of energy per kg of LMNPs produced. The results suggest that when the concentration of lignin particles exceeded 20 wt.%, they tended to overlap, resulting in less effective size reduction during UFG. This study's significance lies in discovering concentration limits for grinding, and improving water and energy use efficiency, such that UFG could emerge as a feasible mechanical treatment and an asset for the industrialization of LMNP.

5.2 Introduction

The production of LMNP has gained significant attention in recent decades, as highlighted in recent literature.[22, 27, 64, 65, 145] Lignin has a wide range of applications,

with its final use determined by its state, particularly the particle size and morphology. With the development of advanced technologies, nanoengineering is becoming increasingly affordable, making it a more viable option for manufacturing LMNPs.[65] LMNPs' nano size allows for more uniform blending with other materials[146], since their large surface area and particle surface charge enable them to form Van der Waals and hydrogen bonds.[20] As an environmentally friendly and renewable material[147], lignin is used in various fields, including heavy metallic ion adsorption[148], oil recovery[149], emulsions[150], antioxidants[151], UV protection[152], pesticides delivery[153], activated carbon production[154], electrode materials[155], polymer composites[156] and even nano diamond[114]. Consequently, the development of an easy and cost-effective method for producing LMNPs will open new opportunities for lignin's use.

The primary constituents of lignin include coniferyl alcohol, sinapyl alcohol, and p-coumaryl alcohol, derived from the phenylpropanoid pathway[107]. Variations in monolignol proportions and types across different plant species contribute to the diverse forms of lignin. The challenges associated with extracting lignin from the lignocellulosic matrix arise from its intricate structure, chemical and thermal stability, heterogeneity, covalent linkages, solubility obstacles, and the risk of losing its structural integrity.[25, 75, 157] Ongoing endeavors focus on developing efficient and environmentally sustainable methods for lignin extraction.

The extraction of LMNPs from wood without the addition of solvents presents a formidable challenge due to lignin's inherent insolubility and the necessity to dismantle its complex structure. Nonetheless, researchers have explored various solvent-free methods to address this challenge. One such approach involves mechanical treatment coupled with enzymatic or chemical pretreatments.[65] The overall process encompasses mechanical treatments such as ball milling[158] or grinding and high-pressure homogenization.[26, 88] These methods subject wood or lignocellulosic biomass to intense mechanical forces, leading to the breakdown of plant cell walls and facilitating the release of lignin nanoparticles. Enzymatic

treatment, utilizing enzymes like cellulases, aids in breaking down cellulose and hemicellulose components, leaving lignin nanoparticles behind.[159] Following mechanical and/or enzymatic/chemical treatments, the resulting mixture typically undergoes fractionation and separation techniques to isolate lignin nanoparticles from other biomass components. However, these methods are not widely adopted in practical applications due to their intricate procedural nature. More commonly, LMNP synthesis relies on obtaining them directly from commercial lignin, a byproduct of industries such as the pulp and paper industry.

There are two main methods for preparing LMNPs from raw lignin: bottom-up and top-down. Bottom-up methods involve the production of LMNPs from a molecular level by changing solvents or adjusting the pH, causing lignin particles to precipitate from the solution.[160] Although the solvent exchanging method often yields lignin particles in sphere shape, it typically requires a high consumption of organic solvents, including toxic ones, which can be a concern.[22, 161, 162] Top-down methods involve the preparation of LMNPs from macro particles using techniques such as grinding[71], ultrasonication[79], microwave treatment, and others[163]. Whether employing a top-down or bottom-up approach, both entail substantial water consumption, typically amounting to 50 times the net lignin weight during LMNP production.[78] Reducing water usage often leads to less wastewater generation during the preparation process. Also, by optimizing water usage, manufacturers can lower their operational costs associated with water procurement, treatment, and disposal. Lower water consumption helps to maintain the ecological balance and protects aquatic habitats, as well as overall biodiversity. However, among existing low-water consuming techniques, ultrasonication and microwave treatments are highly energy-sensitive and can result in significant temperature increases, which can be detrimental to the LMNP manufacturing process.[79] On the other hand, grinding, which can continuously process materials, offers advantages in terms of energy consumption and large-scale processing compared to the aforementioned methods. Hence, reducing water usage in

techniques like grinding would pave the way for sustainable LMNP production.

To industrially scale up mechanical manufacturing of LMNPs, the energy consumption must be low enough to be competitive with other nano materials. Although the yield of LMNPs has been greatly enhanced, there is still room for improvement in terms of unit energy consumption. Many mechanical methods, such as gas-driven shearing and high-pressure homogenization, use high shear delamination to break down plant material into small particles. It is pertinent to note that the energy consumption associated with these methods is not readily comparable due to the diverse sources of lignin. Lignin, being a complex plant-derived material, undergoes intricate extraction, separation, and nanonization processes. This complexity renders direct comparisons of energy consumption challenging, especially when considering lignin derived from different sources. While these methods exhibit suitability for scaling up LMNP production, it is crucial to highlight that their energy efficiency has not been fully optimized. Further efforts are wanted to enhance the energy efficiency of these processes for more sustainable and scalable LMNP production. Many mechanical methods, such as gas-driven shearing and high-pressure homogenization, use high-shear delamination to break down plant material into small particles. These methods are suitable for scaling up LMNP production but have yet to achieve optimal energy efficiency. Except for the twin-screw extrusion process, which employs $\leq 30\%$ solids concentration[80], most mechanical methods typically use a low solids concentration of $\leq 5\%$.[28, 64, 81-83] This not only leads to higher energy consumption per unit weight of dry lignin, but also adversely affects water usage, and the subsequent transport, drying, storage, separation, and utilization of LMNP.

This current research aims to develop a UFG method that performs at high concentration of lignin suspension to address the challenges of producing LMNPs at reduced water usage and improved energy efficiency. We hypothesize that the particle size of LMNPs has a non-linear relationship with the lignin concentration under the same processing conditions, such as grinding cycles and temperature. Specifically, the

median particle size increases slowly at first with increasing lignin concentration and then increases significantly as the concentration continues to rise. By identifying the optimal working interval that balances the particle size requirements and production efficiency, we can produce high-quality LMNPs while minimizing energy consumption. The main contribution of this work was the quantification of the energy required to achieve LMNPs of the same particle size at different concentrations and the investigation of the effect of concentration on the morphology of LMNPs.

5.3 Experimental methods

5.3.1 Materials and sample preparation

The kraft softwood lignin used in this study is described in Section 3.1, and the preparation of LMNPs is detailed in Section 3.2.1.

5.3.2 Characterizations

Fourier-transform infrared (FTIR) spectroscopy analysis is described in Section 3.4.1.2, while thermal analysis is discussed in section 3.4.1.4. and morphological and particle size analysis was detailed in section 3.4.2. Water and energy consumption assessment was described in section 3.3.

5.4 Results and discussion

5.4.1 LMNPs produced by UFG

The application of UFG has enabled the production of LMNPs at high solid contents. The UFG system's profile, depicted in **Figure 3.1**, comprises a stationary grinding disk and a rotating grinding disk that can encounter each other. The shearing zones, which are shown in **Figure 5.1**, consist of two closely positioned rigid grinding surfaces that are in contact with each other. To facilitate the movement of lignin feeds towards the shearing zone, the grinder disk was equipped with infusion channels. These infusion channels are designed to guide the lignin feeds using the aid of a high rotation disk. As evident from **Figure 5.2**, at 25 ºC and a concentration of 40 wt.%, the formulated LMNPs suspension exhibits a dense liquid consistency

Figure 5.1 Photographic representation of the grinding disks of the ultrafine friction grinder

Figure 5.2 Photographic depiction of water based LMNP suspension produced at 25 ºC, 40 wt. %.

reminiscent of a milkshake. Remarkably, this rheological behavior enables seamless passage through the grinding disc clearance, without encountering issues such as clogging or the occurrence of solid-liquid separation. This observation underscores the potential of the lignin nanoparticle suspension for practical applications, highlighting its ability to maintain a homogeneous and pumpable state under specific conditions. By reducing the distance between the two grinding disks, the crushing force can be significantly increased, leading to more effective particle size reduction. The flow rate and maximum processing rate are heavily influenced by factors such as the distance between the grinding disks, lignin morphology, and solid content. In our specific conditions, with a working distance of -200 μm and a concentration of 20 wt.%, UFG process enables the production of LMNPs at a rate of 0.6 kg/h in the dry state or 3 kg/h in the wet state. These results are consistent with a previous report [164], although they used the UFG for cellulose nanofiber (CNF) production. It is worth noting that these rates do not represent the maximum processing capacity of the grinder.

5.4.2 Size and morphology

The particle size and morphology of lignin play a pivotal role in shaping the subsequent application of lignin nanoparticles.[22] Following UFG process, lignin particles undergo substantial changes in both their particle size and morphology. Moreover, various processing parameters such as solid concentration and processing temperature exert discernible effects on the ultimate morphology of the resulting lignin nanoparticles. SEM images of our lignin particles, both before and after undergoing the UFG process at 70 °C and 25 °C, are presented in **Figure 5.3** and **Figure 5.4** respectively. The particle size of lignin particles transitioned from the scale of dozens of microns (as depicted in **Figure 5.3a**) to a particle assemblage characterized by a size distribution spanning from tens to hundreds of nanometers. Consistent with previous findings[74, 88], the grinding process exhibited a pronounced impact on the nano-sizing of lignin, leading to a reduction in dimensions. In general,

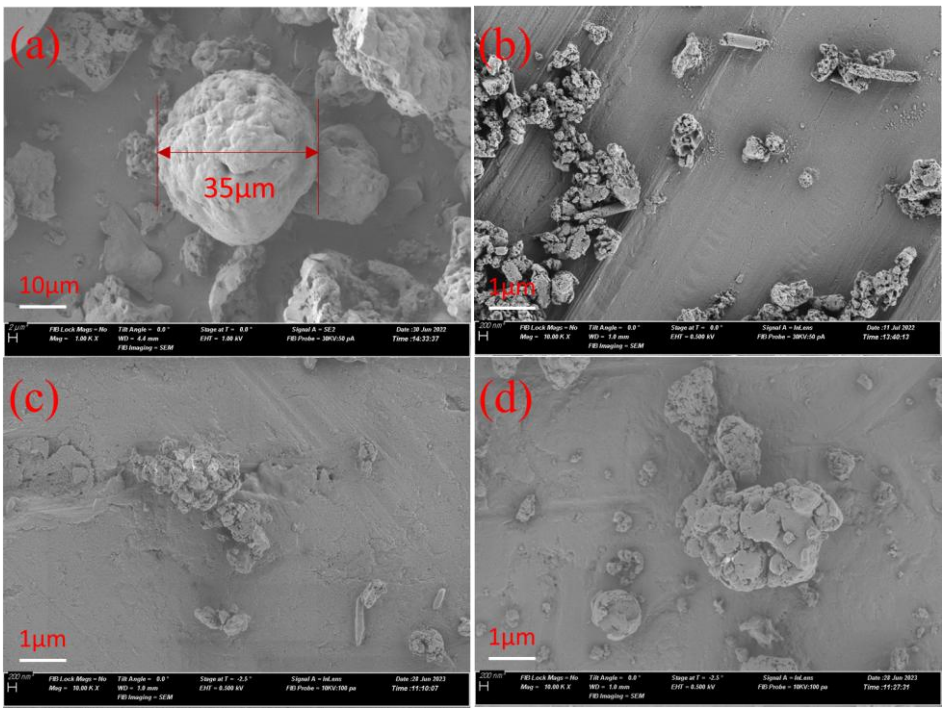

Figure 5.3 SEM images of LMNPs after 10 grinding cycles, manufactured at 70 °C; (a) original raw lignin, (b) 1 wt. %, (c) 20 wt. %, (d) 30 wt. %.

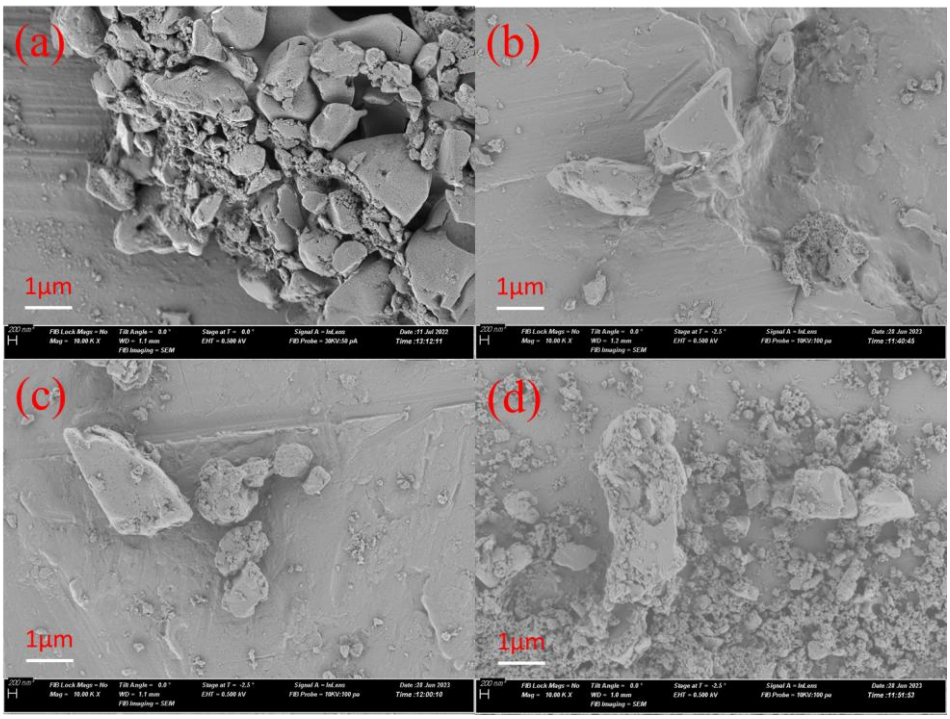

Figure 5.4 SEM images of LMNP manufactured at 25 °C after 10 grinding cycles, (a) 1 wt. %, (b) 20 wt. %, (c) 30 wt. %, (d) 40 wt. %.

the particle size of LMNP at high concentrations was found to be larger compared to that at low concentrations, for the same number of grinding cycles. However, it is important to note that both high and low concentration samples exhibited nano-sized lignin particles after the grinding process. These LMNPs produced at relative low temperature (25 °C) typically depicted an irregular cubic shape with sharp fluting and uneven cross-section, as seen in **Figure 5.5**. The glass transition temperature range of lignin is notably low, typically spanning from 120°C to 160°C.[165-167] Consequently, at the temperature of 70°C employed in this study (the actual internal temperature exceeds the measured outlet material temperature), lignin tends to undergo a softening process. This thermal softening results in particle reshaping and adhesion to one another during the grinding procedure.[168] As a result, particle aggregation resulted in the persistence of micro-sized particles even after ten cycles in the case of high concentration samples (**Figure 5.3c**). Consistent with findings from other disintegration methods such as twin-screw extrusion[80, 164] and high pressure homogenization[70], it has been demonstrated that the nano-sizing effect increases with an increasing number of UFG cycles, although these studies did not vary the feed concentration. Moreover, there is a point where the number of grinding cycles no longer has a significant impact on further nano-sizing of lignin. Our previous study has shown that, at a lignin concentration of 1 wt.%[88], LMNPs could be obtained after four UFG cycles at 70 °C and additional cycles may result in degradation.

In line with the previous report of LMNPs obtained after four cycles[88], we limited the number of UFG cycles to ten to avoid excessive degradation while achieving the desired nano-sizing effect. At a processing temperature of 25 °C, LMNPs at a concentration of 1 wt.%, depicted in **Figure 5.4**, exhibited a final particle size of about 100 nm, while LMNPs at a concentration of 20 wt.%, shown in **Figure 5.6b**, displayed a diameter of about 150 nm. These results align with the existing literature and are consistent with those obtained using a grinder.[22, 64, 68, 169] Especially the SEM images of samples produced at 70 °C and 30 wt. % (**Figure 5.7**) revealed

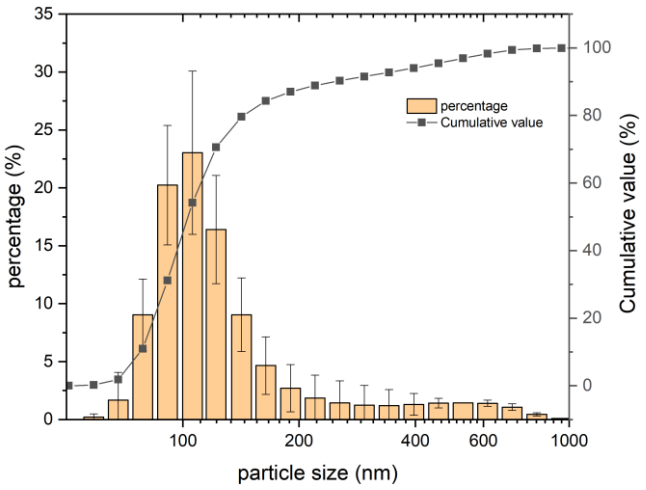

Figure 5.5 Particle size distribution of LNPs L-25-1 after 10 grinding cycles

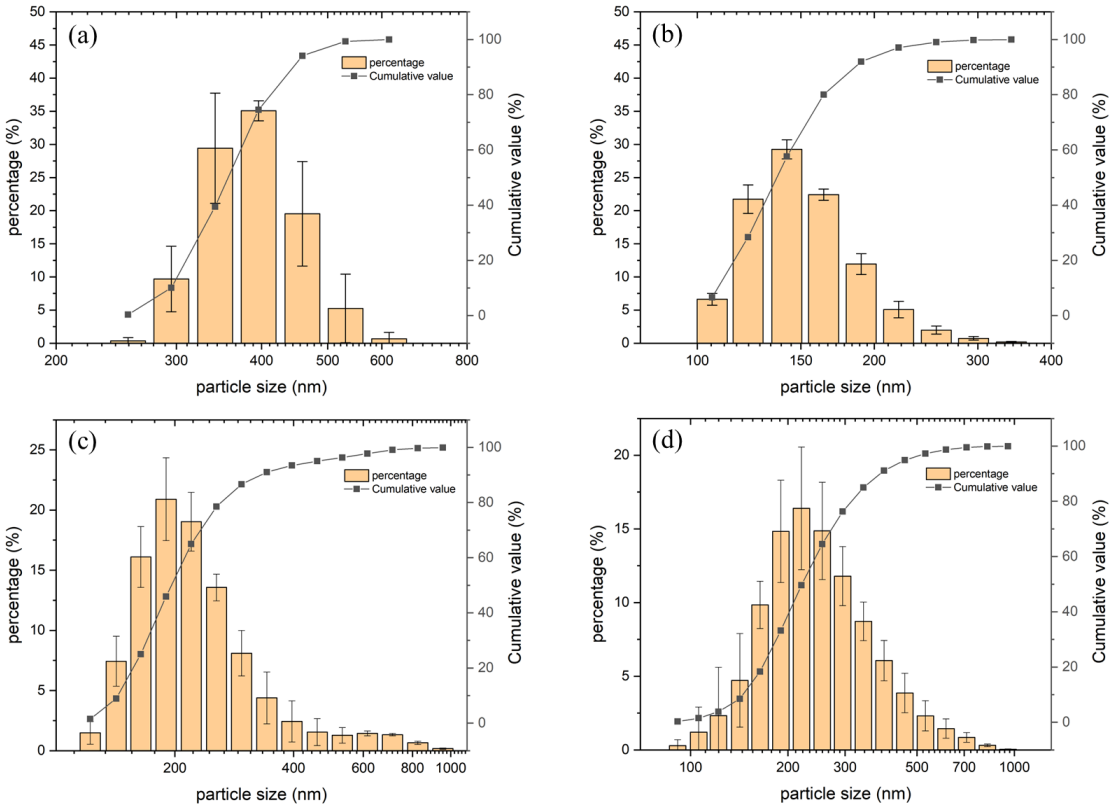

Figure 5.6 Particle size distribution of LMNPs (a) L-25-20 after 4 grinding cycles, (b) L-25-20 after 10 grinding cycles, (c) L-70-20 after 4 grinding cycles, (d) L-70-20 after 10 grinding cycles.

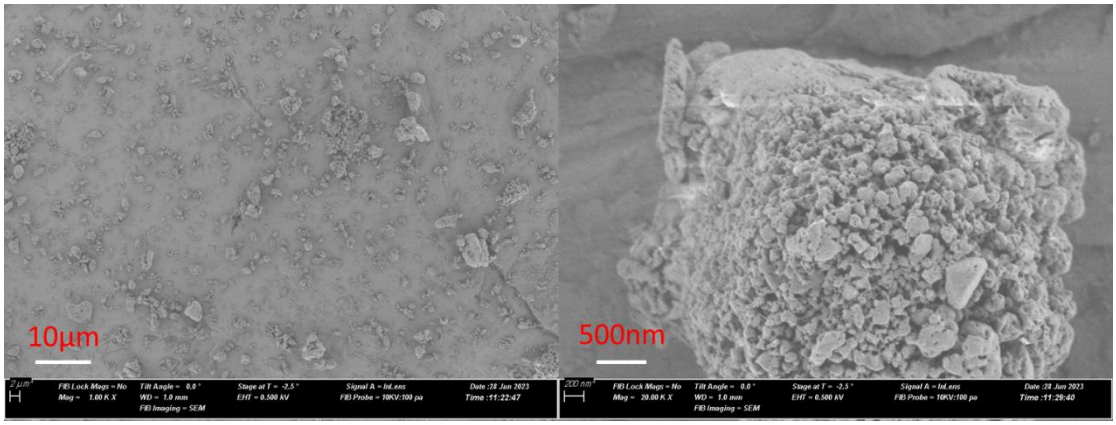

Figure 5.7 SEM image of L-70-30 obtained after 10 UFG cycles.

that these LMNPs exhibited a high degree of entanglement compared to those prepared at relatively lower concentration (20 wt.%) and lower temperature (25 ºC). In previous reports, LMNPs produced by aerosol flow reactors, ultrasonication, and high pressure homogenization were found to contain ~70 %, ~90 %, and 99 %, respectively, of submicron particles [28, 70, 79]. Sample L-25-20 exhibited a fraction of ~94.1 % under 500 nm after four UFG cycles (**Figure 5.6a**), which increased to ~99.9 % under 500 nm after ten cycles (**Figure 5.6b**). Fewer submicron fractions were observed in sample L-70-20 produced at 20 wt. % and higher temperature of 70 °C (**Figure 5.6c** and **d**), which may be because of particle slipping as well as lower surface charge content under high temperature conditions.[170] In summary, UFG allows to produce LMNPs with similar morphologies to those produced conventionally, while the submicron fraction achieved through UFG compares well with literature findings and commercial LMNPs, even under a high solid concentration of 20 %.

The stability of LMNPs in suspension plays a pivotal role in subsequent processes, influencing their thorough integration with other materials and the creation of composite materials with exceptional performance.[22] As large-scale storage of LMNPs typically involves dry solid particles, we established a new suspension by reintroducing the prepared LMNP powders in water, resulting in a 0.5% mass concentration, as illustrated in **Figure 5.8**. Notably, the dry LMNPs exhibited excellent dispersion in water, forming a relatively uniform suspension. **Figure 5.9** depicts the lignin nanoparticle suspension after standing for 24 hours, revealing the occurrence of settling, particularly evident in the form of larger particles concentrated at the bottom, creating a gradient with increasing concentration from top to bottom. This settling phenomenon is attributed to the broad particle size distribution resulting from mechanical grinding, including particles exceeding the micron scale, which tend to settle over time. However, the surface functional groups of the mechanically prepared nanoparticles show minimal alteration, thereby preserving the surface charge and enhancing suspension stability.[171] Despite the observed settling, a substantial

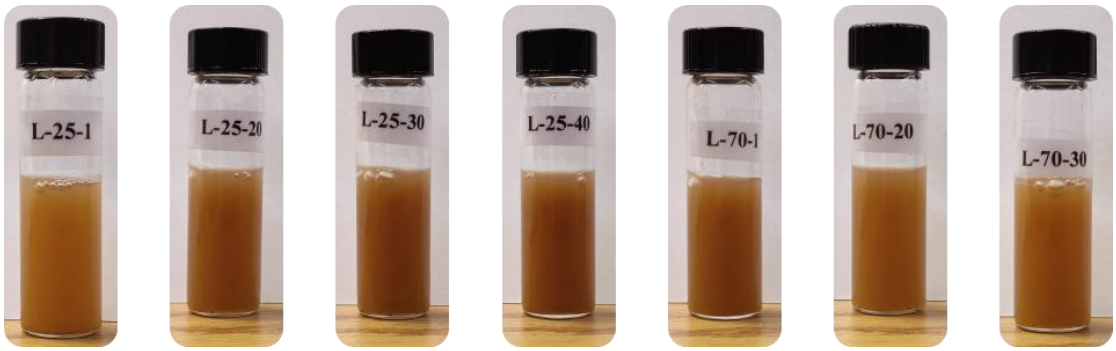

Figure 5.8 Photographic depiction of the new prepared water based LMNPs suspension at 0.5 wt.%

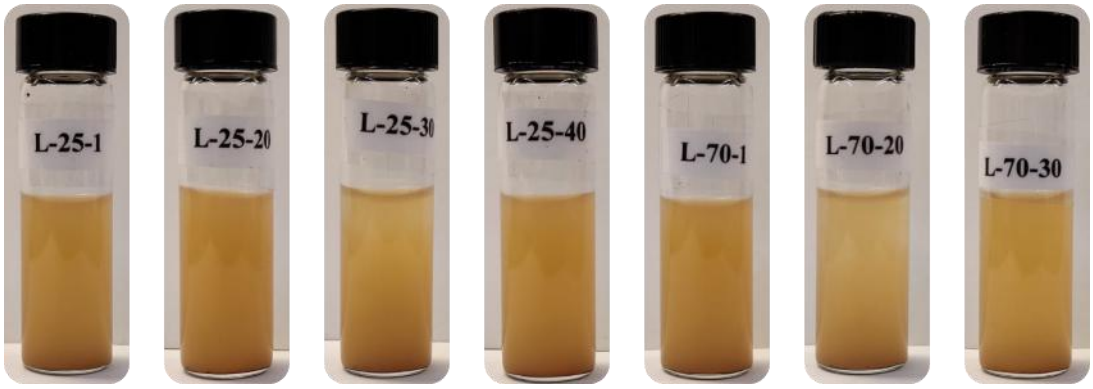

Figure 5.9 Photographic depiction of the water based LMNPs suspension at 0.5 wt.% settled for 24 hours.

number of nanoscale particles remain suspended, a dynamic influenced by particle sedimentation dynamics.[172] Generally, smaller particle sizes correlate with slower settling speeds, contributing to the sustained suspension of numerous nanoscale particles. In summary, while the freshly prepared suspension from dried lignin particles is relatively uniform, it may not exhibit colloidal stability. Nevertheless, LMNPs prepared through mechanical methods hold promising prospects for the fabrication of composite materials, given their favorable characteristics for various applications.

5.4.3 Energy expenditure under varied conditions

LMNP exhibits considerable promise as a green material; however, its potential for widespread industrialization is hindered by its significant energy consumption. The particle size analysis data revealed that the sample of L-25-20 had a peak particle size distribution below 150 nm (**Figure 5.10b**), whereas the peak particle size increased to 200 nm when the solid content reached 30 and 40 % (**Figure 5.10c** and **d**). The size distribution also narrowed as the solid content decreased, which is indicative of an increase in uniformity. The power consumption during each grinding cycle was determined by measuring the current and voltage with an ammeter. While previous publications have reported the energy consumption during UFG by considering only the energy used for cellulose fibril feeds[164], our study accounts for the total energy consumption required to sustain the grinder's rotation and facilitate both the grinding operation and nano-sizing of lignin. The relationship between power consumption, grinding cycles, and particle size during LMNP manufacturing is illustrated in **Figure 5.10** (25 °C) and **Figure 5.11** (70 °C). Remarkably, the sample with a 40 % solid content demonstrated the capacity for ambient temperature grinding. However, when heated to 70 °C, the lignin suspension exhibited a non-flowing state and became resistant to grinding due to its significantly increased viscosity. The energy required to achieve the same particle size (i.e.,150nm) was significantly reduced when the lignin concentration was increased to 20 wt. % at both

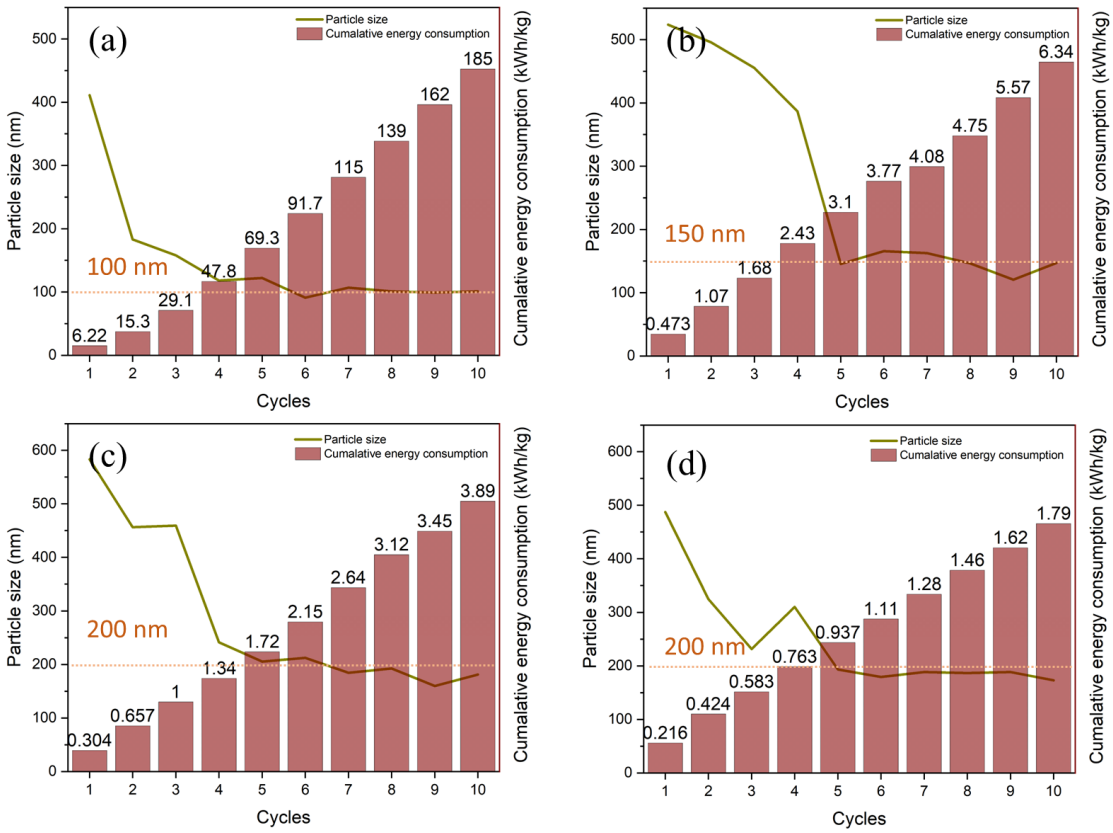

Figure 5.10 Comparing the power consumption per kilogram of lignin nanoparticle and the corresponding particle size reduction during UFG at 25°C, (a) L-25-1, (b) L-25-20, (c) L-25-30, (d) L-25-40. Notably, the dashed line within the figures signifies the equilibrium particle size.

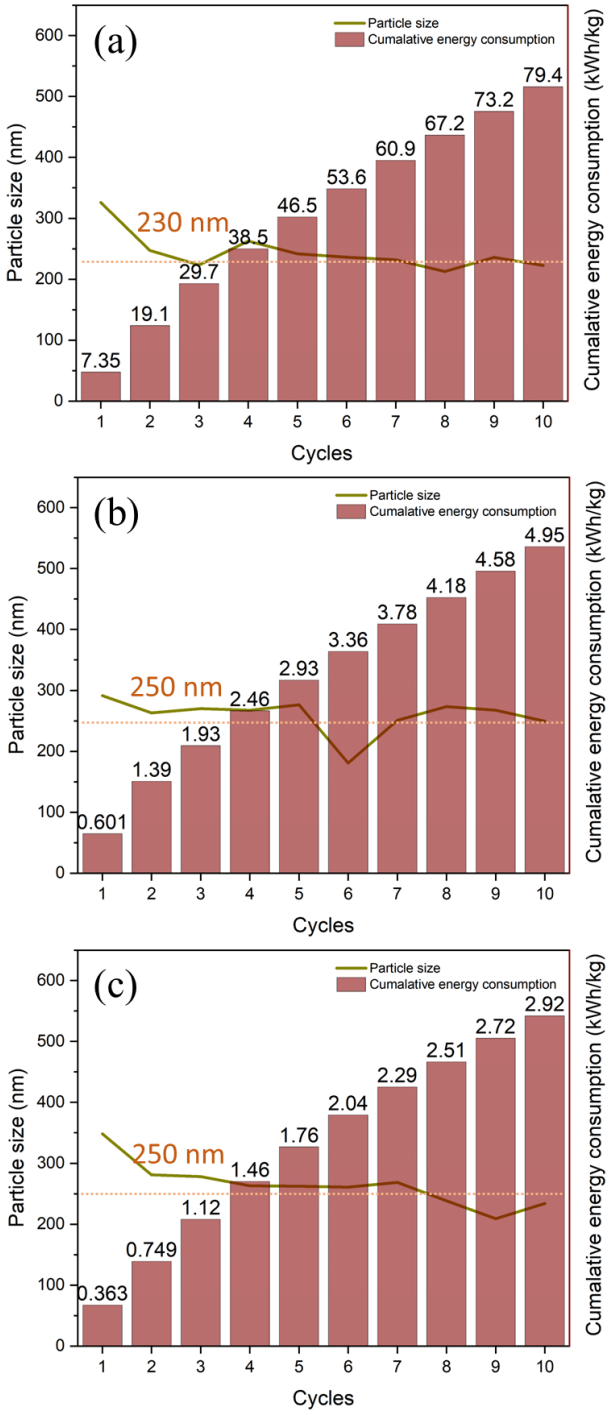

Figure 5.11 Comparing the power consumption per kilogram of lignin nanoparticle and the corresponding particle size reduction during ultrafine friction grinding (UFG) at 70°C, (a) L-70-1, (b) L-70-20, (c) L-70-30. Notably, the dashed line within the figures signifies the equilibrium particle size.

25°C and 70°C. Specifically, the energy consumption was less than one-tenth of the original energy consumption at 1 wt. % concentration. The data from the 1 wt. %, 20 wt. %, and 30 wt. % concentrations show that increasing the temperature was beneficial for reducing energy consumption per kg of lignin prepared via UFG. However, the final stable particle size achieved at 70 °C was larger than the particle size achieved at 25°C. Upon detailed examination of **Figure 5.3b-c**, it becomes evident that numerous minute particles coalesced, forming larger structures at 70°C. Previous investigations have demonstrated alterations in lignin's micromorphology when exposed to elevated temperatures, resulting in increased softness and flowability.[135, 136] Hence, it is plausible to hypothesize that, at lower temperatures, lignin exhibits enhanced brittleness, leading to the creation of sharply angled LMNPs. As the temperature approaches the glass transition (T_g), the interfaces of the newly formed LMNPs undergo a transition towards softness. Upon cooling, these LMNPs adopt a configuration characterized by low surface free energy, manifesting in the formation of spherical structures. This pattern is consistent with our previous work[88], where lignin nano-sizing was achieved only after four UFG cycles at 70°C as opposed to 12 cycles at 25°C.

Our results thus show that it is possible to achieve ~150 nm LMNP size while consuming less water and energy, and requiring only 5 UFG cycles at 25 °C. We also demonstrate the optimization of energy consumption based on the target LMNP size. As seen in **Table 5.1** and **Table 5.2**, when the target LMNP size is 300 nm, the corresponding energy consumption will be 0.749 kWh/kg at 70 °C and 30 wt. % concentration. Similarly, when the target LMNP size is 200 nm, the corresponding energy consumption will be 0.937 kWh/kg at 25 °C and 40 wt. % concentration. Thus, increasing solid concentration improves the potential for industrial scale LMNP production.

5.4.4 Comparative analysis of water utilization

Minimizing water usage during lignin nanoparticle production offers a range

Table 5.1 Specific particle size targets and the corresponding energy consumption during ultrafine friction grinding (UFG) at 25 ˚C.

Sample name / Energy consumption (kWh/kg)	Particle size targets (nm)		
	100	150	200
L-25-1	91.7	29.1	15.3
L-25-20	N/A	3.1	3.1
L-25-30	N/A	N/A	2.64
L-25-40	N/A	N/A	0.937

Table 5.2 Energy consumption (kWh/kg) corresponding to a targeted particle size of 300 nm at different grinding temperatures and solid concentration.

Grinding temperature (˚C)	Lignin concentration (wt. %)			
	1	20	30	40
25 ˚C	15.3	3.1	1.34	0.937
70 ˚C	19.1	1.39	0.749	N/A

of significant advantages. Firstly, it promotes resource efficiency by conserving water for other essential needs while reducing the environmental footprint associated with its extraction and treatment. Secondly, it leads to cost savings by decreasing operating expenses and conserving energy, particularly in heating, cooling, and wastewater treatment processes. This, in turn, can enhance the economic viability of nanoparticle production. Additionally, lower water usage contributes to a more environmentally friendly process by reducing wastewater discharge and the potential for pollution. Moreover, optimizing water consumption often improves overall process efficiency, resulting in more consistent and higher-quality nanoparticle production. In methods of LMNPs production mediated by water, the solid concentration consistently remains at a notably low level, typically well below 2 wt. %.[169] We investigated four distinct concentrations, namely 1, 20, 30, and 40 wt. %. **Table 5.3** presents the corresponding water consumption per kilogram of produced lignin nanoparticles for each concentration. Elevating the solid concentration within lignin suspensions leads to a substantial reduction in water consumption when contrasted with conventional 1 % concentrations. Transitioning from a 1 % concentration to 20 % results in a reduction of water usage to merely 4 % of the initial amount. Moreover, by raising the concentration to 40 wt. %, water consumption can be further reduced to as little as 1.5 % of the initial amount. However, this reduction in water usage is accompanied by an increase in particle size, growing from 100 nm to 300 nm. Based on our experimental findings, it can be inferred that compromising a slight degree of particle size requirement can lead to a significant reduction in water consumption. This revelation holds promise for the future of lignin nanosizing, as it opens the possibility of achieving a more sustainable and efficient production process.

5.5 Conclusion

The industrialization and application of nanoparticles in various fields are driven by two key factors: high solid content and energy efficiency. High solid content enables efficient production of nanoparticles, while the emphasis on energy

Table 5.3 Comparative assessment of water consumption (kg / kg lignin nanoparticles) at varied concentrations.

Working condition	Concentration of lignin suspension (wt. %)			
	1	20	30	40
Water consumption (kg/kg LMNPs)	99	4	2.3	1.5

efficiency ensures sustainable and cost-effective manufacturing processes. In this study, a water and energy saving one-pot LMNP production method was successfully demonstrated. LMNPs of ~150 nm size were successfully produced from softwood kraft lignin at high solid content (20 wt. %) and five UFG cycles at 25°C. The energy requirement for nano-sizing was found to be 90 % lower at a solid content of 20 wt. % than at 1 wt. % lignin concentration. Furthermore, the water usage per kg of LMNP production was remarkably reduced to only 4 % of that consumed at a 1 wt. % concentration. Reducing water usage and energy requirements will thus contribute towards improving the feasibility and viability of LMNPs production for widespread industrial use. Moreover, we demonstrated that the LMNP properties are highly influenced by the number of grinding cycles and the solid concentration. Our results will thus enable the production of various LMNP grades by controlling the number of UFG cycles at a specific solid concentration. This flexibility in manufacturing allows for the customization of LMNPs, catering to diverse application requirements.

CHAPTER SIX : A FULLY PLANT-BASED WATER- AND OIL-RESISTANT PAPER COMPOSITE

A version of this chapter was originally published as:

Zhongjin Zhou, Kalavathy Rajan, Shahab Saedi, Nicole Labbé, Mi Li, Wei Wang, Siqun Wang. (2024). A Fully Plant-Based Water-and Oil-Resistant Paper Composite. *ACS Sustainable Chemistry & Engineering*, 12, 50, 18043-18057.

Author contributions are listed as follows. **Zhongjin Zhou**: Conceptualization, Methodology, Formal analysis, Investigation, Writing-original draft, Writing - Review & Editing. **Siqun Wang**: Conceptualization, Methodology, Formal analysis, Investigation, Review & Editing, Supervision, Project administration, Funding acquisition. **Kalavathy Rajan**: Investigation, Validation, Review & Editing. **Shahab Saedi**: Review & Editing. **Nicole Labbé**: Conceptualization, Resources, Review & Editing, Funding acquisition. **Mi Li**: Resources, Review & Editing, NMR test. **Wei Wang:** Water contact angle test and analysis, Review & Editing.

6.1 Abstract

Disposable tableware commonly used at gatherings and for take-out has switched from plastic to paper due to concerns about micro- and nano-plastic pollution. Their water and oil resistance are typically achieved by using either per- and polyfluoroalkyl substances (PFAS), which are harmful and persistent in the environment, or plastic coating, which exacerbate the plastic pollution issue. Hence, safe, and eco-friendly water and oil-resistant materials are a crucial need. Emulating natural plant properties, we applied a seamless lignin film on paper via the hot-pressing method. By varying parameters such as lignin coating weight (10-40 g/m^2), hot-pressing pressure (1-5 MPa), temperature (120-180 °C), and moisture content (10-50 wt.%) of LMNP suspension before hot-pressing, we determined that 40 g/m^2 of lignin coating weight applied at 3 MPa pressure, 160 °C temperature, and 30 wt.% moisture content are the optimal condition. This yielded a lignin layer with exceptional waterproofing (100 minutes) and oil resistance (25 minutes). The paper composite board biodegraded within 56 days in garden soil, thereby providing a promising eco-friendly alternative to non-biodegradable plastics and PFAS.

6.2 Introduction

In the municipal solid waste (MSW) domain, plastics emerge as a rapidly expanding constituent. The foremost contributor to plastic volume is single-use containers and packaging, accumulating a notable quantity of over 35.7 million tons in 2018.[31] These wastes are easily spread into the environment, especially in developing countries and regions, causing damage to the local communities, environment and ecology.[173-175] Micro and nano plastics, the products of plastic degradation, end up in human organs via the food chain.[176] Consequently, there has been increased attention to paper-based tableware and packaging. Unfortunately, paper made from cellulose fibers without water and oil proofing agents cannot be directly used to store foods, especially at higher temperatures, due to their interactions with the hydrophilic domains of ordinary cellulose.[177] Paper loses its structural

integrity in the presence of liquids as it swells and the hydrogen bonding between cellulose fibers weaken.[178] One potential solution is to coat the paper with a layer of plastic. Although plastic-coated paper has shown advancements in biodegradability, it remains incapable of fully eliminating plastic accumulation in the environment. Plastic films used in paper packaging materials are more difficult to collect and recycle, especially when compared with the bulky plastic used in bottles and other containers. It is noteworthy that the overall plastic recycling rate was only 8.6% in 2018.[31]

Another commercially viable solution involves the use of wet-end chemical additives, such as per- and poly-fluoroalkyl substances (PFAS), to enhance durability. It is paramount to recognize the profound safety concerns linked to PFAS, even if its additives are being phased out from food packaging.[18] These concerns encompass a spectrum of environmental and health-related issues. Notable among the potential detriments of PFAS are their persistence, bioaccumulative nature[12, 14], adverse health effects[15], environmental contamination[179], and contamination of drinking water sources[15]. The quest for substitute material to replace PFAS and nondegradable plastic is of pressing significance.

Cellulose and lignin are the world's most abundant renewable, degradable plant materials.[65, 180] Lignin naturally has antioxidant properties, because of its chemical structure of aromatic rings[181], which makes it attractive in food preservative films.[182-184] It is also widely accepted that lignin is hydrophobic[185], so the application of lignin in water repellent packaging materials is a topic worthy of investigation. Lignin is also considered a natural binder and is used in the reinforcement of cellulosic composites.[178, 186] The density of composite and pores size are considered to play an important role in the barrier properties of paper packaging.[89, 187] Lignin could potentially block the pores in paper and form a protective hydrophobic layer, when melted under the hot press molding process. Rojo et al.,[188] reported that the softened

lignin has the ability to glue and fill in the pores of cellulose nanofibers resulting in a very smooth surface.

Cellulose nanofibers have excellent mechanical strength and oxygen barrier properties, which makes them one of the premier functional additives for food packaging materials.[189, 190] However, cellulosic materials are not highly compatible with hydrophobic additives, making it difficult to form a strong, flat, and uniform hydrophobic film on the surface of paper without adhesives.[191, 192] Up until now, there are no studies on the formation of pure lignin-based continuous films as barrier layer for paper composite. The size of commercial lignin particles is between tens to hundreds of microns[19], making it difficult to be embedded between cellulose or nanocellulose fibril. When combined with cellulose to form a paper composite, lignin tends to agglomerate and distribute unevenly. During the thermoforming process, uneven heat can cause partial decomposition, making it difficult to achieve a uniform and smooth-textured film. LMNPs have a size from 100-1000 nm, which can theoretically fill in the cavities between fibers. Application of heat and increased hydrogen bonding could improve the compatibility between cellulose fiber and lignin layers.[96-99] Thus, a composite or layered film can be formed. Bhagia et al.,[89] prepared lignocellulose-based paper under hot pressing between 150 °C and 180 °C. The mechanical strength of the resulting paper was doubled compared with air-dried paper. We speculate that under hot pressing conditions, LMNPs will melt and fill into the voids of cellulosic paper and form a continuous dense layer on the surface, thus blocking the penetration of oil droplets.

The primary objective of this study is to achieve a continuous layer of LMNPs on the surface of cellulose paper. Our hypothesis posits that the introduction of lignin onto paper surface, under high temperature molding conditions, will lead to the formation of a three-layered structure. This structure will comprise of a bottom layer of cellulose fiber, a middle layer consisting of a mixture of cellulose and melted lignin, and a continuous lignin layer as the top. Our aim is to exploit this laminated

structure to achieve oil resistance and hydrophobic properties. Notably, the lignin is applied without any chemical modification and exhibits hydrophobicity. To investigate the reaction mechanism of LMNPs in the production of a paper composite, we conducted a comparative experiment by varying the amount of LMNPs used, temperature and pressure of hot press, and moisture content of wet lignin layer before hot-pressing. Furthermore, this LMNP-paper composite's biodegradation in an aerobic environment was tested.

6.3 Experimental methods

6.3.1 Materials and sample preparation

The kraft softwood lignin used in this study is described in Section 3.1, and the preparation of LMNPs is detailed in Section 3.2.1. LMNP-paper composites preparation was described in section 3.2.2.

6.3.2 Characterizations

Fourier-transform infrared (FTIR) spectroscopy analysis is described in Section 3.4.1.2, while thermal analysis is discussed in section 3.4.1.4. and morphological and particle size analysis was detailed in section 3.4.2. Performance of paper composites including oil and water resistance, and mechanical strength assessment was described in section 3.4.4 Biodegradation was described in section 3.5

6.4 Results and discussion

6.4.1 Size and micromorphology of LMNP

The particle size distribution of LMNP, determined by DLS, showed that the mean particle size was 150 nm (**Figure 6.1a**), whereas the polydispersity was 0.5 ± 0.03, indicating that the lignin particles were not a uniform system. The particle size of LMNP was also verified by SEM, as shown in **Figure 6.1b**, which revealed that the micromorphology of our LMNPs varied and was not in the form of spherical nano solids.

6.4.2 Chemical characterization of the paper composites

The chemical properties of the paper composites of C80-P3-T120-M30,

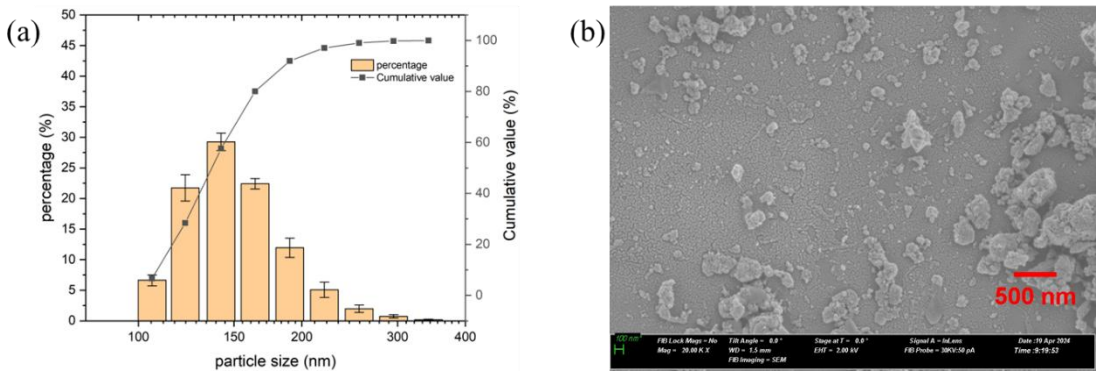

Figure 6.1 (a) Particle size distribution, and (b) Scanning electron microscopy image of lignin micro- and nanoparticles (LMNP).

C80-P3-T140-M30, C80-P3-T160-M30, C80-P3-T180-M30 along with uncoated paper and LMNP as references were investigated by FTIR (**Figure 6.2a**). The dominant bands at 1053 and 1030 cm^{-1} in the uncoated paper are attributed to C-O-C and C-O stretching modes respectively.[193] A broad band at 3300 cm^{-1} was observed across all samples, corresponding to O-H stretching vibrations from intermolecular and intramolecular hydrogen bonds.[194] The relatively weak peaks at 2927 cm^{-1} and 2855 cm^{-1}, also present in samples, represent asymmetric and symmetric C-H stretching vibrations.[195] Characteristic lignin peaks are also evident, particularly around 1591 cm^{-1} and 1511 cm^{-1}, which correspond to the aromatic skeletal vibrations of lignin.[123] These peaks confirm the successful deposition of a lignin layer on the cellulose paper surface.

Principal component analysis (PCA) was employed to further investigate the chemical variations among the samples, with the scores plot presented in **Figure 6.2b**, and the corresponding loadings plots in **Figure 6.2c**. The scores plot reveals distinct clustering based on hot-pressing temperatures. Samples treated at 140°C and 160°C group closely in the positive region of PC1, which accounts for 74% of the total variance, suggesting only minor chemical differences between these two groups. Conversely, samples processed at 180 °C exhibit greater separation along PC1, indicating more substantial chemical changes. The loadings plot for PC1 highlights three major negative bands, 2927 cm^{-1} and 2855 cm^{-1} (C-H stretching in methyl and methylene groups)[196], and at 1747 cm^{-1} (C=O stretching)[197], responsible for the separation, suggesting molecular rearrangements. The positive peaks for lignin aromatic skeletal vibrations (1591 cm^{-1} and 1511 cm^{-1}) and for guaiacyl and syringyl units (1270 cm^{-1} and 1215 cm^{-1}) indicate a potential thermal degradation of lignin at higher processing temperature. Further quantitative insights were obtained through 2D-HSQC NMR analysis, confirming the chemical alterations observed by FTIR.

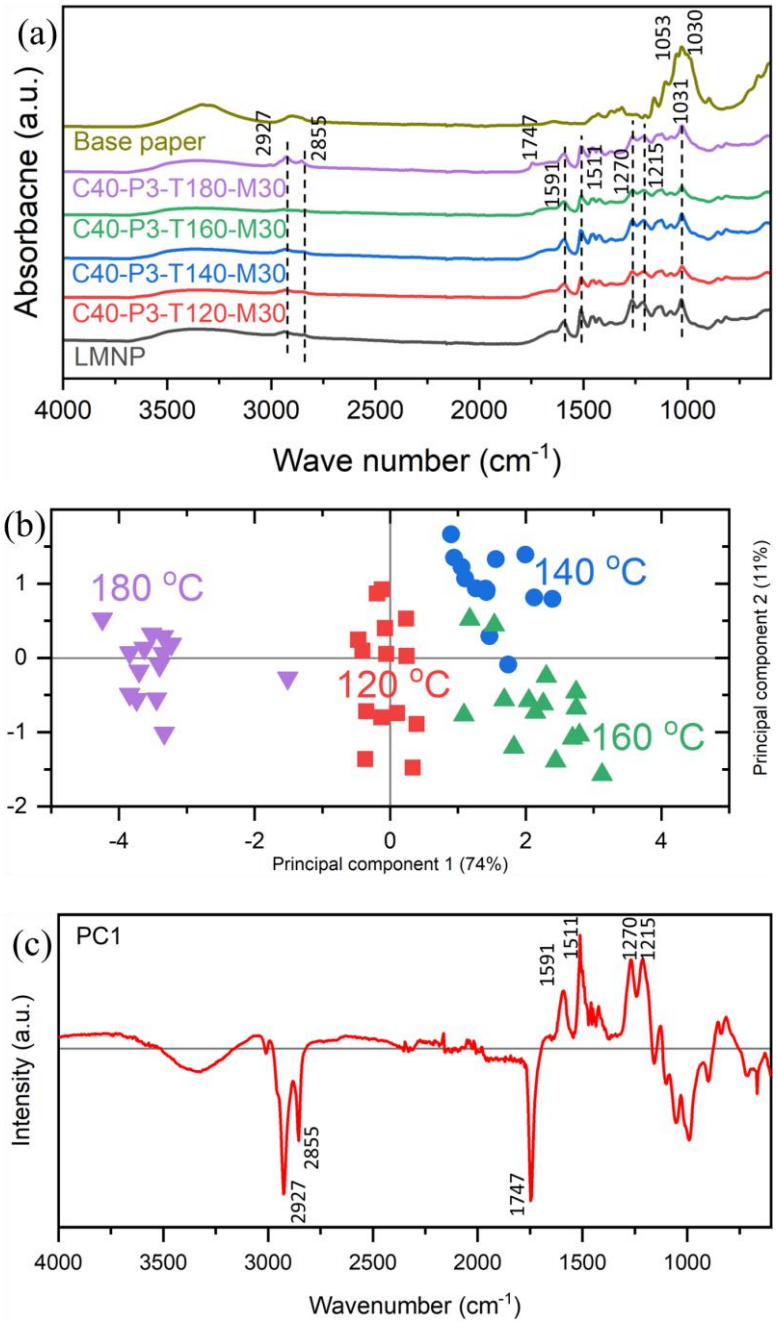

Figure 6.2 (a) The ATR-FTIR spectra of uncoated and LMNP-paper composites under different hot-press temperatures, (b) Scores plot of the principal component analysis (PCA) of the FTIR spectra for paper composites subjected to hot-pressing at 120, 140, 160, and 180°C. (c) Loadings plot of principal component 1 (PC1), which explains 74% of the variance in the data.

The aryl ether bonds (β-O-4') and condensed linkages, namely β-β′, β-5', and β-1', constitute the primary substructures of lignin (**Figure 6.3**) [41, 44, 45]. The analysis of side chain linkages (Aα+Bα+Cα+Fα = 100), as seen in **Figure 6.4**, reveals that, following hot-pressing, the proportion of β-O-4 linkages declined significantly from 65% to 59% at 120 °C; this decline levels out to 54% when hot-pressed above 120 °C and below 180 °C. Concurrently, the proportion of C-C bonds originating from β-β′, β-5, and β-1 linkages increases from 29% to 41% at 120 °C, and further escalating to 46% when heated to 180 °C. This trend underscores the degradation of native ether linkages during hot-pressing and the emergence of condensed C-C bonds upon repolymerization when cooling. Given the higher energy associated with C-C bonds compared to ether bonds [46], the resultant lignin film from hot-pressing may exhibit enhanced chemical stability relative to the original LMNP. However, the heightened prevalence of condensed bonds renders the lignin film stiffer and more brittle. Consequently, increased brittleness elevates the susceptibility to surface cracking, thereby compromising the sealing properties of the lignin film to a certain extent.

6.4.3 Properties of LMNP-paper composites

6.4.3.1 Visual appearance

Lignin content significantly influences the optical properties of wood-derived structural materials. A similar property is observed in our fabricated LMNP-paper composites. While cellulose is inherently white, lignin possesses an intricately structured, dark-colored appearance. Consequently, as the lignin coating weight increases from 10 to 40 g/m^2, the color of the cellulose/lignin composite transitions from brown to black, which can be seen in, **Figure 6.5**.

6.4.3.2 Thermal stability analysis

The thermal stability of the composite paper was assessed using TGA. For comparison, the thermogravimetric profiles of pure paper and LMNP powder prior to hot- pressing were also evaluated. The mass loss as a function of temperature is depicted in **Figure 6.6a**, while the first derivative of mass with respect to temperature

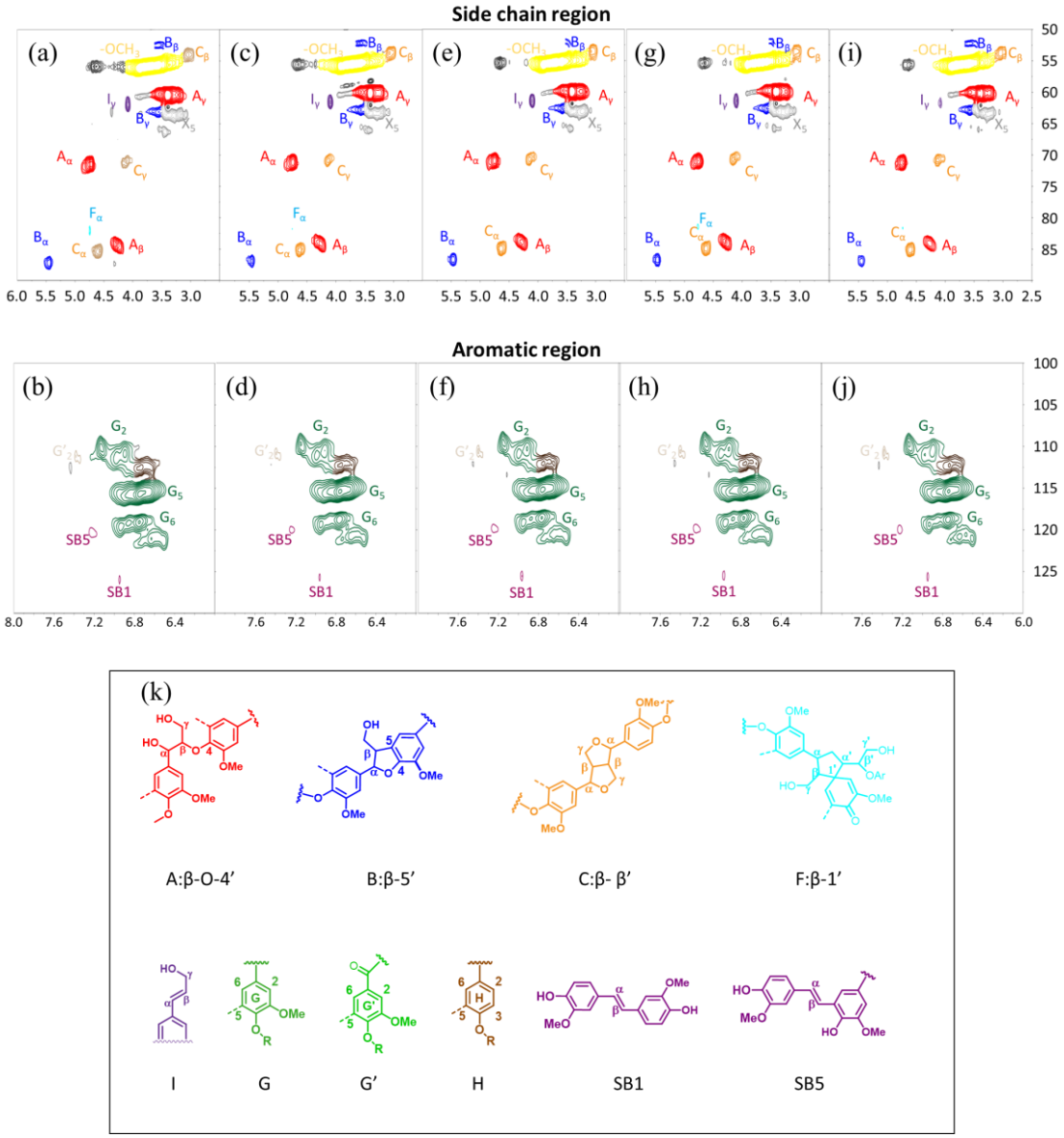

Figure 6.3 2D-HSQC NMR analysis of the sidechain and aromatic substructures of (a) and (b) lignin micro- and nanoparticles (LMNPs) feedstock; (c) and (d) LMNP compressed at 120 °C; (e) and (f) LMNP compressed at 140 °C; (g) and (h) LMNP compressed at 160 °C; (i) and (j) LMNP compressed at 180 °C; (k) legend of lignin substructures.

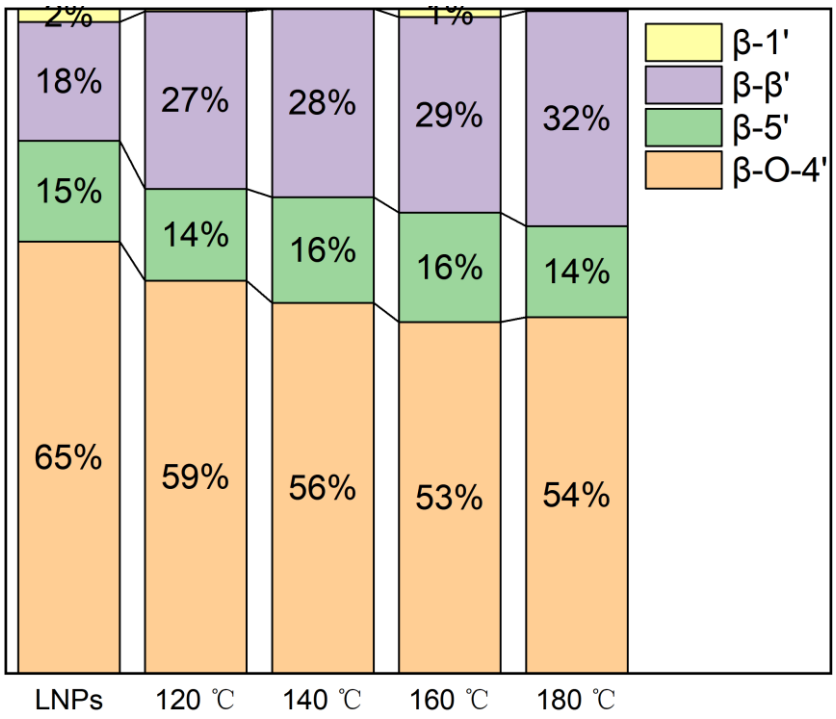

Figure 6.4 Changes in LMNP inter-unit linkages, namely β-O-4 (aryl ether), β-5 (phenyl coumaran), β-β′ (resinol) and β-1 (spirodienone), as a function of hot-pressing temperature.

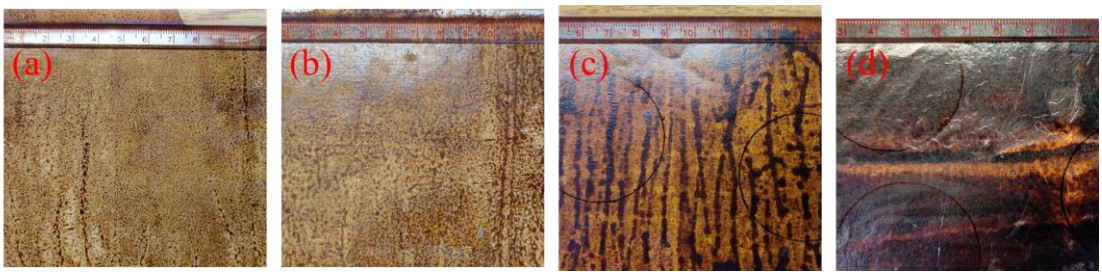

Figure 6.5 photos of lignin coated paper with different coating weight, (a) C10-P3-T160-M30, (b) C20-P3-T160-M30, (c) C30-P3-T160-M30, (d) C40-P3-T160-M30.

(DTG) is shown in **Figure 6.6b**. The initial mass loss observed from room temperature to approximately 110 °C corresponds to the volatilization of adsorbed water, a feature common to all three samples. The first plateau, occurring between 110 °C and 240 °C, indicates thermal stability in both pure and composite paper. In contrast, LMNP exhibits a mass loss beginning around 160 °C, suggesting partial decomposition of components. In the composite, the LMNP layer underwent structural changes during the hot-pressing process, resulting in no significant mass change. Both the uncoated and LMNP-composite paper show rapid mass loss between 240°C and 380°C, with a singular peak in the DTG curves at ~360 °C, attributable to the decomposition of cellulose's main structure. In contrast, the original LMNP powder exhibits a continuous mass loss with less pronounced peaks in the DTG curve. In summary, the LMNP-paper composite retains the thermal characteristics of both cellulose and lignin, with distinct differences in the 160-240 °C range. These differences arise from the heat treatment during the hot-pressing process, rendering the composite more thermally stable below 240 °C compared to uncoated paper.

6.4.3.3 Density analysis

Low porosity is an advantage for any barrier paper.[180, 198, 199] We hypothesized that the porosity of the paper composite would be reduced when the apparent density of paper composite increased. **Figure 6.7a** showed the density of paper with different LMNP coating grammage. **Figure 6.7b** showed the density of paper under different hot-pressing pressures and **Figure 6.7c** showed the density changed as a function of hot-pressing temperature. Finally, **Figure 6.7d** showed the density of paper composite as a function of moisture content of wet LMNP before hot-pressing. As can be seen in **Figure 6.7a**, as the LMNP coating weight increases from 10 to 40 g/cm^2, the density value increases from 0.87 to 0.93 g/cm^3. This is because the melted lignin fills in the gaps of cellulose fibrils and increases its density; moreover, the paper substrate could have been densified under high pressure. We hypothesized that the aromatic backbone of LMNP stacks densely on top of each other, compared to the cellulose fibrils, and

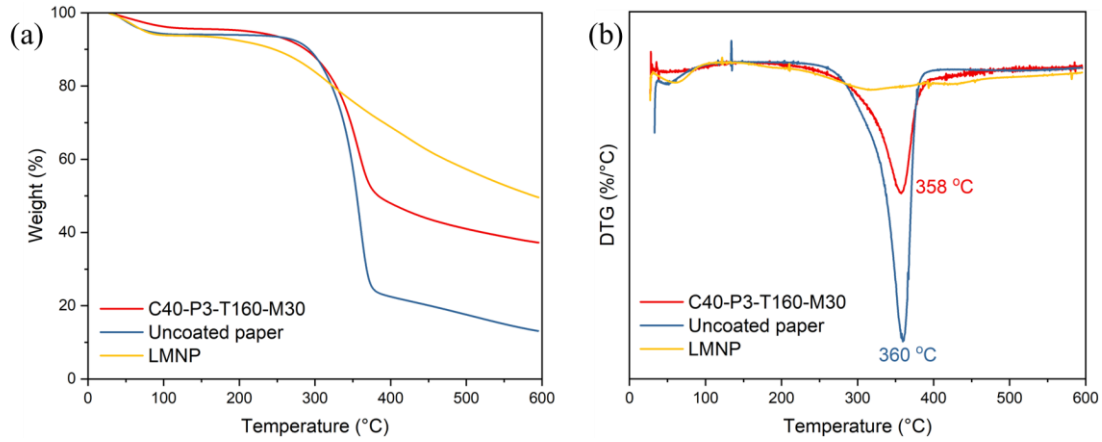

Figure 6.6 (a) TGA curves and (b) first-order derivative thermograms (DTG) of LMNP-paper composite (C40-P3-T160-M30), uncoated paper, and LMNP.

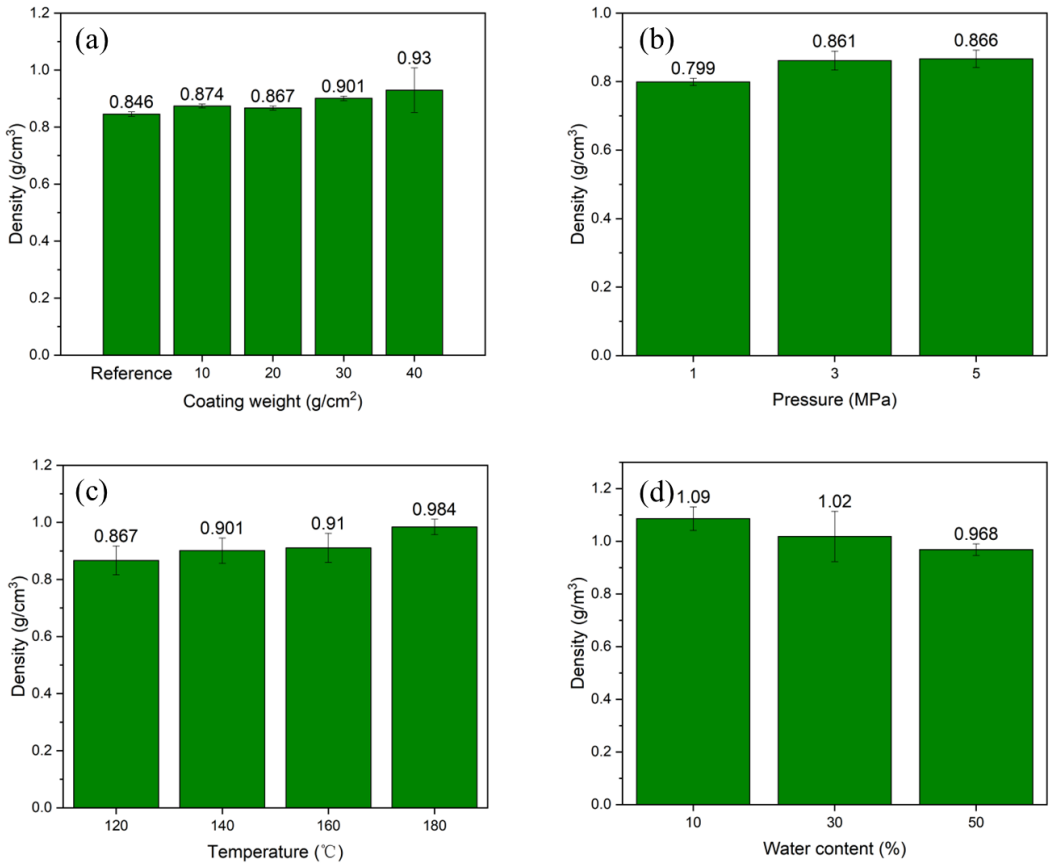

Figure 6.7 Density of LMNP-paper composites (a) at different LMNP coating weight, (b) at different pressing pressure, (c) pressing temperature, and (d) at different water content of wet LMNP before hot press.

henceforth the composite's density increased with the increase in LMNP coating grammage. Similarly, the composite's density increased as a function of hot-pressing temperature and pressure (**Figure 6.7b and c**). This could be correlated to the degradation of lignin at severe hot-pressing conditions and an increase in condensed lignin substructures that may stack tightly compared to the native aryl ether linkages. The increase in density as a function of pressure may be a straightforward effect of increased compression. Finally, the paper composite's density increased with a decrease in water content of wet LMNP before hot press (**Figure 6.1d**). Despite these differences, it is important to note that the changes in composite density as a function of temperature, lignin coating grammage, and LMNP concentration were not significant compared to other studies, where the density increased from 0.75 to 1.64 g/cm^3 [44].

6.4.3.4 Mechanical strength analysis

Mechanical strength is crucial for the application of paper composites in biodegradable foodware. The tensile property testing revealed the effects of LMNP coating weight, hot-pressing pressure, temperature, and moisture content on the composite's mechanical properties, as seen in **Table 6.1**. **Figure 6.8a** showed that at a lignin coating weight of 10-20 g/m^2, the tensile strength of the composite increases by 30% compared to pure paper. This improvement is due to lignin forming a hard polymer during hot pressing, which integrated with paper fibers. However, at an LMNP weight above 30 g/m^2, the tensile strength decreased, resembling that of uncoated paper. This occurred because a thicker lignin layer reduced the mixing zone portion in paper composite, weakening the reinforcement. For lignin weights of 10-20 g/m^2, maximum elongation was around 2.4%, and Young's modulus reached 4 GPa，35% higher than uncoated paper. This indicates that while lignin enhanced tensile strength, reduced toughness, aligning with its reinforcing role. **Figure 6.8b** shows that increasing hot-pressing pressure boosted tensile strength. At 5 MPa, tensile strength reached 35 MPa, 20% higher than uncoated paper, due to increased lignin penetration,

Table 6.1 Summary of Mechanical Properties.

Sample ID	Tensile properties		
	Young's modulus (MPa)	Maximum tensile stress (MPa)	Ultimate strain (%)
C10-P3-T160-M30	3953 ± 534	38.1 ± 2.3	1.9 ± 0.2
C20-P3-T160-M30	4443 ± 281	41.7 ± 2.7	2.3 ± 0.3
C30-P3-T160-M30	2676 ± 387	28.7 ± 0.6	4.2 ± 0.5
C40-P3-T160-M30	2763 ± 145	27.2 ± 1.5	3.2 ± 0.1
C40-P1-T160-M30	3506 ± 279	28.9 ± 5.1	1.8 ± 0.5
C40-P5-T160-M30	4239 ± 85	34.8 ± 0.6	1.6 ± 0.1
C80-P3-T120-M30	1953 ± 104	18.7 ± 0.8	4.0 ± 0.1
C80-P3-T140-M30	1761 ± 252	16.0 ± 0.7	3.3 ±0.7
C80-P3-T160-M30	2254 ± 336	19.8 ± 3.2	2.7 ± 0.9
C80-P3-T180-M30	3618 ± 544	30.8 ± 3.7	2.6 ± 0.5
C40-P3-T160-M10	1940 ± 203	16.7 ± 1.7	3.0 ± 0.2
C40-P3-T160-M50	4999 ± 379	37.0 ± 4.4	1.7 ± 0.3
Uncoated paper	2569 ± 166	28.6 ± 0.5	3.8 ± 0.3

higher density, and enhanced structural integrity. **Figure 6.8c** demonstrates that higher temperatures increased tensile strength. Around 180 °C, lignin molecules restructure, forming a more rigid polymer. 2D-NMR analysis shows an increase in high-energy C-C bonds, strengthening the polymer (**Figure 6.4**). The rise in Young's modulus and the decrease in the maximum strain at break with temperature confirms this. **Figure 6.8d** indicates that higher moisture content in the LMNP layer improved mechanical strength. At 50% moisture, tensile strength reached 37 MPa, 28% higher than uncoated paper. Increased LMNP moisture during hot pressing allowed lignin to penetrate deeply into the paper, expanding the mixing area and enhancing strength. This led to increased strength and brittleness, as seen in the increased Young's modulus and decreased maximum strain at break.

In conclusion, optimizing the mechanical properties of paper composites requires balancing lignin coating weight, hot-pressing pressure, temperature, and moisture content. Each factor significantly influences the composite's strength and toughness.

6.4.3.5 Oil and water resistance

The oil and grease resistance (OGR) of LMNP-paper composites were measured using the TAPPI kit test, where a higher value means superior resistance. As shown in **Table 6.2**, the OGR rating increases from 1.5 to 7 as the weight of the lignin coating increases from 10 to 30 g/cm^2. Secondly, the OGR rating increased from 1 to 7 as a function of hot-pressing pressure, provided all other variables are kept constant. Similarly, the oil holding time increases from 3 to 15 mins when the hot-pressing pressure increases from 1 to 3 MPa. This could be because at higher pressure, the LMNP-paper composite's density increased significantly. An increase in density will result in a decrease in porosity, which subsequently could lead to an improvement in oil and grease resistance. Another important observation is that the OGR rating increased from 2.5 to 8 as the moisture content of wet lignin layer before hot press increased from 10 to 50 wt.%. The oil resistance capacity also increased

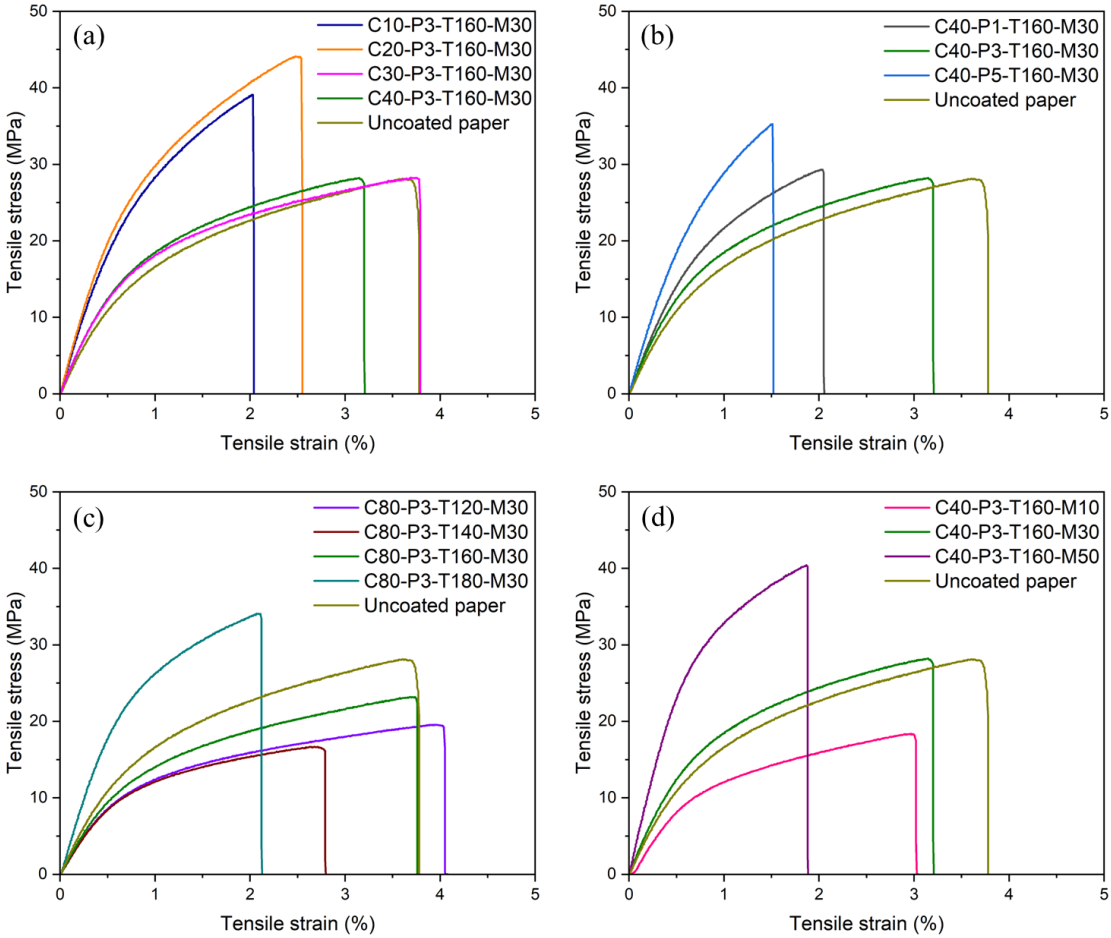

Figure 6.8 Stress−strain curves of LMNP-paper composites under varying conditions: (a) different lignin coating weights, (b) different hot press pressures, (c) different hot press temperatures, and (d) different moisture contents of wet LMNP layer prior to hot press.

Table 6.2 Manufacturing parameters and physical property of LMNP-paper composites.

Paper Composite code	**OGR rating***	**Water holding duration† (min)**	**Oil holding duration‡ (min)**
C10-P3-T160-M30	1.5	60±9	3±1
C20-P3-T160-M30	2	70±7	5±3
C30-P3-T160-M30	7	70±23	10±5
C40-P3-T160-M30	8	100±5	25±3
C40-P1-T160-M30	2	5±2	3±1
C40-P5-T160-M30	1	60±21	3±1
C80-P3-T120-M30	1	60±24	1±1
C80-P3-T140-M30	7	60±18	10±2
C80-P3-T160-M30	8	70±9	20±5
C80-P3-T180-M30	2	60±11	5±1
C40-P3-T160-M10	2.5	3±1	5±2
C40-P3-T160-M50	8	15±4	75±6

Note: LMNP – Lignin micro- and nanoparticle; *OGR – Oil and grease resistance determined as per TAPPI kit test method; Water holding duration† – the time (min) for coated paper to hold water at 25 °C without penetration; Oil holding duration‡ – the time (min) for paper composite to hold water at 25 °C without penetration.

dramatically from 5 to 75 mins. Based on the previous section, it is postulated that OGR may be related to the density of the paper composite and positively correlated with hydrogen bonding between cellulose and lignin. Finally, it is noteworthy that the water and oil holding capacity of the paper composite initially increases with the lignin coating grammage, hot-pressing pressure, and temperature but decreases beyond a certain point. This indicates that the LMNP-paper composite can be optimized for maximum water oil resistance.

6.4.3.6 Film morphology

The assessment of film morphology relies on several pivotal parameters, encompassing film completeness, surface roughness, thickness, and uniformity of thickness. To evaluate the dispersion of LMNP within the cellulose matrix, we utilized scanning electron microscopy (SEM) to capture top surface and cross-sectional images of the LMNP-paper composite.

Figure 6.9 depicted the SEM images illustrating both the top surface and cross-section of uncoated paper. Examination of the surface revealed a crisscross arrangement of cellulose fibers without a discernible single orientation. The fibers exhibited a width spanning from 10 to 100 μm. Moreover, numerous micrometer-sized holes punctuated the interwoven fibers. Analysis of the cross-section reveals that the uncoated paper has an average thickness of 109 μm which is constant with the result measured by micrometer. Additionally, it is evident that the degree of fiber packing is lower in uncoated paper when compared to the LMNP-paper composite after hot-pressing.

Figure 6.10a depicted the surface morphology of the paper composite C10-P3-T160-M30. Meanwhile, **Figure 6.11a** illustrates a cross-sectional view of the paper composite C10-P3-T160-M30, presenting a total thickness of 119 μm with a lignin layer thickness of 10 μm. Notably, microcracks of diverse lengths were discernible on the surface of the lignin layer, with a width averaging approximately 0.5 μm. Similarly, from **Figure 6.11a-d**, we can find that the thickness of the lignin

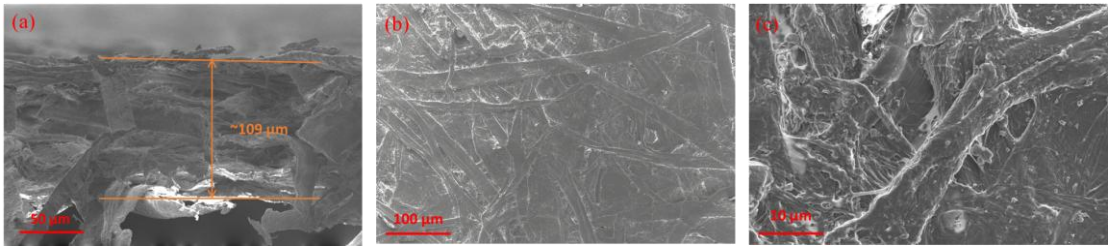

Figure 6.9 Scanning electron microscope (SEM) image of substrate paper, (a) cross section, (b) and (c) top view of paper surface.

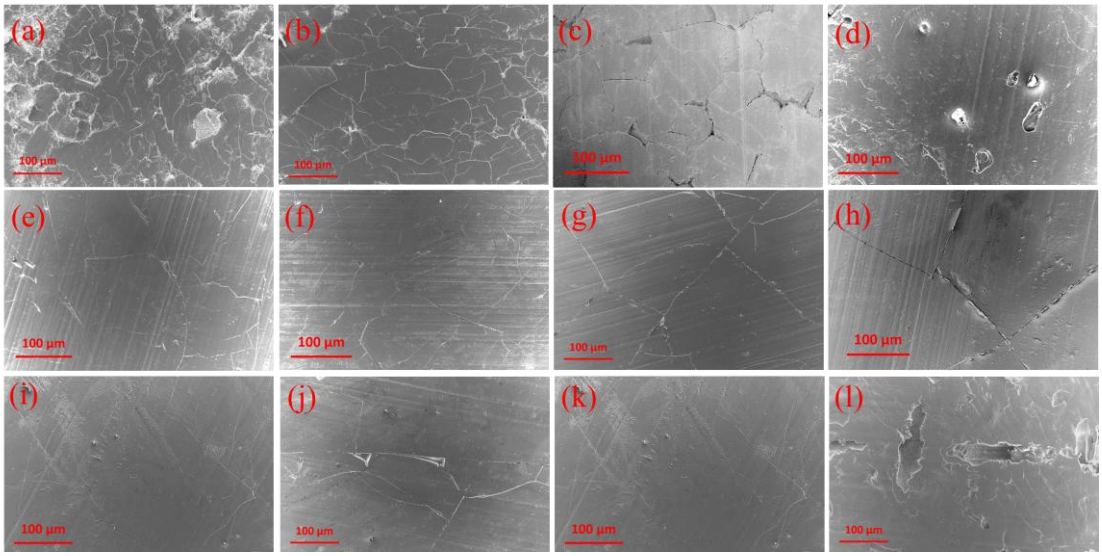

Figure 6.10 SEM image of top view of LMNP-paper composites (a) C10-P3-T160-M30, (b) C20-P3-T160-M30, (c) C30-P3-T160-M30, (d) C40-P3-T160-M30, (e) C80-P3-T120-M30, (f) C80-P3-T140-M30, (g) C80-P3-T160-M30, (h) C80-P3-T180-M30, (i) C40-P1-T160-M30, (j) C40-P5-T160-M30, (k) C40-P3-T160-M10 and (l) C40-P3-T160-M50.

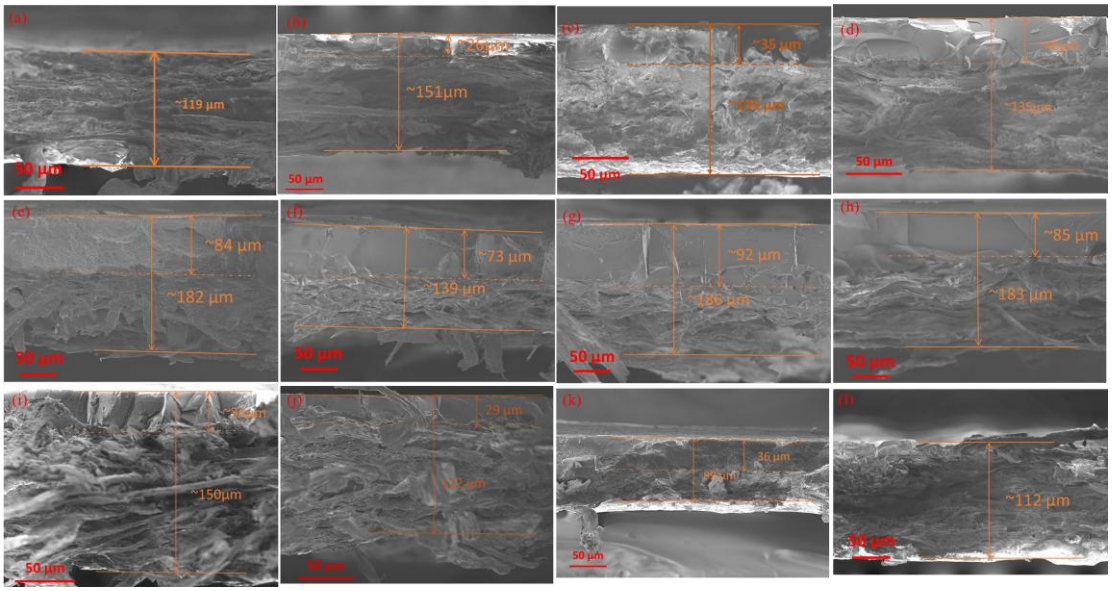

Figure 6.11 SEM image of cross view of LMNP-paper composites (a) C10-P3-T160-M30, (b) C20-P3-T160-M30, (c) C30-P3-T160-M30, (d) C40-P3-T160-M30, (e) C80-P3-T120-M30, (f) C80-P3-T140-M30, (g) C80-P3-T160-M30, (h) C80-P3-T180-M30, (i) C40-P1-T160-M30, (j) C40-P5-T160-M30, (k) C40-P3-T160-M10 and (l) C40-P3-T160-M50.

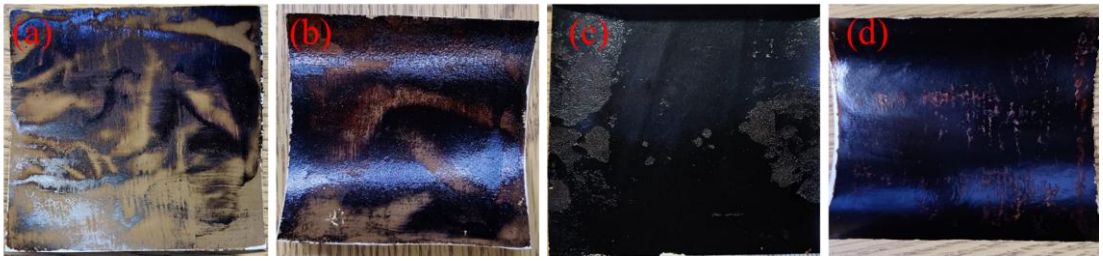

Figure 6.12 photos of LMNP paper composite with different temperatures in the hot press, (a) C80-P3-T120-M30, (b) C80-P3-T120-M30, (c) C80-P3-T160-M30, (d) C80-P3-T180-M30.

layer increased as the weight of the coating increases. When the weight of the LMNP coating reached 40 g/m^2, the thickness reached a maximum of 40 µm. When the weight of the LMNP layer reached more than 30 g/m^2, some pits ranging from a few microns to tens of microns appear on the surface of the lignin film, and some cracks up to 1 µm width also appeared.

In **Figure 6.10e-h and Figure 6.11e-h**, the morphological characteristics of composite materials were depicted as influenced by temperature. Remarkably, variations in temperature did not yield significant changes in the overall thickness of the composite material or the thickness of the lignin layer, which remained relatively constant at about 80 µm. However, notable alterations in the micromorphology of the LMNP layer were observed with temperature fluctuations. Particularly, at 120 °C (considerably lower than the lignin glass transition temperature of 160 °C [33] employed in this study), the cross-section of the formed lignin film exhibited a porous structure seen in **Figure 6.11e.** This phenomenon primarily arisen from incomplete melting and flow of lignin, leading to gaps between nanoparticles remaining unfilled. Notably, **Figure 6.12** illustrated that at 120 °C, certain areas of the formed lignin film retain the shape and color of lignin nanoparticles. Additionally, cracks larger than 1 µm persist on the surface of the lignin film across all samples except the one heated to 160 °C. Furthermore, the 180 °C sample displayed pits with distinct geometric shapes resulting from material loss on its surface. This can be attributed to the highest degree of lignin cross-linking at 180°C, as evidenced by the 2D-HQSC NMR data (**Figure 6.4**). Consequently, the lignin film became brittle, leading to easy breakage and surface pitting. These results recommend that 160 °C was the most suitable for lignin film formation using a hot press.

Figure 6.11i and j demonstrates that with increasing pressure from 1 to 5 MPa, the overall thickness of the paper composite decreased from 150 µm to approximately 120 µm, while the thickness of the lignin layer remained relatively constant at about 30 µm. This reduction in thickness primarily stemmed from the

compression of cellulose fibers, resulting in a reduction in voids within the cellulose fiber layer. Notably, the lignin layer exhibited incompressible properties due to the absence of a porous structure, thus leaving no room for further compression during the pressing process. Additionally, cracks with an average width of approximately 1 µm manifest on the surface of the lignin films formed under varying pressures, accompanied by a greater number of cracks with widths below a micron, which can be seen **Figure 6.10i and j**.

Figure 6.10k, l and Figure 6.11k, l illustrated the evolution of paper composite morphology with varying concentrations of moisture content of wet lignin before hot-pressing. At a moisture content of 10 and 50 wt.%, the boundary between the lignin layer and the cellulose layer remains distinct, with a consistent thickness of approximately 40 µm corresponding to the targeted lignin weight of 40 g/m^2. However, a notable transformation occurred when the moisture content reached 50 wt.%. In this instance, the lignin layer became indiscernible, and upon closer examination of the cross-section (**Figure 6.13**), lignin infiltrated the gaps between cellulose fibers. Additionally, the newly formed lamellar lignin, post-melting, was encompassed by cellulose fibers. Despite these changes, microcracks persisted on the surface of the paper composite, with the sample containing 50 wt.% moisture content displaying large pits exceeding 10 µm, a phenomenon absented in other samples. Furthermore, **Figure 6.14**clearly indicated deviations in some areas of the sample surface compared to typical lignin films. The emergence of these pits can be attributed to the rapid movement of water molecules under hot pressure conditions, displacing lignin nanoparticles from their original positions.

In acquiring cross-sectional morphology, to mitigate the influence of mechanical forces on the material, Forced Ion Beam (FIB) technology was employed to etch thin film materials with varying moisture contents during compression in the hot press. The cross-sectional details were depicted in **Figure 6.15**. The delineation between the lignin layer and the cellulose layer was discernible in both 10 wt.% and

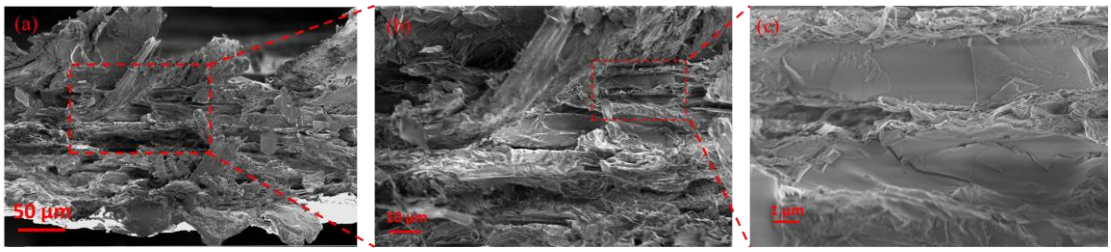

Figure 6.13 SEM images of the cross-section of C40-P3-T160-M50 at high magnification.

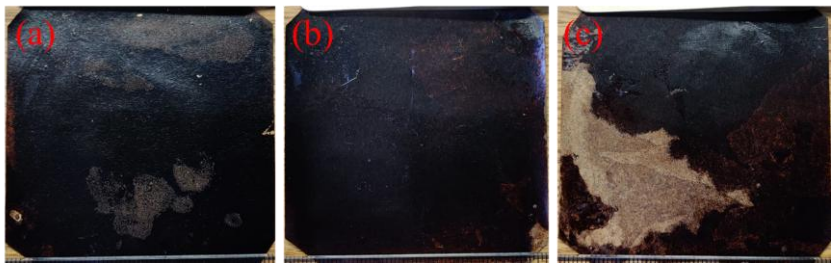

Figure 6.14 photos of LMNP paper composite with the different water content of lignin suspension before the hot press, (a) C40-P3-T160-M10, (b) C40-P3-T160-M30, (c) C40-P3-T160-M50

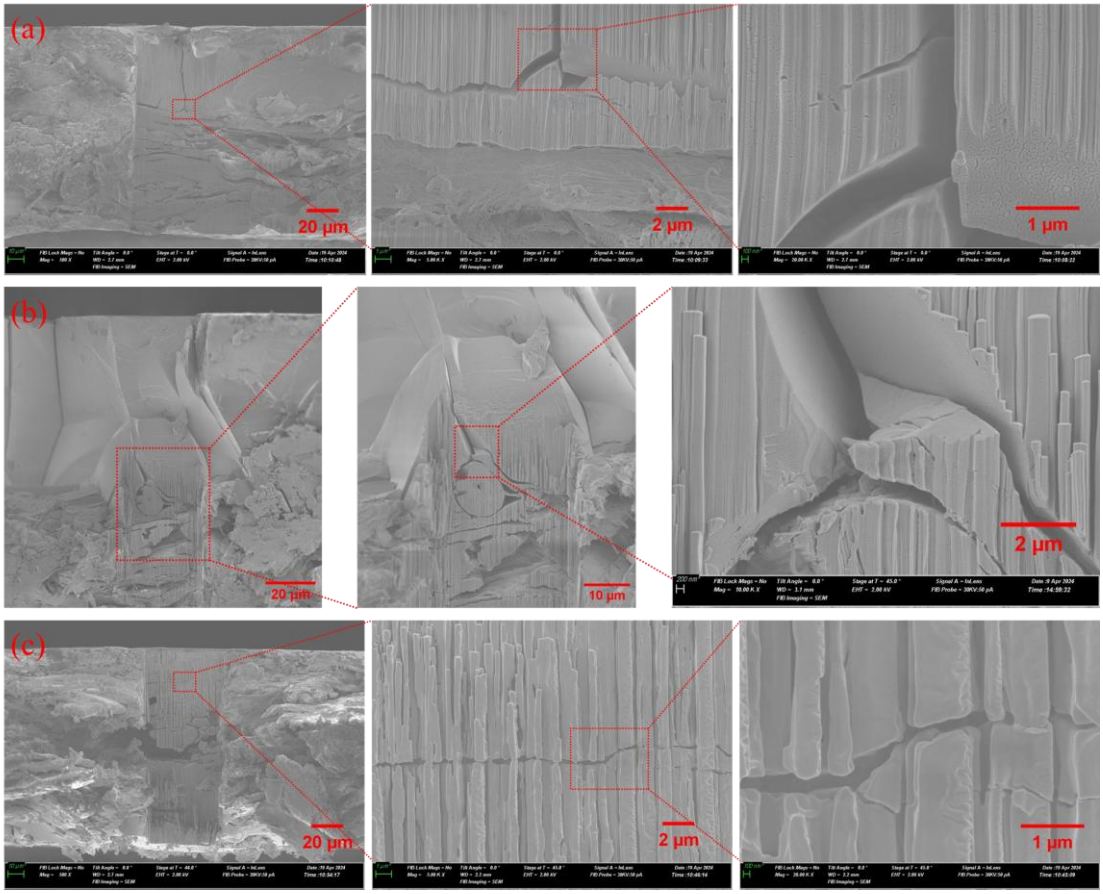

Figure 6.15 SEM images of cross-sections of (a) C40-P3-T160-M10, (b) C40-P3-T160-M30 and (c) C40-P3-T160-M50 prepared using Forced Ion Beam.

30 wt.% moisture content, accompanied by cracks extending from surface to the lignin-cellulose interface. In the case of 50 wt.% moisture content (**Figure 6.15c**), the transition zone between the lignin layer and the cellulose layer was notably broader compared to the other two concentrations. Despite the persistence of cracks, their width had substantially reduced from approximately 1 µm to about 300 nm, and their orientation had shifted from perpendicular to parallel to the film direction. This alteration was highly advantageous for barrier film materials. However, for samples with high moisture content, achieving a smooth surface finish became challenging due to the intense movement of water molecules.

6.4.3.7 Contact angle analysis

The dynamic water contact angle was measured to investigate the surface energy properties of LMNP-paper composite, and to elucidate the influence of manufacturing parameters, such as coating weight, hot-pressing temperature and pressure, and moisture content of wet LMNP layer prior to hot-pressing.

As depicted in **Figure 6.16a**, the contact angles at 60s across varying coating weights ranged from 67° to 80°, without discernible patterns correlating with the weight of the lignin layer. This observation suggested that, provided the lignin layer uniformly coats the substrate, the contact angle remained unaffected by the weight of the lignin coating. This phenomenon can be attributed to consistent surface properties of the lignin layers under comparable conditions, such as temperature and pressure during hot-pressing, leading to minimal alterations in water contact angle.

As illustrated in **Figure 6.16b**, the contact angle at 60s demonstrated an upward trend with increasing pressure during hot press molding, ranging from 64° to approximately 78°. This phenomenon can be attributed to the effect of pressure on the adhesion of lignin to the substrate surface. At lower pressures, inadequate adhesion resulted in incomplete coverage of the substrate surface by lignin, leading to the formation of defects within the lignin layer. These defects contributed to a reduction in the contact angle.

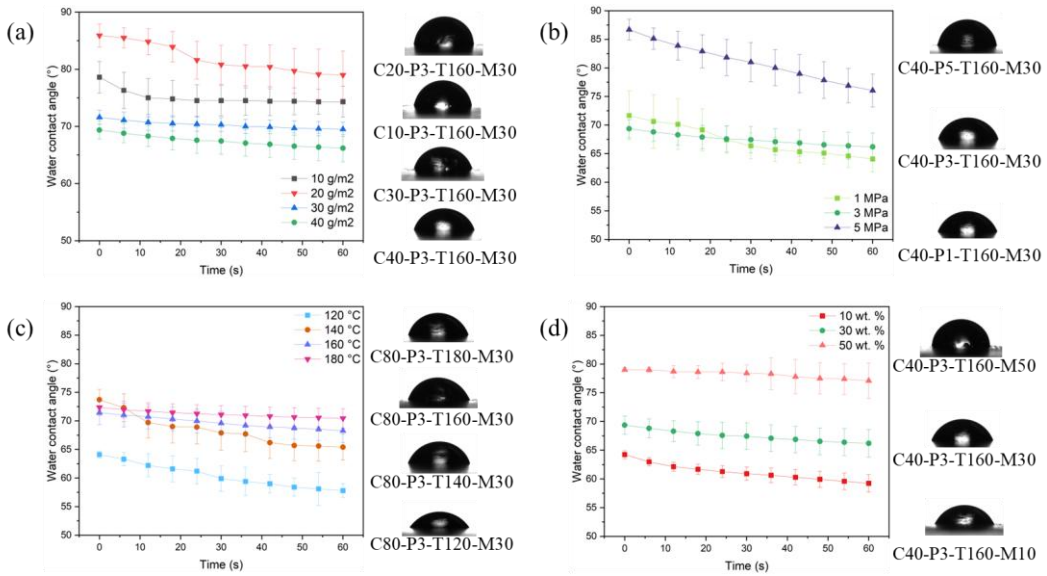

Figure 6.16 The water contact angle over time of LMNP-paper composite with photo at 60s at different (a) coating weight, (b) pressing pressure, (c) pressing temperature, and (d) moisture content of wet LMNP layer prior to hot press.

The influence of hot press temperature on the water contact angle was delineated in **Figure 6.16c**. Notably, the contact angle at 60s increased with rising temperature, ranging from 58° to 72°. The diminished contact angle observed at 120 °C can be attributed to its considerable distance from the glass transition temperature of the used lignin (approximately 160 °C). At this temperature, the LMNP failed to achieve complete melting and flow, thereby precluding the formation of a dense and uniform lignin film. Consequently, the resulting surface defects contributed to the reduction in the contact angle. The surface quality improved as the temperature increased, resulting in a high WCA compared to that at 120 °C.

The impact of the moisture content of wet LMNP layer on the contact angle was elucidated in **Figure 6.16d**. Notably, the contact angle risen as moisture content increased. Specifically, at a moisture content of 10 wt.%, the contact angle at 60s measured 58°, whereas at 50 wt.% moisture content, it peaked at 78°. At lower moisture content levels, the reduced contact angle can be attributed to insufficient wetting of nano-lignin particles, impeding their complete flow under hot-pressing conditions. Consequently, fewer intermolecular hydrogen bonds were formed compared to higher moisture content levels, resulting in compromised lignin film quality and the emergence of surface defects (as depicted in **Figure 6.14**). Conversely, at higher moisture content levels, excess water evaporated rapidly under hot pressure conditions, leading to the discharge of non-evaporated water into the surroundings due to the rapid movement of species. This phenomenon caused a significant detachment of lignin nanoparticles from the substrate surface, thereby compromising the integrity of the lignin film. Interestingly, this surface got the highest contact angle.

Overall, the water contact angles at 60s of LMNP-paper composite prepared in this study ranged from ~60 to ~90°. And the contact angle decreased over time on certain samples, likely as a result of water wicking into the material. However, these values fall short of the threshold exceeding 90° typically associated with hydrophobic materials.[192] Consequently, the waterproof and oil-resistant properties of these

composites were largely contingent upon their ability to block liquids away by forming barrier films.

6.4.4 Biodegradation analysis

Nondegradable materials used in disposable tableware and packaging accumulate in the environment, posing risks to wildlife and human health.[3, 32, 200] The degradability of the developed LMNP-paper composite is crucial for its future application. Given that cellulose and lignin are biodegradable[103, 105, 201], their derived composites should also exhibit biodegradability. Preliminary aerobic biodegradation studies of one of the LMNP-paper composites C40-T160-P3-M30, in garden soil showed that the LMNP-paper composite became wet and soft within the first 7 days, broke into several parts after 14 days, and progressively disintegrated over time. By 56 days, the composite had disappeared or too small to be observed (**Figure 6.17**). This demonstrated that the hot-pressed LMNP-paper composite offers a significant advantage over plastic coatings or PFAS additives for paper products.

6.5 Conclusion

The development of a fully plant-based water- and oil-resistant paper composite presents a significant advancement in the quest for sustainable disposable tableware. Through the optimal application of a lignin film using hot-pressing, we have demonstrated a method to achieve high levels of water and oil resistance without relying on harmful PFAS or plastic coatings. The study identified the optimal conditions for the lignin film application as 40 g/m² LMNP film weight, 3 MPa pressure, 160 °C temperature, and 30 wt.% moisture content of wet LMNP layer. These conditions result in a paper composite with excellent durability, capable of holding water for 100 minutes and oil for 25 minutes. Importantly, the composite biodegrades within 56 days in garden soil, underscoring its environmental benefits. This research not only addresses the immediate need for eco-friendly disposable tableware but also sets the stage for further innovations in sustainable packaging solutions.

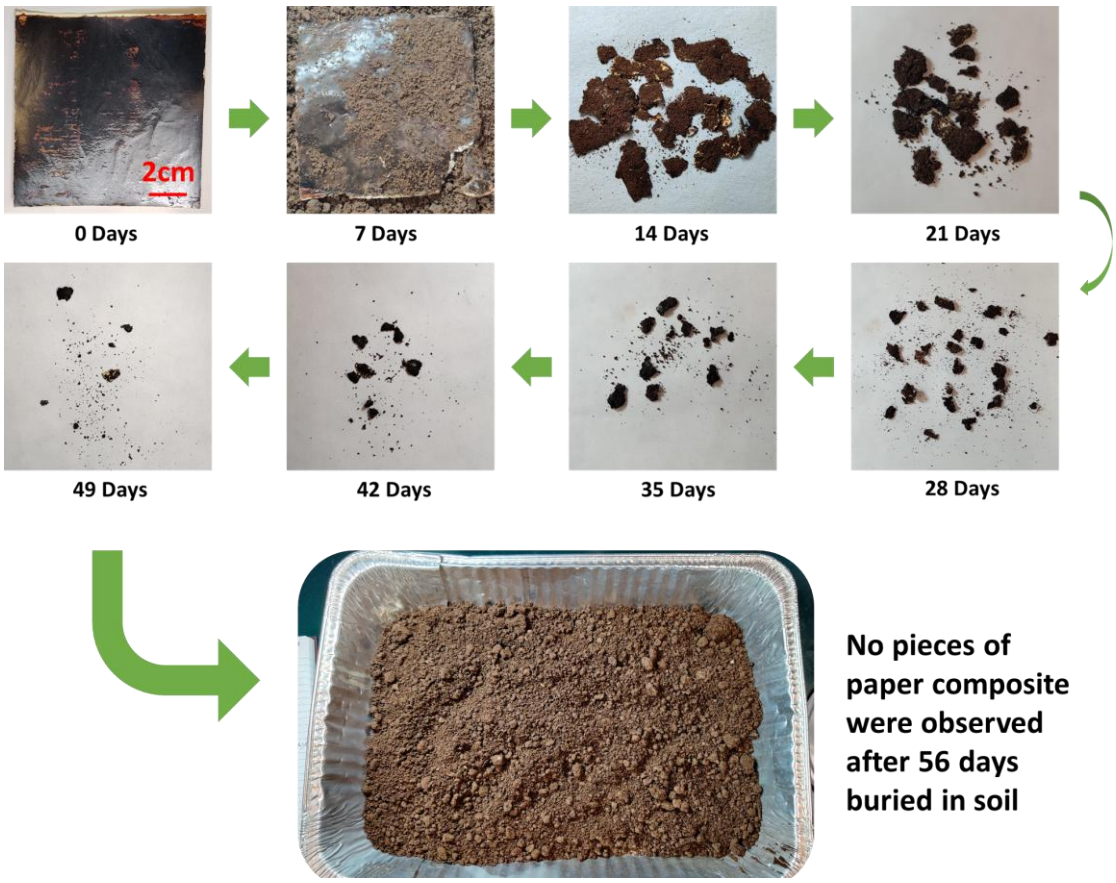

Figure 6.17 Degradation of LMNP-paper composite in garden soil.

CHAPTER SEVEN : SANDWICH-STRUCTURED PAPER COMPOSITE WITH WATER AND OIL RESISTANCE FOR FOOD PACKAGING AND TABLEWARE APPLICATIONS

A version of this chapter is originally written and considered for submission as: Zhongjin Zhou, Lauren Merrill, Xianhui Zhao, Shahab Saedi, Nicole Labbé, Tong Wang, Harry M. Meyer III, Sanjita Wasti, Siqun Wang. (2025). Sandwich-structured paper composite with water and oil resistance for food packaging and tableware applications. *Composites Part B: Engineering*.

Author contributions are listed as follows. **Zhongjin Zhou:** Conceptualization, Methodology, Formal analysis, Investigation, Writing, Original Draft, Writing, Review & Editing. **Siqun Wang:** Conceptualization, Methodology, Formal analysis, Investigation, Review & Editing, Supervision, Project Administration, Funding Acquisition. **Lauren Merrill:** Investigation, Validation, Review & Editing. **Xianhui Zhao:** Experimentation and Analysis of XPS and EDX, Review & Editing. **Shahab Saedi:** Review & Editing. **Nicole Labbé:** Conceptualization, Resources, Review & Editing, Funding Acquisition. **Tong Wang:** Resources, Review & Editing. **Harry M. Meyer III:** Experimentation and Analysis of XPS. **Sanjita Wasti**: Experimentation and Analysis of SEM and EDX

7.1 Abstract

The growing environmental challenges posed by plastic waste from disposable tableware highlight the urgent need for sustainable alternatives. Traditional plastics decompose over centuries, generating microplastics that threaten ecosystems and human health. While lignin has emerged as a promising material for plastic replacement, its inherent dark brown color and processing challenges in paper-based products have limited its application, particularly in food-contact materials. To address these limitations, we have developed biodegradable sandwich-structured paper composites comprising parchment paper as surface layers and a lignin-polymer core with polyvinyl alcohol (PVA) and polylactic acid (PLA). This innovative structure eliminates the need for binders, minimizing potential food contamination, and enables direct application as packaging or molded tableware. Lignin enhances durability and provides natural water and oil resistance without harmful additives, such as per- and polyfluoroalkyl substances (PFAS), while PVA and PLA improve the composite's tenacity. The resulting material, composed of 65 wt.% lignin, demonstrates excellent water and oil resistance, with no penetration exceeding one hour, and exhibits enhanced tensile strength (45 MPa), making it a viable and eco-friendly alternative for disposable tableware.

7.2 Introduction

The widespread use of disposable plastic tableware has significantly contributed to the global plastic waste crisis [3]. Plastics may take centuries to degrade, and as they break down, they release microplastics that contaminate soil and water, infiltrate the food chain, and harm wildlife and human health [4, 202]. Although biopolymers have been extensively researched as sustainable alternatives, most degradable biopolymers, such as polylactic acid (PLA), Polycaprolactone (PCL), Polyvinyl alcohol (PVA), Polyglycolide (PGA), Polyhydroxyalkanoates (PHA), and Polyhydroxybutyrate (PHB), require specific environmental conditions to achieve complete degradation [1, 202-206]. Furthermore, the high cost of these biopolymers

remains a major barrier to their widespread adoption when compared to conventional petroleum-based plastics [207]. In response to these challenges, there is growing interest in natural fiber-based tableware as an eco-friendly alternative. However, pure cellulose fiber paper is inherently unsuitable for containing water or oily foods, particularly at elevated temperatures [9]. To address these limitations, commercial solutions have often relied on wet-end additives, such as per- and polyfluoroalkyl substances (PFAS) or the application of plastic films or aluminum films to achieve necessary oil and water resistance. Despite their effectiveness, PFAS are persistent, bioaccumulative, and linked to severe health risks due to environmental contamination and polluted drinking water [12, 15]. Regulatory restrictions on PFAS further emphasize the need for sustainable alternatives [2]. Consequently, identifying substitute materials that eliminate nondegradable plastics and PFAS is an urgent priority in advancing eco-friendly tableware solutions.

To address the challenges of sustainable disposable tableware, plant-based polymer materials have emerged as promising alternatives [103, 208, 209]. Among these, lignin, a natural polymer and protector in plants, stands out due to its inherent hydrophobic properties, which provide resistance to water [210, 211]. This characteristic makes lignin particularly suitable for containers designed to hold liquids without significant leakage over time. Unlike many synthetic materials, lignin is biodegradable, allowing lignin-based products to break down in an environmentally friendly manner at the end of their lifecycle, thereby minimizing environmental impact [112, 212-214]. As a byproduct of the paper and pulping industry, lignin is abundant, renewable, and its use aligns with sustainable practices by reducing dependence on non-renewable resources. The development of nano-lignin has further expanded the application potential of lignin [68]. For instance, Zhou and colleagues successfully prepared a high-solid-content lignin micro- and nano- particles (LMNP) suspension using ultrafine grinding. This LMNP suspension was subsequently coated onto paper and transformed into a dense, functional coating through hot pressing, demonstrating

its potential for producing durable, biodegradable tableware [30]. However, application of lignin in materials such as disposable tableware has been limited by its poor mechanical properties.

To overcome this limitation, blending LMNP with thermoplastics such as PVA and PLA, along with specific additives like ZnO, can enhance its mechanical performance. PVA, rich in hydroxyl groups, interacts with lignin's functional groups, improving interfacial adhesion and creating a mechanically robust composite. This interaction enhances tensile strength, elasticity, and durability, making the material resistant to cracking and suitable for practical applications. PVA's flexibility, toughness, and excellent film-forming capability facilitate the processing of lignin-PVA composites into desired shapes. For example, in Shao et al.'s research, lignin nanoparticles significantly reinforced PVA-based organogels [215]. Choe et al. [216] reported a biodegradable, biocompatible, and high-barrier paper coating using boric acid-crosslinked PVA. The coated papers showed enhanced oxygen (~0.89 cc m^{-2} d^{-1}), water vapor (~5.17 g m^{-2} d^{-1}) barrier properties, oil resistance (grade of 12 based on TAPPI T 559) and retained tensile strength (~53.0 MPa) in moist conditions. PVA's water solubility also ensures uniform blending with LMNP suspension, promoting consistent distribution and preventing localized failures under stress. These advancements highlight the potential of lignin-PVA composites as sustainable, high-performance materials for applications such as disposable tableware. Moreover, the inclusion of PLA further enhances the properties of the composite. PLA, derived from renewable resources like corn starch or sugarcane, provides excellent mechanical strength (~50-70 MPa) and thermal stability, improving the durability and heat resistance of the composite [214]. PLA's compatibility with lignin and PVA ensures a uniform and stable material with enhanced performance. Additionally, PLA imparts good barrier properties against moisture and gases, making the composite more suitable for storing food and liquids[9]. Li et al. [208] developed a method to coat PLA onto cellulose nanofiber (CNF)extracted from sargassum by

soaking CNF in melted PLA. The resulting biodegradable composite exhibited excellent water (~14 wt% absorption) and oil (~0.8 wt% absorption) resistance over 24 hours. ZnO in polymer composites functions as a UV absorber, antimicrobial agent, mechanical reinforcer, thermal stabilizer, and electrical conductor, enhancing durability, strength, and functional properties [182, 217, 218].

Despite extensive research and the development of numerous lignin-based packaging materials, their commercial adoption remains limited, particularly in food packaging and disposable tableware. A major challenge is the inherent dark brown color of the lignin, which many consumers find unappealing. For instance, Hu et al. developed a strong, water-stable, and biodegradable lignin-based paper that outperforms many plastics in tensile strength and barrier properties; however, its color ranges from light brown to black depending on the lignin content, limiting its aesthetic appeal and marketability[201]. Additionally, while lignin-based coatings and films have demonstrated promising water and oil resistance, their direct contact with food raises concerns about potential contamination from extractable components, including unreacted functional groups, residual chemicals from lignin processing, or additives such as melamine-formaldehyde resin, bleaching agents, alkyl ketene dimer (AKD), and PFAS [17, 219-223].

To address these challenges, we developed a sandwich-structured paper composite optimized for roll-to-roll coating processes. Unlike traditional lignin-based coatings, which are either applied as surface layers or blended into fiber matrices, our approach strategically embeds the functional polymer layer between two layers of parchment paper, effectively eliminating direct contact between lignin-based materials and food. This design mitigates concerns about food contamination while maintaining the oil and water resistance essential for disposable tableware applications. The use of a LMNP-PVA-PLA-ZnO blend further distinguishes our work from previous studies by balancing hydrophobicity, mechanical strength, and biodegradability, offering an environmentally friendly alternative without the need for

additional plastic films or chemical binders. Furthermore, our study employs a mixture design approach using JMP software to systematically optimize the composition of each component, ensuring enhanced material performance in terms of water and oil resistance, and mechanical integrity. Unlike previous studies that primarily report empirical formulations, our data-driven optimization provides a structured approach to tailoring material properties for scalable manufacturing. The sandwich structure not only enhances durability but also minimizes microplastic migration, a growing concern in both polymer films and fiber-based tableware. This innovative composite can be directly utilized as biodegradable food packaging or molded into tableware, offering a commercially viable alternative that bridges the gap between laboratory research and real-world applications.

7.3 Experimental methods

7.3.1 Materials and sample preparation

The kraft softwood lignin used in this study is described in Section 3.1, and the preparation of LMNPs is detailed in Section 3.2.1. Polymer blend preparation was described in section 3.2.3. Sandwich structure LMNP-paper composites preparation was described in section 3.2.4.

7.3.2 Characterizations

Fourier-transform infrared (FTIR) spectroscopy analysis is described in Section 3.4.1.2, while thermal analysis is discussed in section 3.4.1.4, HSQC-NMR was described in section 3.4.1.5 and morphological and particle size analysis was detailed in section 3.4.2. Performance of paper composites including oil and water resistance, and mechanical strength assessment was described in section 3.4.4.

7.4 Results and discussion

7.4.1 Size and micromorphology of LMNP

The LMNPs used in this study were the same as those described in our previous publication [30]. The size of the lignin particles was measured using dynamic light scattering (DLS), which revealed a mean particle size of 120 nm with a

polydispersity index (PDI) of 0.50 ± 0.03, indicating a non-uniform particle system. The particle size distribution was further corroborated by scanning electron microscopy (SEM) images shown in **Figure 7.1**. The SEM analysis also highlights the micromorphological characteristics of the lignin particles, demonstrating that they are irregularly shaped rather than spherical nanosolids.

7.4.2 Chemical functional groups

The Fourier-transform infrared (FTIR) spectra of samples 10# (63 wt.% LMNP, 13 wt.% PLA, 13 wt.% PVA, and 10 wt.% Zn $(NO_3)_2$) and 20# (100% LMNP) (shown in **Figure 7.2**) exhibit characteristic lignin peaks at 1592 cm^{-1}, corresponding to aromatic skeletal stretching in lignin, as reported previously [224]. These peaks confirm the presence of LMNPs in the composite. Additionally, typical peaks at 2936 cm^{-1} (asymmetric stretching of CH_2) and 2906 cm^{-1} (symmetric stretching of CH_2) from PVA [225], as well as a peak at 1750 cm^{-1} representing C=O stretching in PLA[226], were observed in the spectra of both samples. These findings confirm the successful incorporation of LMNPs, PVA, and PLA into the composite.

7.4.3 Thermal analysis

The thermal stability of sandwich structure paper composites was assessed using TGA, as shown in **Figure 7.3**. Sample 10# and sample 20# were tested alongside two reference materials of pure LMNP and uncoated paper. From room temperature to 105 °C, all samples exhibited a slight weight loss, attributed to the evaporation of adsorbed water. The key differences were observed in the derivative thermogravimetric (DTG) curves. Unlike pure LMNP, which displayed a gradual weight loss without distinct peaks due to the broad distribution of functional groups, the other three samples exhibited clear peaks. For uncoated paper, a peak at 360 °C in the DTG curve corresponded to the pyrolysis of crystalline regions of cellulose [227]. Samples 10# and 20# showed similar peaks, located at 350 °C and 358 °C, respectively, influenced by the incorporation of other polymers like LMNP. Additionally, sample 20# displayed a broad peak at 254 °C, indicating the early

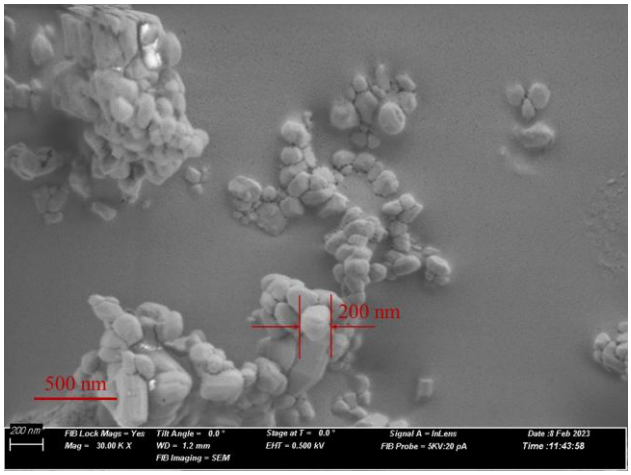

Figure 7.1 SEM image showing morphology and dimensions of LMNPs

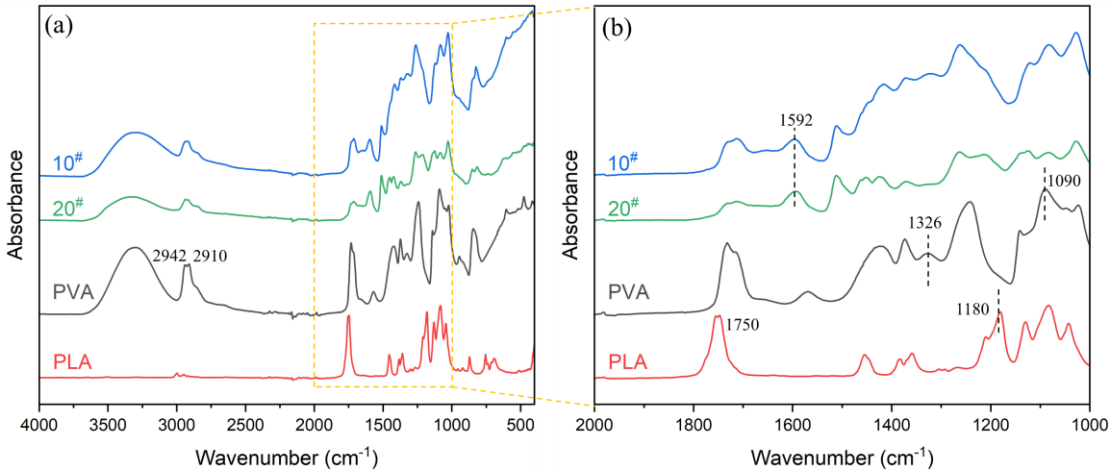

Figure 7.2 (a) FTIR spectra of samples 10# and 20#, with PVA and PLA as reference materials, (b) magnification of the region between 1000–2000 cm^{-1}.

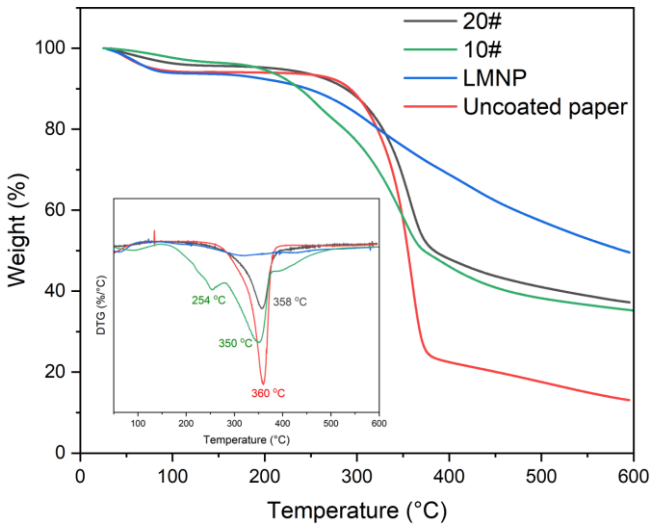

Figure 7.3 Thermogravimetric analysis (TGA) and derivative (DTG) analysis of sandwich structure paper composite

degradation of PLA, catalyzed by MgO and its interactions with other components in the composite, such as lignin and cellulose. This peak also reflects the decomposition of PVA through the elimination of water or small volatile compounds [228, 229]. In conclusion, while the paper composites exhibit slightly reduced thermal stability compared to uncoated paper, their thermal performance remains sufficient for practical applications, as temperature for hot press is usually below 200 °C [230].

7.4.4 Characterization of films

Microscale morphology provides valuable insights into the mechanisms underlying the composite's resistance and mechanical performance. **Figure 7.4** illustrates the SEM microscale morphology of sandwich structure composites and their cross-sectional surfaces after tensile testing. **Figure 7.4** presents the elemental distribution of C, O, and Zn within the interlayer of the polymer blend in sandwich structure paper composite sample 10#. The uniform dispersion of all elements indicates that ZnO was well-integrated into the polymer blend. **Figure 7.4b** presents the tensile-fractured surfaces of pure substrate paper and selected sandwich-structured paper composites with varying formulations. The cross-sectional images reveal the formation of a continuous, dense polymer blend layer in all composites. However, differences in the fractured surface details were observed, attributable to variations in polymer blend formulations**. Figure 7.4c** highlights the fractured surface details of sample 10#, where the polymer blend layer exhibited a straight, smooth surface, even under 5,000× magnification. This non-porous structure effectively blocks liquid penetration, such as vegetable oil. In contrast, the fractured surface of sample 20#, which consisted of 100% LMNP, displayed several fractures approximately 1 micron wide, as shown in **Figure 7.4**d. These structural discontinuities explain the inferior liquid resistance of sample 20# compared to sample 10#. Additional high-magnification cross-sectional images of other sandwich-structured paper composites after tensile testing are provided in **Figure 7.5**. Generally, smoother cross-sections with fewer fractures indicate higher resistance to liquid penetration.

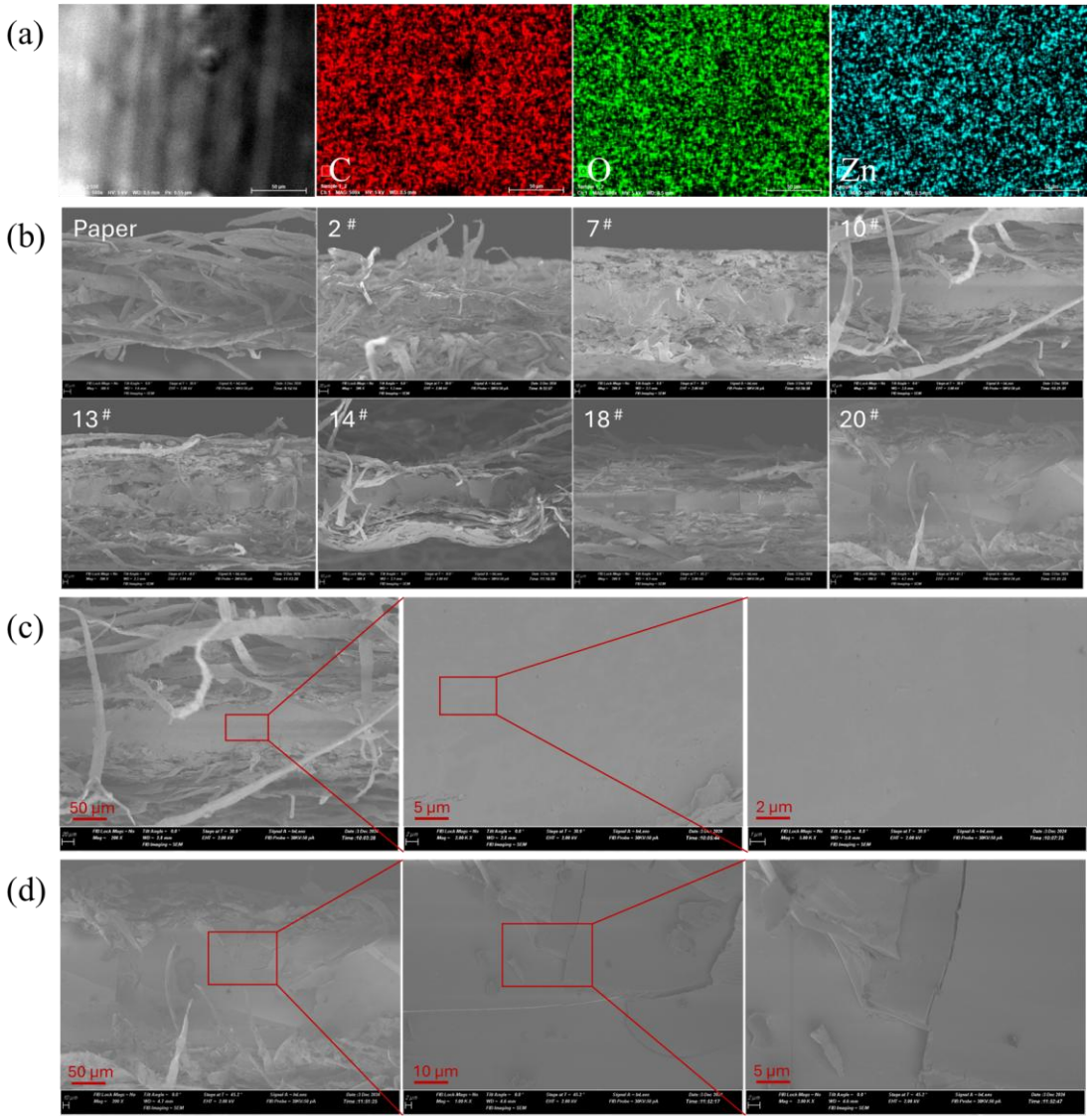

Figure 7.4 SEM and EDX analysis of paper composites: (a) elemental mapping (C, O, Zn) for sample 10#, (b) cross-section of composites, (c) high-magnification view of sample 10#, (d) high-magnification view of sample 20#.

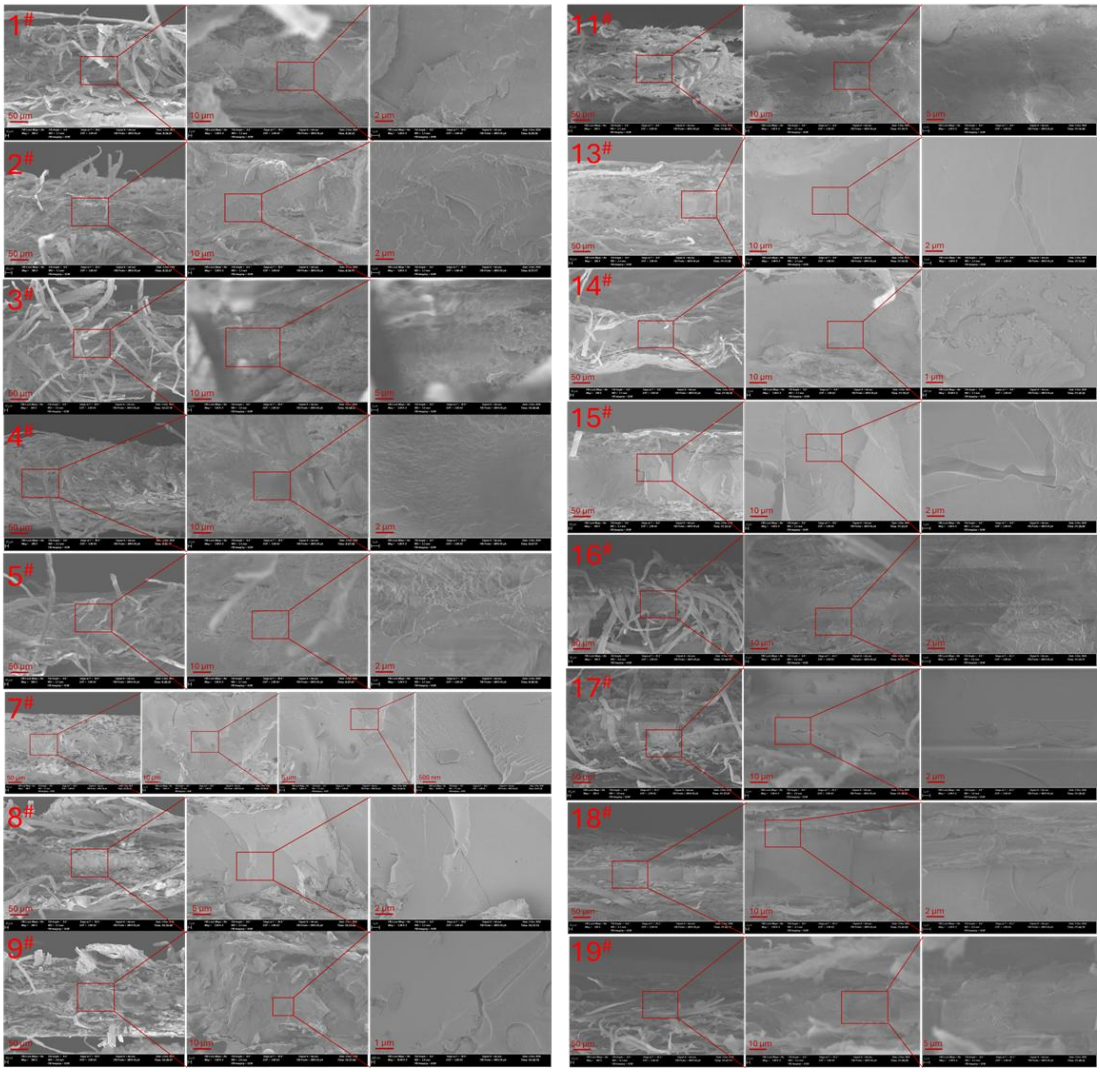

Figure 7.5 SEM Cross-Section Images of Sandwich-Structured Paper Composites at Multiple Magnifications.

7.4.5 Visual appearance

In natural wood, the lignin content significantly influences the optical properties of wood-derived structural materials, and a similar trend is observed in fabricated lignin-cellulose composites. While cellulose is inherently optically colorless or white, lignin possesses a complex, dark-colored structure. **Figure 7.6** illustrates the appearance of the interlayer of the sandwich structure without cover paper, which exhibits a dark color, close to black. This unevenly distributed dark color may raise concerns among consumers regarding the aesthetic appeal of such tableware products, potentially hindering the broader adoption of lignin-based materials. However, the introduction of a sandwich structure has addressed this issue.

Figure 7.7 displays the outer appearance of the sandwich-structured paper composites. In most cases, the dark color of the interlayer was successfully concealed. However, samples 7–9$^{\#}$, 13$^{\#}$, 15$^{\#}$, and 17$^{\#}$ did not perform well in improving the outer appearance, as numerous dark dots were visible on the surface. These dark dots resulted from the migration of the polymer blend through the cover paper. For samples 7–9$^{\#}$, the dark dots were primarily composed of PLA, where the PLA content ranged from 40–50 wt.%. PLA, being water-insoluble, formed large particles that melted and penetrated the cover paper under heat and pressure rather than mixing effectively with LMNP and PVA.

When the PLA concentration decreased to 20–25 wt.% (as in samples 13$^{\#}$, 15$^{\#}$, and 17$^{\#}$) but with 0% PVA, the size of the dark dots reduced but did not disappear. In conclusion, excessive PLA particles tend to penetrate the cover paper during hot pressing. The inclusion of PVA, as demonstrated in samples 4–6$^{\#}$ (containing 20–25 wt.% PLA and PVA), effectively mitigated this issue, resulting in cover paper that retained its original color and improved aesthetic quality. Additionally, this problem can be further addressed by using thicker cover paper, which would provide better resistance to PLA penetration.

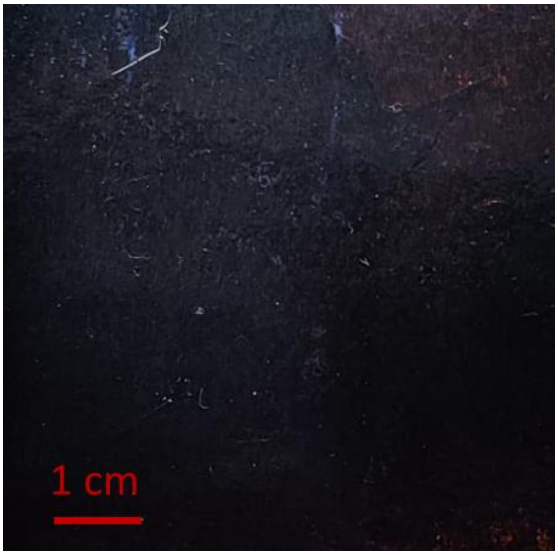

Figure 7.6 View of the Exposed Interlayer in Sandwich-Structured Paper Composite 20# Without Cover Paper.

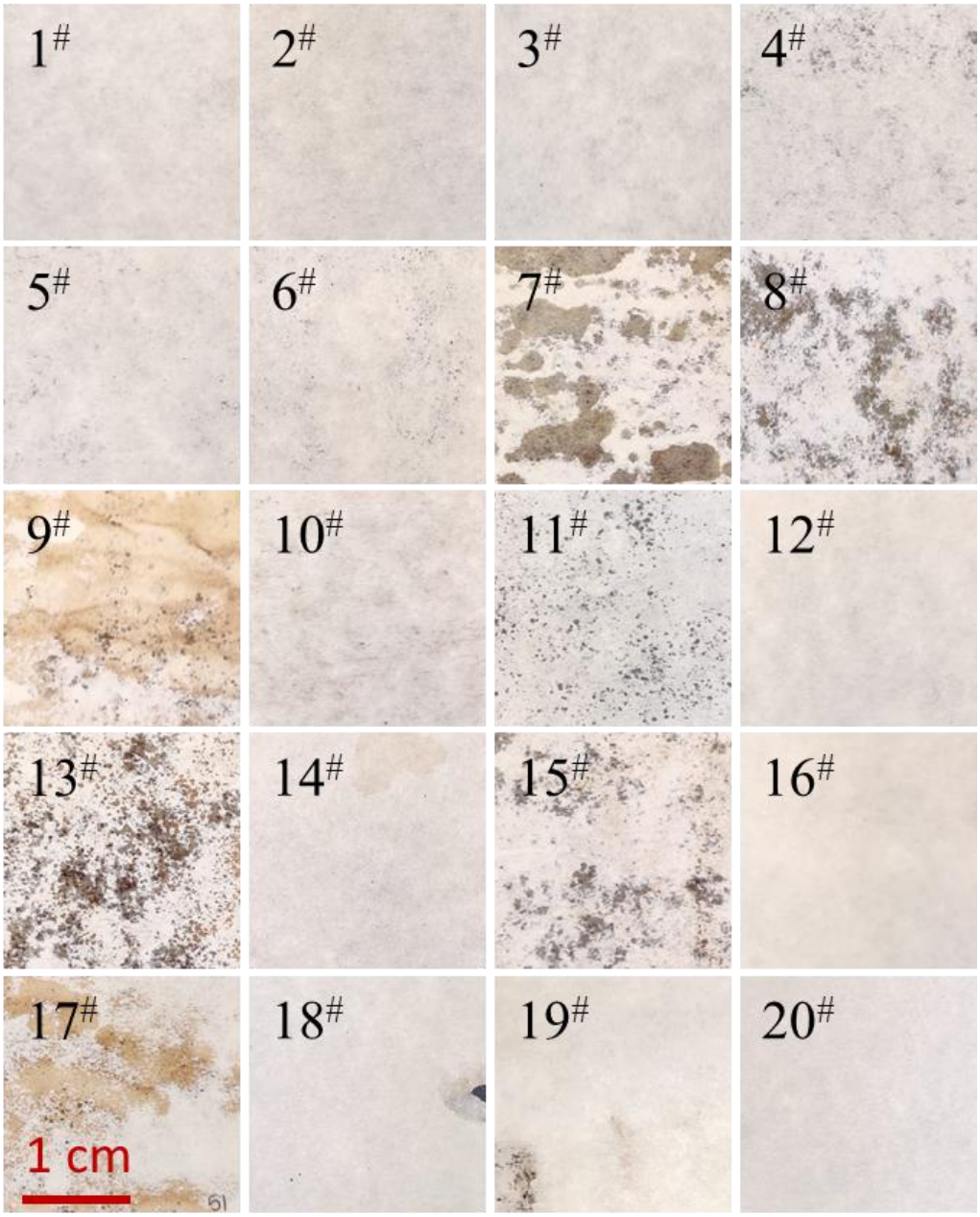

Figure 7.7 Overall view of all sandwich-structured paper composites

7.4.6 Performance of paper composite

Mechanical strength is a critical property of paper plates, ensuring durability and resistance to bending or tearing, which is essential for securely holding food and liquids. Water and oil resistance are equally important, as they determine the plate's ability to repel liquids without soaking, warping, or breaking down. These properties enable the plate to effectively contain moist or greasy foods without leaking or losing structural integrity. In this study, tensile strength, oil-holding time at room temperature and 60 °C, and water-holding time at room temperature were selected as response variables influenced by different formulations of the biodegradable sandwich structure paper composite. The response patterns of the selected variables in relation to the proportions of the four components are illustrated in **Figure 7.8**.

Regarding tensile strength, the addition of PVA was found to enhance this property. This improvement is attributed to the hydroxyl groups in PVA, which promote bonding between lignin and the base paper. For oil resistance, increasing the PVA content significantly improved performance. PVA, being water-soluble, disperses uniformly in water before hot pressing and evenly coats lignin and PLA particles, forming a more consistent polymer layer that reduces defects (**Figure 7.4**) and prevents oil molecules from penetrating the paper composite. This trend was observed at both room temperature and 60 °C, as shown in the PVA column in **Figure 7.8**. Conversely, water resistance exhibited an inverse relationship to oil resistance. As shown in **Figure 7.8** (subfigure with PVA on the x-axis and water retention on the y-axis), water resistance decreased with higher PVA content but improved with increasing PLA content. This can be attributed to PVA's water solubility, which naturally reduces water resistance, whereas PLA, a well-established hydrophobic polymer, effectively enhances waterproofing properties.

The role of Zn in this study was limited, with two possible explanations. First, Zn may not form coordination bonds with oxygen atoms in the other polymers, resulting in no significant enhancement effect. Alternatively, if such bonds do form,

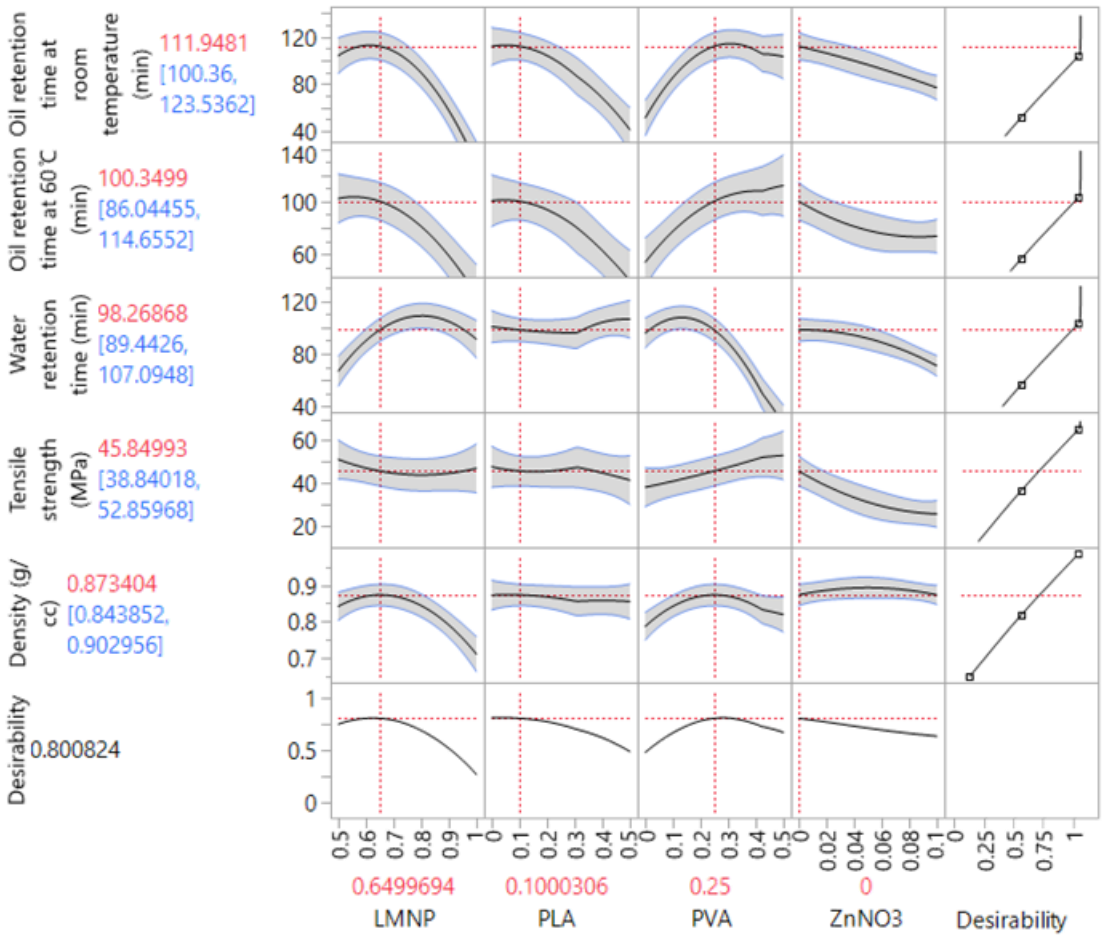

Figure 7.8 Prediction profiler showing five responses as functions of component percentages. The component percentages are shown on the X-axis, and response values are shown on the Y-axis. The gray-shaded area represents the error range along the prediction line.

they may be too weak to provide meaningful reinforcement [231].

Density was also investigated, particularly its correlation with oil resistance. The results showed that density, which varied with the formulation, exhibited a similar trend to water and oil resistance—where higher density corresponded to longer retention times for both— as seen in **Figure 7.8** (density row and liquid retention rows). This can be attributed to the fact that higher density implies a less porous structure, thereby reducing the number of channels available for liquid penetration.

7.4.7 Optimization

To make the optimization results more visually intuitive, a mixed profile was developed, as shown in **Figure 7.9**, based on raw data presented in **Table 7.1**. In this figure, the water holding time was set at 80 minutes, and the oil holding time at room temperature was also set at 80 minutes, both exceeding the market requirement of 30 minutes [10], while the tensile strength was set to 44 MPa, matching the strength of existing market products[232]. The shaded areas in **Figure 7.9** indicate regions that do not meet these criteria, whereas the unshaded (colorless) areas represent results that exceed the set values. Thus, the colorless region identifies the conditions under which all requirements are satisfied. From the data corresponding to the colorless points in **Figure 7.9**, it was observed that when the LMNP content was 65 wt.%, the PLA content was 10 wt.%, the PVA content was 25 wt.%, and the Zn content was zero, the resulting composite met all specified performance requirements. Regarding the influence of Zn content, **Figure 7.10** shows that the presence of Zn (5 wt. %) eliminated the colorless region that met all conditions, further confirming that Zn had no positive effect on performance. Among the affected properties, tensile strength experienced the most significant reduction, decreasing from approximately 46 MPa to ~30 MPa, likely due to the catalytic effect of ZnO on polymer decomposition. However, ZnO did lead to a slight increase in density.

Table 7.1 Performance (Mechanical Strength and water and oil resistance) and Physical Characteristics of Sandwich-Structured Paper Composites.

Species Order	Thickness (mm)	Grammage (g/m^2)	Density (g/m^3)	Tensile strength (MPa)	Elongation at break (%)	*Water retention time (min)	*Oil retention time at room temperature (min)	*Oil retention time at 60℃ (min)
1	0.267±0.008	218±4	0.813±0.018	34.0±11.9	3.88±1.75	23±6	100±0	100±0
2	0.252±0.004	214±6	0.847±0.035	45.0±13.0	4.37±1.58	27±3	100±0	100±0
3	0.253±0.004	207±4	0.817±0.029	49.6±20.8	5.55±1.88	22±6	100±0	100±0
4	0.252±0.003	215±11	0.852±0.039	31.2±10.9	1.81±0.17	20±0	33±7	100±0
5	0.261±0.009	223±1	0.854±0.027	39.5±14.0	3.30±0.96	100±0	100±0	100±0
6	0.259±0.005	217±6	0.835±0.012	37.8±20.1	6.00±1.67	100±0	100±0	100±0
7	0.285±0.008	246±7	0.861±0.046	17.9±6.2	0.80±0.09	100±0	8±6	38±12
8	0.274±0.005	245±2	0.893±0.022	23.2±5.9	1.33±0.21	100±0	13±6	100±0
9	0.298±0.017	258±17	0.866±0.018	46.6±3.6	4.13±0.30	100±0	23±6	17±3
10	0.279±0.021	232±4	0.833±0.049	17.5±7.7	1.20±0.05	100±0	23±3	38±12
11	0.272±0.003	259±7	0.951±0.033	56.0±2.2	4.97±0.30	100±0	100±0	33±16
12	0.261±0.006	237±3	0.908±0.028	19.2±7.6	1.39±.032	100±0	100±0	23±8
13	0.309±0.018	282±9	0.914±0.045	14.9±4.4	0.72±0.11	100±0	13±3	100±0
14	0.284±0.007	252±4	0.884±0.034	21.1±1.3	5.09±0.69	100±0	100±0	33±16

Table 7.1 continued

15	0.302±0.008	272±22	0.899±0.059	22.0±6.6	1.25±0.29	100±0	17±3	60±0
16	0.257±0.006	214±3	0.832±0.014	54.0±1.1	4.68±0.32	100±0	100±0	100±0
17	0.409±0.060	311±12	0.767±0.084	16.7±11.2	4.58±1.29	100±0	100±0	15±0
18	0.251±0.006	205±8	0.814±0.035	22.7±8.8	2.47±0.75	100±0	5±0	100±0
19	0.269±0.020	206±11	0.764±0.020	27.8±11.3	6.48±2.43	100±0	7±3	72±25
20	0.257±0.005	191±2	0.740±0.008	45.3±0.9	4.27±0.19	100±0	5±0	15±0

Note: * 100 mins and above will be noted as 100 mins

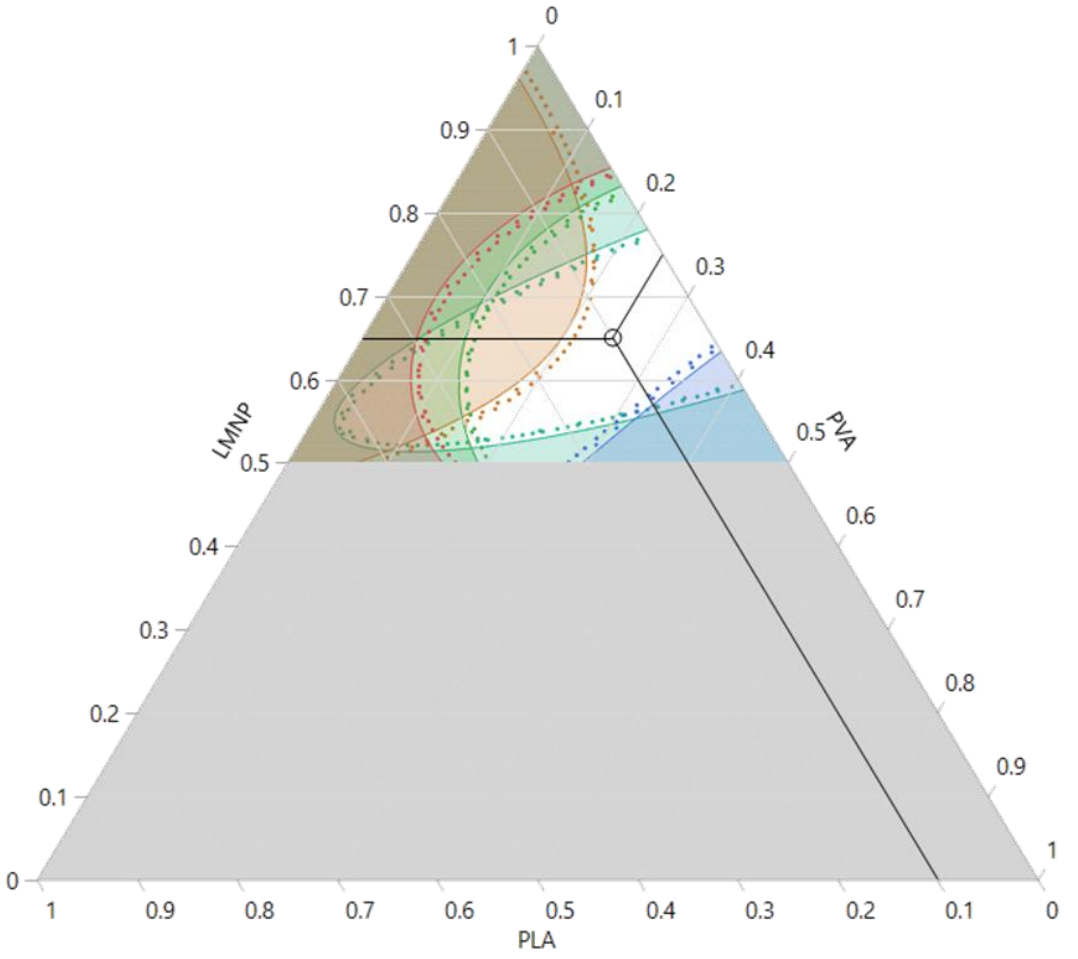

Mixture Profiler

T	L	R	Factor	Current X	Lo Limit	Hi Limit
●	○	○	LMNP	0.65	0.5	1
○	●	○	PLA	0.1	0	0.5
○	○	●	PVA	0.25	0	0.5
○	○	○	ZnNO3	0	0	0.1

Change

Response	Contour	Current Y	Lo Limit	Hi Limit
Time for oil holding (room temperature)	80	111.94862	80	.
Time for oil holding (60 °C)	80	100.35006	80	.
Time for water	80	98.27076	80	.
Tensile strength (MPa)	44	45.849961	44	.
Density (g/cm3)	0.86	0.8734043	0.86	.

Figure 7.9 Mixture profiler showing 5 responses as functions of lignin, PVA, and PLA percentages at 0 wt.% $Zn(NO_3)_2$.

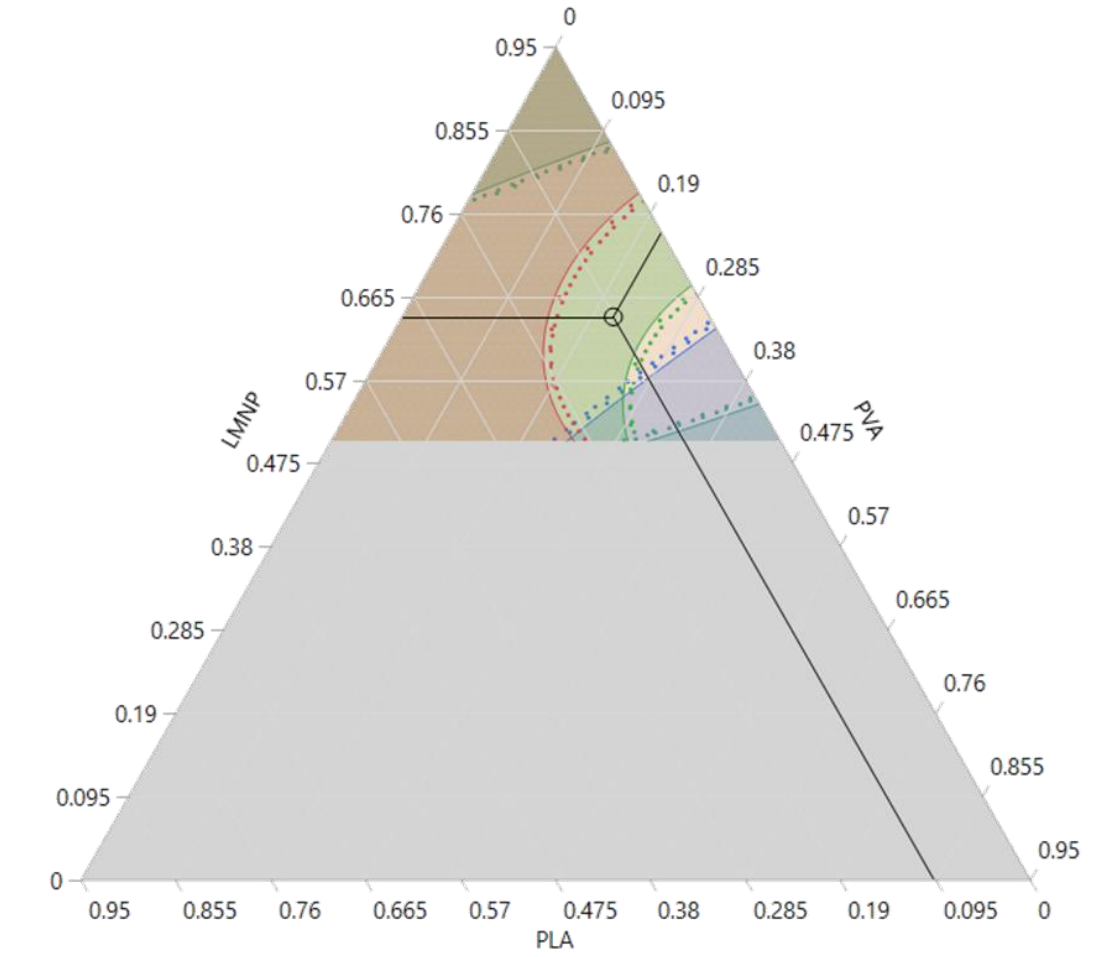

Mixture Profiler

T	L	R	Factor	Current X	Lo Limit	Hi Limit
◉	○	○	LMNP	0.64205	0.5	1
○	◉	○	PLA	0.0963916	0	0.5
○	○	◉	PVA	0.2115584	0	0.5
○	○	○	ZnNO3	0.05	0	0.1

Change

Response	Contour	Current Y	Lo Limit	Hi Limit
Time for oil holding (room temperature)	80	93.347742	80	.
Time for oil holding (60 °C)	80	74.931966	80	.
Time for water	80	97.319762	80	.
Tensile strength (MPa)	44	30.140898	44	.
Density (g/cm3)	0.86	0.8955855	0.86	.

Figure 7.10 Mixture profiler of 5 responses against the percentage of lignin, PVA and PLA, when percentage of $Zn(NO_3)_2$ was set as 5 wt. %.

7.4.8 Effects of ZnO on morphology and mechanical strength

ZnO has the potential to form Zn-ligand coordination interactions with carboxylic and other oxygen-containing groups present in lignin, PVA, and PLA under high temperatures [231]. Such interactions are expected to enhance the mechanical strength of the lignin polymer blend. The chemical state of Zn in the composite was evaluated using XPS analysis of Zn $2p^{3/2}$ spectrum. **Figure 7.11** presents the elemental chemical states for samples $10^{\#}$ and $20^{\#}$. Both samples exhibited signals for C and O; however, Zn was detected only in sample $10^{\#}$, consistent with the EDX results presented in and **Table 7.2**, confirming the successful incorporation of Zn in sample $10^{\#}$. The C 1s spectra of samples $20^{\#}$ and $10^{\#}$ are shown in **Figure 7.11b and e**, respectively. The peaks observed at binding energies of 284.8, 286.3, 287.8, and 289.0 eV correspond to C–C, C–O, C=O, and O=C–O bonds, respectively [233-235]. The concentration of C–C was approximately 42% in both samples; however, the concentration of C–O in sample $10^{\#}$ (21%) was lower than in sample $20^{\#}$ (27%). This suggests that ZnO in the lignin polymer blend facilitates the degradation of C–O bonds due to its catalytic activity [236], while the stability of the C–C backbone was confirmed. The O 1s spectrum of samples $20^{\#}$ and $10^{\#}$ are depicted in **Figure 7.11c and f**, respectively. Peaks at 530.1, 531.6, 532.5, and 533.6 eV were attributed to oxygen ions, C=O, C–OH/C–O–C, and COOH groups, respectively [70, 233, 237]. The presence of oxygen ions coordinated with ZnO, indicated by the peak at 1022 eV in **Figure 7.11d**, was observed only in sample $10^{\#}$, further verifying the incorporation of ZnO in the lignin polymer blend. Additionally, the higher C=O concentration in sample $10^{\#}$ (27%) compared to sample $20^{\#}$ (12%) correlates with the presence of PLA's C=O groups. However, based on **Figure 7.11d**, it remains inconclusive whether Zn-ligand coordination interactions with carboxylic groups were successfully formed.

7.4.9 Molded products

Our sandwich-structured paper composite offers broad application potential and promising future prospects. It can be utilized for both flat sheets and molded products. **Figure 7.12** illustrates a molded paper plate with the optimized formula, demonstrating its oil resistance exceeding one hour. The choice of cover paper in this structure is flexible and can be tailored to specific applications, ranging from thin to thick paper.

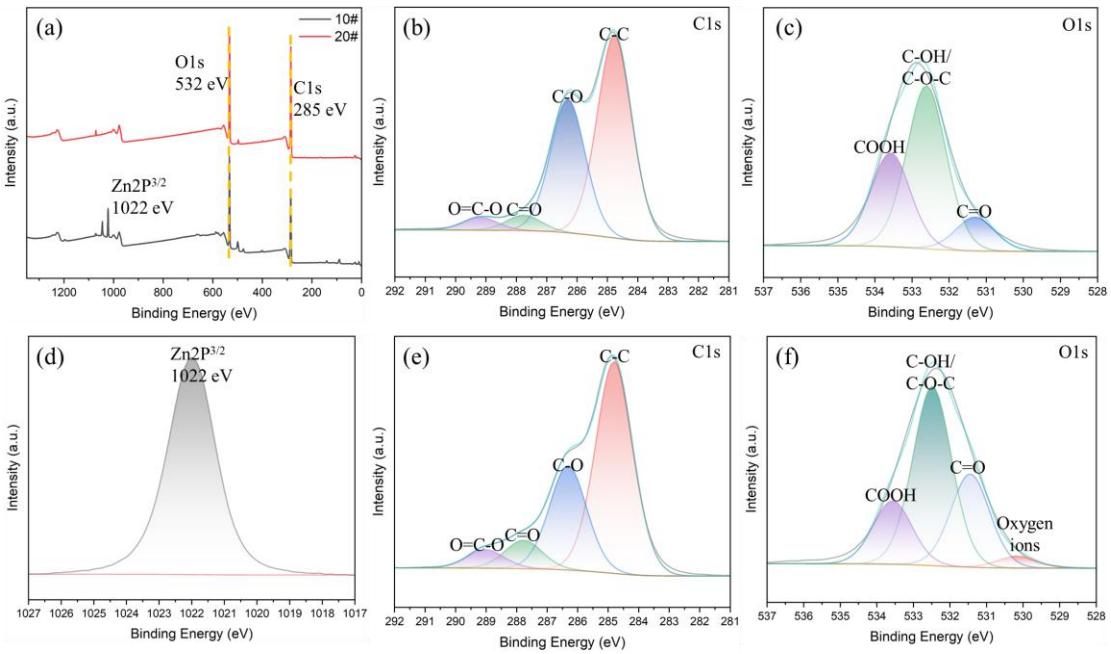

Figure 7.11 XPS characterization of samples $10^{\#}$ and $20^{\#}$: (a) full elemental survey, (b) C1s spectrum of $20^{\#}$, (c) O1s spectrum of $20^{\#}$, (d) Zn $2p^{3/2}$ spectrum of $10^{\#}$, (e) C1s spectrum of $10^{\#}$, (f) O1s spectrum of $10^{\#}$.

Table 7.2 Result of elemental Composition of the Interlayer in Sandwich-Structured Paper Composite $10^{\#}$ via EDX.

Element	Atomic number	Net counts	Norm. mass concentration (%)	1σ uncertainty (mass%)
Carbon	6	61834	48.58	0.37
Nitrogen	7	0	0	0
Zinc	30	5962	6.65	0.41
Oxygen	8	36675	44.76	0.40
Sum			100.00	

Additionally, as shown in **Figure 7.13** , the cover paper is printable, allowing manufacturers to incorporate logos or branding elements—such as the *Center for Renewable Carbon (CRC)* logo—enhancing market appeal. This high level of customization, combined with the availability of all composite components on the market, makes it an accessible and scalable solution. As a result, this biodegradable paper composite holds strong potential for widespread adoption across various industries, particularly as a sustainable alternative in food packaging and disposable tableware.

7.5 Conclusion

In this study, we successfully developed a biodegradable, water- and oil-resistant LMNP-PVA-PLA sandwich-structured paper composite, optimized with 65 wt.% lignin, 25 wt.% PVA, and 10 wt.% PLA as the core layer. This composite demonstrates strong potential for eco-friendly tableware applications. Its mechanical properties, including tensile strengths exceeding 45 MPa, meet the practical requirements for food packaging. The achieved oil and water resistance, exceeding 60 minutes, underscores the effectiveness of the innovative integration of LMNP, PLA, and PVA, positioning this composite as a viable alternative to conventional plastic-based or PFAS-containing products. Furthermore, the sandwich structure minimizes the migration of microplastics and other potential pollutants into food, enhancing its safety for consumer use. The choice of cover paper in this structure is highly flexible, it can be thick or thin and is available in various colors, making it adaptable for different product designs. Additionally, the printability of the cover paper allows manufacturers to incorporate logos or branding elements, further enhancing marketability. This flexibility and ease of customization make the composite particularly suitable for new disposable tableware manufacturers, providing a straightforward, scalable, and commercially viable solution using readily available components.

Further research should focus on reducing the reliance on high-cost biopolymers, such as PVA and PLA, by optimizing LMNP modification and refining processing parameters like hot pressing temperature and duration. Additionally, a deeper understanding of lignin film formation mechanisms is needed to improve material performance and expand its applications.

Figure 7.12 Molded plate-shaped sandwich-structured paper composite retaining vegetable oil for over 1 hour without leakage.

Figure 7.13 Molded plate-shaped sandwich-structured paper composite with a printed Center for Renewable Carbon (CRC) logo.

CHAPTER EIGHT : ECOFRIENDLY BIOCOMPOSITES: DEVELOPING WATER AND OIL RESISTANT LIGNIN – PULP FIBER COMPOSITE VIA DRY FORMING

A version of this chapter is originally written and considered for submission as:
Zhongjin Zhou, Xianhui Zhao, Ercan Cakmak, Shahab Saedi, Nicole Labbé, Siqun Wang. (2025). Ecofriendly biocomposites: developing water and oil resistant LMNP – pulp fiber composite via dry forming. *Composites Part B: Engineering*.

Zhongjin Zhou: Conceptualization, Methodology, Formal analysis, Investigation, Writing, Original Draft, Writing, Review & Editing. **Siqun Wang:** Conceptualization, Methodology, Formal analysis, Investigation, Review & Editing, Supervision, Project Administration, Funding Acquisition. **Xianhui Zhao:** Investigation, Validation, Review & Editing. **Ercan Cakmak:** Experimentation and Analysis of X-CT, Review & Editing. **Shahab Saedi:** Review & Editing. **Nicole Labbé:** Conceptualization, Resources, Review & Editing, Funding Acquisition.

8.1 Abstract:

Plant-based materials, such as cellulose fibers and lignin, offer promising solutions to mitigate plastic waste and reduce the use of volatile organic compound (VOC)-emitting adhesives and environmentally persistent functional agents such as PFAS, which are commonly used for oil repellency. Traditionally, fiber products are manufactured using wet processing methods, which are water intensive. In contrast, the underdeveloped dry-forming method presents an energy-efficient alternative by eliminating the need to suspend fry pulp in water and then redrying; however, its practical applications have been limited due to poor forming capabilities and insufficient liquid resistance. In this study, lignin micro- and nanoparticles (LMNP), produced through ultrafine grinding (UFG), were incorporated into dry pulp fibers as both binders and liquid-resistance agents. During hot pressing, the melted LMNP fills pores and cavities within and between pulp fibers. Upon cooling, the resulting pulp fiber-lignin composite forms a cohesive structure with excellent mechanical properties, achieving a tensile strength of 30 MPa. Additionally, the composite exhibits impressive liquid resistance, absorbing only 15 wt.% water after 24 hours and showing no oil penetration after 3 hours. This composite also demonstrates potential for 3D-molded product applications. Compared to petrochemical-based plastics, the pulp fiber-lignin composite offers high performance, presenting a sustainable alternative for structural or packaging materials.

8.2 Introduction

Replacing non-degradable materials with pulp fibers in molded products offers a sustainable solution to address escalating environmental concerns associated with plastic pollution, low recycling rates, and the long-term impact of non-degradable materials on ecosystems.[6] Plastics persist in the environment for centuries, accumulating in oceans[238], soil and landfills, with recycling efforts hindered by complex sorting and processing challenges.[1,238] In contrast, pulp fibers are biodegradable, renewable, and possess a lower carbon footprint, making them an eco-friendly alternative. Beyond sustainability, pulp fibers offer functional benefits such as lightweight durability, customizability, and improved barrier properties through advanced treatments.[239] As industries face increasing regulatory pressures and growing consumer demand for greener products,[240] pulp-based

molded materials present a viable and cost-effective solution that supports environmental sustainability while maintaining essential functionality.

The wet process is a commonly employed method in the manufacturing of paper-based tableware, where cellulose fibers are dispersed in water to form a slurry, which is then molded into desired shapes [100]. Although this process allows for uniform fiber distribution and smooth surface formation, it is associated with significant challenges. A large volume of wastewater is generated during fiber washing and molding, often containing fine fiber residues and chemical additives, which require extensive treatment to meet environmental discharge standards [241]. Additionally, the high moisture content of molded products leads to substantial energy consumption during the drying stage. This drying process not only increases production costs but also contributes to the overall carbon footprint of paper tableware manufacturing [100]. Therefore, addressing wastewater treatment and drying efficiency remains critical for sustainable and cost-effective production.

A promising innovation in this field is the dry-forming method for molded fiber-based products. This process involves four steps: (1) separating fluff pulp into individual fibers, (2) pre-pressing these fibers into a fluff mat, (3) incorporating binding or functional agents into the mat, and (4) thermally forming the mat into a molded product.[101, 242] Unlike the traditional wet process, dry forming eliminates the need for pulp suspension and using of water. Moreover, by avoiding a drying stage, dry forming reduces energy consumption associated with water evaporation and shortens hot-press cycle times, offering substantial energy and time savings.

Despite these advantages, dry forming faces two major challenges: oil resistance and mechanical strength. While the process enhances efficiency, it does not inherently improve the barrier properties of fiber-based products. Oil resistance remains reliant on external agents, with per- and polyfluoroalkyl substances (PFAS) being the most commonly used—despite their environmental persistence and associated health risks, such as bioaccumulation in drinking water sources.[12, 14] Another challenge lies in achieving sufficient mechanical strength; unlike wet forming, which relies on hydrogen

bonding between fibers, dry-formed materials lack this natural reinforcement, raising concerns about their structural integrity.

One potential solution is the use of biopolymers to bind fibers without enough hydrogen bonds. However, common biopolymers like polylactic acid (PLA)[243], polyvinyl alcohol (PVA)[72] and polyhydroxybutyrate (PHB)[243, 244] are cost-prohibitive compared to pulp. A more sustainable and cost-effective alternative lies in developing plant-based biocomposites, particularly with lignin, a biopolymer with a glass transition temperature of ~120 - 180°C.[165, 167, 168] Lignin becomes soft beyond its glass transition temperature, allowing it to flow and fill cavities under pressure during hot pressing. As the second most abundant natural polymer after cellulose and a byproduct of the paper industry, lignin offers a significant economic and environmental advantage.[107, 245]

Recent studies highlight lignin's potential as a natural binder. Blánquez et al.[246] demonstrated that solid-state fermentation with *Streptomyces* can effectively tune lignin properties for adhesive applications. Hu et al. [201] further confirmed that lignin forms strong hydrogen bonds and self-bonding networks within cellulose fibers during hot pressing, significantly improving mechanical strength, water resistance, and thermal stability. However, the interaction mechanisms between lignin dry powder and pulp fibers during hot pressing remain unclear. Most existing dry-forming methods rely on liquid-phase binders, leaving a gap in understanding how lignin particles bond with fibers in the dry state.

Particle size is a critical factor influencing dry-forming performance and mechanical strength. Several studies have shown that reducing particles or fiber size enhances the mechanical properties of fiber composites. For instance, Youssef[195] demonstrated that smaller nanocellulose particles improve tensile strength and Young's modulus due to better dispersion and stronger interfacial interactions. Similarly, Bhagia[89] showed that ultra-friction grinding of biomass fibers increases surface area and inter-fiber bonding, enhancing mechanical strength. Horseman[72] highlighted that reducing lignocellulose nanofibril size improves tensile properties due to more uniform fibril distribution, while Wang[178] revealed that reducing lignin particle size enhances the

mechanical strength and hydrostability of cellulose-lignin composite straws through improved bonding and densification.

In lignin-containing fiber composites, several forces, including electrostatic interactions, hydrogen bonding, ionic cross-linking, and van der Waals forces, contribute to enhanced fiber binding.[178, 201] Additionally, under hot-pressing conditions, fibers undergo deformation, with cell lumens collapsing to form dense composites that increase mechanical strength. Heat treatment also partially hydrolyzes hemicellulose and lignin, facilitating the formation of new chemical bonds (e.g., C–C bonds in lignin), which further enhance the rigidity of the matrix.[30]

This study hypothesizes that hot pressing enables the formation of a dense fiber-LMNP composite with improved mechanical strength and water/oil resistance, inspired by, but not replicating, the structural efficiency of natural wood. Due to nanoscale effects, LMNPs increase contact area, improve uniformity, and attach more effectively to fiber surfaces through electrostatic attractions. In this research, LMNPs were introduced during the fiber separation phase of pulp sheet processing. We investigate the influence of LMNP content on mechanical strength and liquid resistance, with varying LMNP loadings. To better understand the underlying mechanisms, particularly how LMNPs flow and fill pores and cavities within the fiber network, X-ray computed tomography (X-CT) was employed to analyze the inner morphology of the resulting pulp fiber-lignin composites. With applications spanning diverse fields such as foodware, automotive, construction, and furnishings, combined with high efficiency, the dry-formed pulp LMNP composite holds significant promise for future advancements.

8.3 Experimental methods

8.3.1 Materials and sample preparation

Pulp, printing paper, soybean oil, deionized water, and LMNPs were described in section 3.1 and 3.2.1. LMNP-pulp fiber composite by dry forming method was described in section 3.2.5. In short, Dry pulp sheets were disintegrated into individual fibers using a Ninja® blender (Madison, TN, USA) with a peak power of 1700 W, operating in Max-Crush mode for 2 minutes. The resulting fibers were then mixed with LMNPs at predetermined weight percentages under dry conditions. Three LMNP loading (10, 30,

and 50 wt.%) were selected to examine the effect of LMNP loading on composite properties. The mixtures were subsequently hot-pressed at 200°C under 5 MPa for 3 minutes to form composites, designated as L1-PF9, L3-PF7, and L5-PF5 according to their LMNP content. Additionally, pure pulp fibers were used to produce molded samples (L0-PF10) as control sample, where 30% water was added during hot pressing to facilitate hydrogen bonding.

8.3.2 Characterizations

Fourier-transform infrared (FTIR) spectroscopy analysis is described in Section 3.4.1.2, while thermal analysis is discussed in section 3.4.1.4. and morphological and particle size analysis was detailed in section 3.4.2. Performance of paper composites including oil and water resistance, and mechanical strength assessment was described in section 3.4.4.

8.4 Results and discussion

8.4.1 FTIR analysis

The IR spectra of LMNP, pulp fiber, and LMNP-pulp fiber composites are shown in **Figure 8.1**. The broad absorption band at 3300 cm^{-1} corresponds to O–H stretching vibrations [208], while the bands within 2837–2950 cm^{-1} are attributed to C–H stretching [247]. Characteristic peaks associated with the lignin aromatic skeleton, observed at 1593 cm^{-1} and 1512 cm^{-1} [201], were present in all composites, confirming the successful incorporation of LMNP into the pulp fiber matrix. Additionally, the C–O stretching peak of phenolic groups at 1267 cm^{-1} [201] was detected alongside the lignin-associated peaks at 1593 cm^{-1} and 1512 cm^{-1}. This peak was absent in pure pulp fiber but became increasingly pronounced as the LMNP content increased from 10% to 50%, serving as a clear indicator of LMNP presence in the composites.

8.4.2 Out appearance and physics

The appearance of LMNP-pulp fiber composites, from raw materials to pre-pressed and final composite sheets, is shown in **Figure 8.2** - **Figure 8.5**. The color of the composites darkened with increasing LMNP loading, regardless of the hot-pressing stage. Notably, LMNPs adhered well to pulp fibers during dry mixing; however, at 50% LMNP

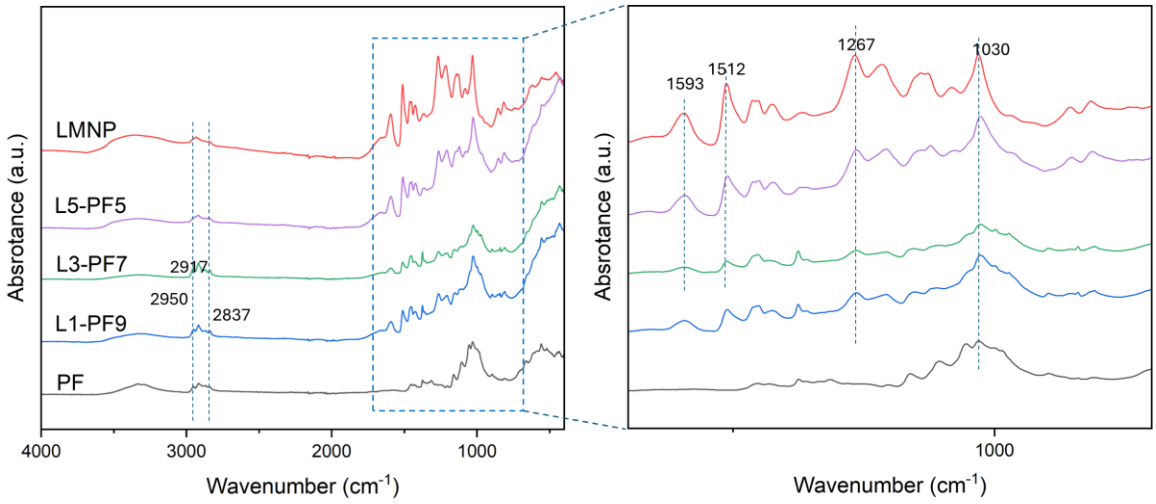

Figure 8.1 FTIR spectra of pulp fiber (PF), lignin micro/nanoparticles (LMNP), and LMNP-pulp fiber composites with different LMNP loading (L1-PF9, L3-PF7, L5-PF5). The right panel presents a magnified view of the 1700–700 cm^{-1} region, highlighting key functional group peaks.

Figure 8.2 (a) Individual pulp fibers in their raw form, (b) fiber assembly before hot pressing, and (c) final product of L0-PF10 after hot pressing.

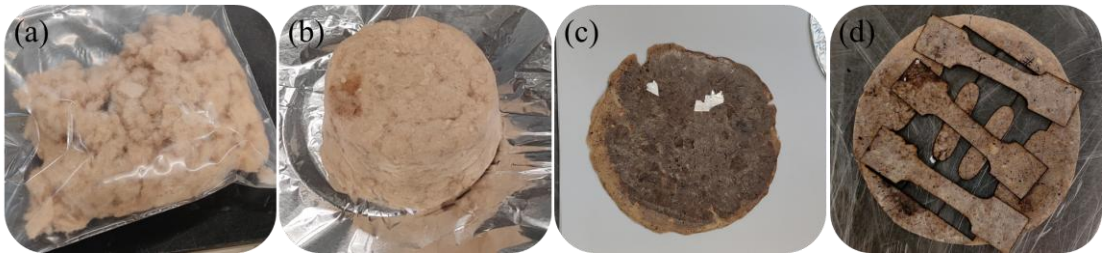

Figure 8.3 Preparation and processing of L1-PF9 composite. (a) Individual pulp fibers mixed with LMNPs, (b) fiber assembly before hot pressing, (c) final product of L1-PF9 after hot pressing, and (d) laser-cut sample for tensile testing.

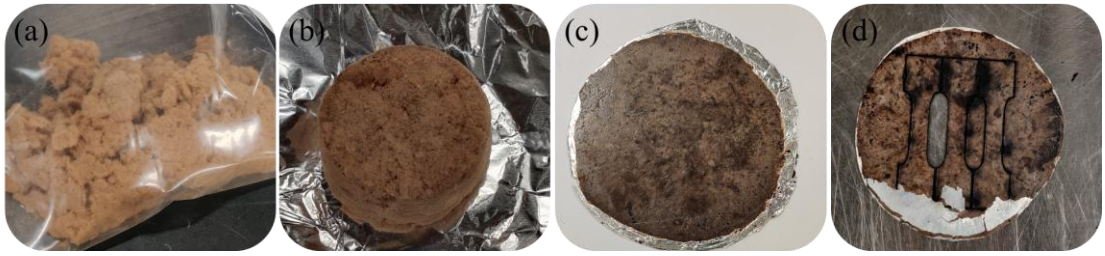

Figure 8.4 Preparation and processing of L3-PF7 composite. (a) Individual pulp fibers mixed with LMNPs, (b) fiber assembly before hot pressing, (c) final product of L3-PF7 after hot pressing, and (d) laser-cut sample for tensile testing.

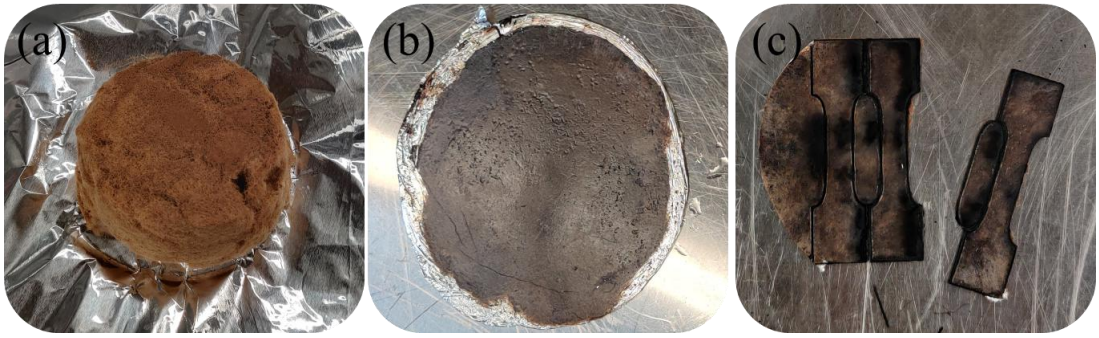

Figure 8.5 Preparation and processing of L5-PF5 composite. (a) Individual pulp fibers mixed with LMNPs, (b) fiber assembly before hot pressing, (c) final product of L5-PF5 after hot pressing, and (d) laser-cut sample for tensile testing.

loading, some LMNPs detached from the fiber surface. This suggests that 50% represents the maximum LMNP load capacity under dry mixing conditions.

The grammage and density of LMNP-pulp fiber composites at varying LMNP contents are presented in **Figure 8.6**. Both parameters exhibit a non-linear trend, indicating that LMNP incorporation influences structural compactness and mass per unit area. Grammage increased with LMNP content up to 30%, peaking at approximately 1220 g/m², before slightly decreasing at 50% LMNP. However, high variability was observed due to the manual nature of fabrication steps. Density followed a similar pattern, rising sharply from 0.8 g/cm³ (0% LMNP) to over 1.2 g/cm³ (30% LMNP), before slightly declining at 50% LMNP. The increased density suggests that LMNPs contribute to void reduction and enhanced matrix consolidation, improving fiber packing efficiency. The slight decline at 50% LMNP may result from structural disruptions, where excess LMNPs hinder uniform fiber bonding and introduce localized defects.

These results suggest that LMNP incorporation at 10–30% can improve grammage and density, contributing to a more compact composite structure. However, visual inspection revealed some surface heterogeneity even at the 10% loading level, indicating that uniform LMNP distribution remains a challenge. Furthermore, industrial feedback highlights cost concerns associated with using high additive loadings. Therefore, optimizing LMNP content—potentially below 10%—is essential to balance structural reinforcement, barrier performance, visual uniformity, and economic viability.

8.4.3 Oil and water resistance

8.4.3.1 Oil resistance

The oil resistance of LMNP-pulp fiber composites was evaluated using TAPPI T 559 cm-22 [248] and ASTM F119 [102] methods, as shown in **Figure 8.7**. The kit number provides a measure of resistance to low-surface-energy liquids, with higher values (maximum of 12) indicating superior resistance. The incorporation of LMNPs enhanced oil resistance, as demonstrated by the increase in kit number with rising LMNP content. The ASTM F119 test, which quantifies the time required for oil penetration, revealed a more pronounced effect. Oil penetration time increased from minutes to several hours as LMNP content rose, confirming a significant improvement in barrier properties.

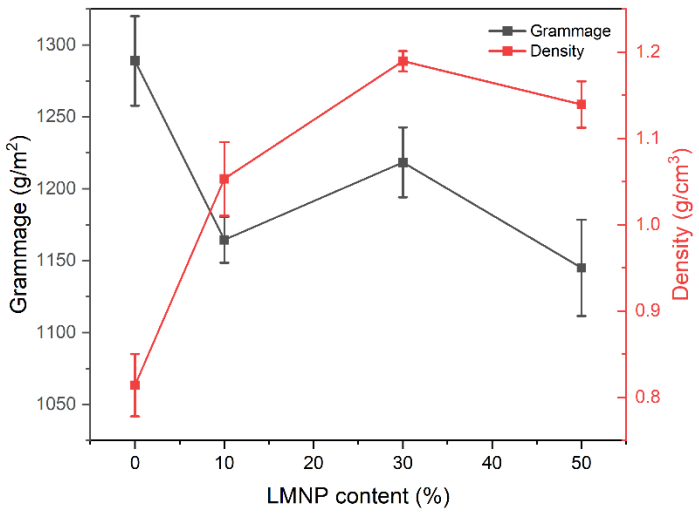

Figure 8.6 Grammage and density of LMNP-pulp fiber composites at varying LMNP content. The black squares represent grammage (g/m²), while the red squares represent density (g/cm³).

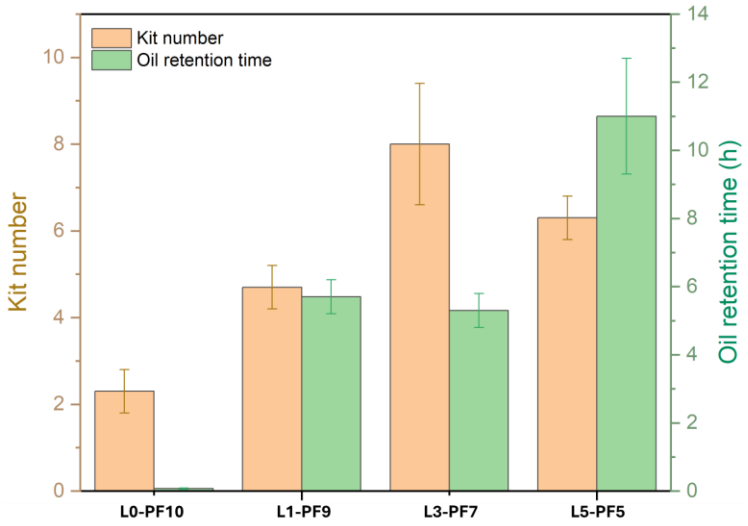

Figure 8.7 Oil resistance test results of LMNP-pulp fiber composites. The kit number (left y-axis, orange bars) indicates the oil repellency level, while the oil retention time (right y-axis, green bars) represents the duration before oil penetration. Error bars denote standard deviations.

This enhanced oil resistance can be attributed to the formation of a denser lignin matrix around pulp fibers under hot-pressing conditions. At higher LMNP loadings, lignin fully encapsulated fiber surfaces, while fiber lumens collapsed under pressure, resulting in a more compact composite structure. This structural transformation will be further analyzed using X-CT and SEM cross-sectional imaging.

8.4.3.2 Water resistance

Figure 8.8 illustrates the water resistance of LMNP–pulp fiber composites, evaluated by immersing samples in water at 20 °C. Water absorption declined from 45% to 15% as LMNP content increased. While the trend suggests improved resistance with higher LMNP loading, statistical significance between formulations has not yet been confirmed and will require further analysis. This improvement in composite stability demonstrates significantly enhanced performance compared to commercially available fiber-based materials.

8.4.4 Mechanical strength analysis

The mechanical properties of LMNP-pulp fiber composites were evaluated based on tensile strength, Young's modulus, and strain at break, as shown in **Figure 8.9**. The incorporation of LMNPs significantly influenced mechanical performance, exhibiting distinct trends across different LMNP loadings. The tensile strength and Young's modulus displayed a non-linear relationship with LMNP content. At 0% of LMNP, the composite exhibited relatively low tensile strength (~18 MPa) and Young's modulus (~1500 MPa). At 10% of LMNP, both properties increased notably, reaching approximately 42 MPa and 2200 MPa, respectively. This enhancement is likely due to the reinforcing effect of LMNPs, which promote interfacial interactions between lignin and pulp fibers, improving load transfer efficiency. At 30% of LMNP, Young's modulus peaked at ~2600 MPa, indicating increased stiffness. However, tensile strength showed slight fluctuations, likely due to LMNP agglomeration, which may introduce stress concentrations and compromise mechanical integrity. A clear inverse trend was observed between strain at break and LMNP content: At 10% LMNP, the strain at break peaked (~1.9%), suggesting improved ductility, possibly due to enhanced fiber-matrix adhesion, which facilitates energy dissipation under tension. At higher LMNP loadings (30% and 50%), strain at break

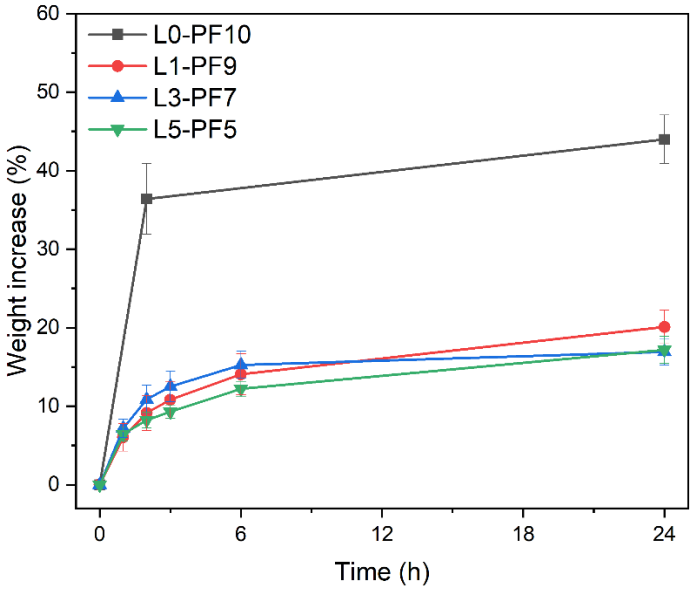

Figure 8.8 Weight increase of LMNP-pulp fiber composites over time when soaked in water at 20 °C. The weight gain percentage reflects the water absorption capacity of different composite formulations (L0-PF10, L1-PF9, L3-PF7, and L5-PF5). Error bars indicate standard deviations.

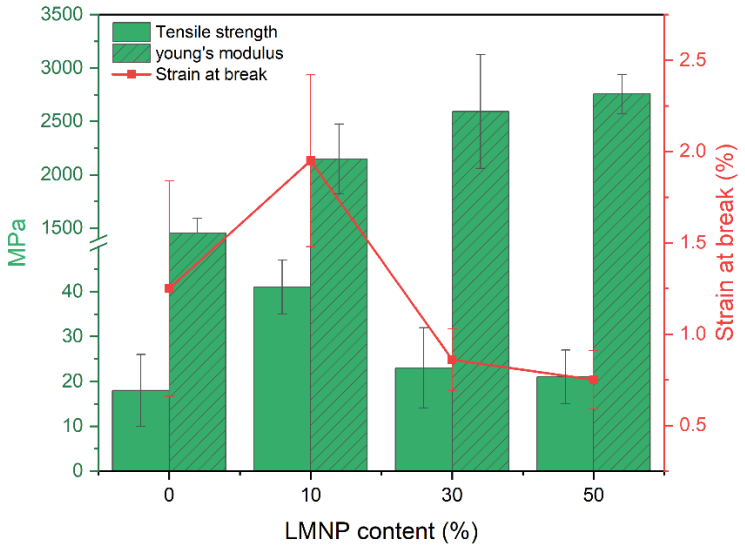

Figure 8.9 Tensile test results of LMNP-pulp fiber composites. The tensile strength (solid green bars) and Young's modulus (hatched green bars) are plotted on the left y-axis (MPa), while the strain at break (red line with square markers) is plotted on the right y-axis (%). Error bars indicate standard deviations.

dropped below 1.0%, indicating increased brittleness. This reduction may result from excessive LMNP aggregation, which restricts fiber flexibility and introduces microstructural defects.

These findings suggest that moderate LMNP incorporation (10%) optimizes stiffness and tensile strength while maintaining acceptable ductility. However, excessive LMNP loading (50%) may lead to phase separation and weaker stress transfer efficiency, compromising mechanical performance. These trends align with previous studies on lignin-based fiber reinforcements, emphasizing the importance of optimizing LMNP content for balanced mechanical properties.

8.4.5 Morphology

8.4.5.1 SEM analysis

SEM images of pulp fibers, LMNPs, and LMNP-pulp fiber composites before hot press are shown in **Figure 8.10**. The morphology of LMNPs (**Figure 8.10a**) revealed irregularly shaped particles with an average diameter ranging from 100 to 1000 nm. The average pulp fiber diameter was approximately 100 μm. Numerous LMNPs adhered to pulp fiber surface due to electrostatic forces (**Figure 8.10c**), driven by the attraction between oppositely charged species [249]. In the cross-sectional view (**Figure 8.11a**), fiber lumens remained open, potentially acting as pathways for liquid penetration. In composites, low LMNP loadings resulted in fiber-dominant structures, where lignin coverage was insufficient to fully coat the fibers. At 30 wt.% LMNP loading, a significant increase in lignin volume was observed. At 50 wt.% LMNP, lignin formed a continuous matrix, fully embedding the individual fibers. Further volume distribution analysis is provided in the X-CT analysis.

8.4.5.2 Internal Morphology Analysis through X-CT analysis

The internal structure of LMNP-pulp fiber composites (L5-PF5) was examined using X-CT, as shown in **Figure 8.12.** The 3D reconstructions provide a detailed visualization of material components and their spatial distribution, offering insights into the composite's structural integrity and functional properties.

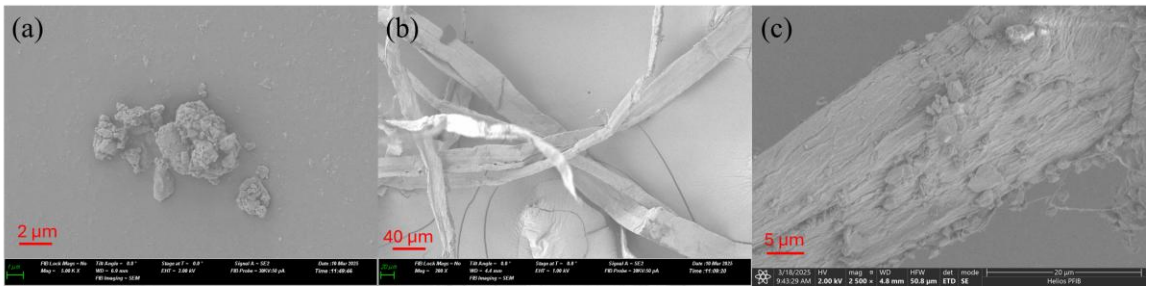

Figure 8.10 Scanning electron microscopy (SEM) images of (a) lignin micro/nanoparticles (LMNPs) and (b) pulp fibers, (c) LMNP attached to pulp fiber surface before hot press.

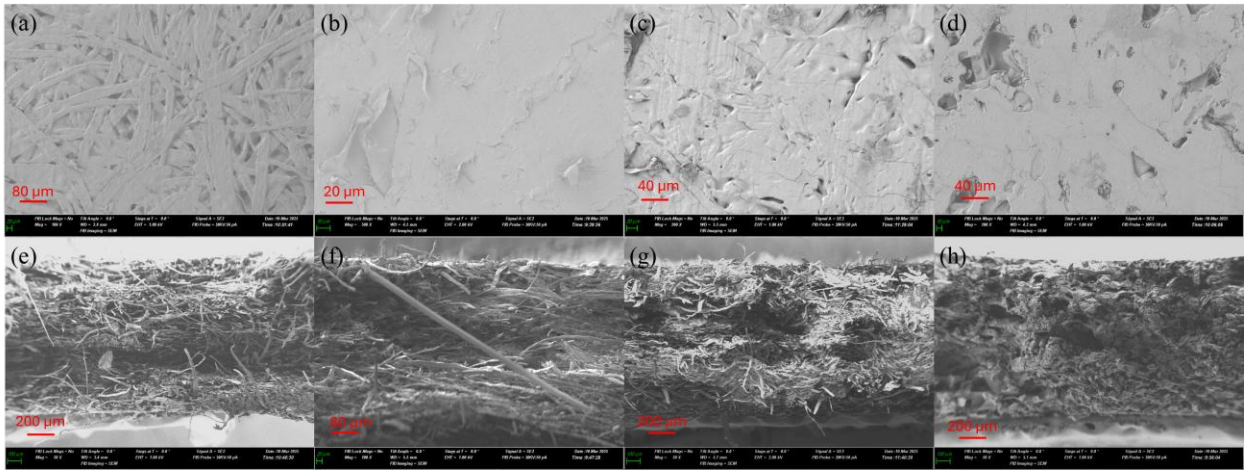

Figure 8.11 Scanning electron microscopy (SEM) images of the top surface (a–d) and cross-section (e–h) of LMNP-pulp fiber composites after tensile testing. (a, e) L0-PF10, (b, f) L1-PF9, (c, g) L3-PF7, and (d, h) L5-PF5.

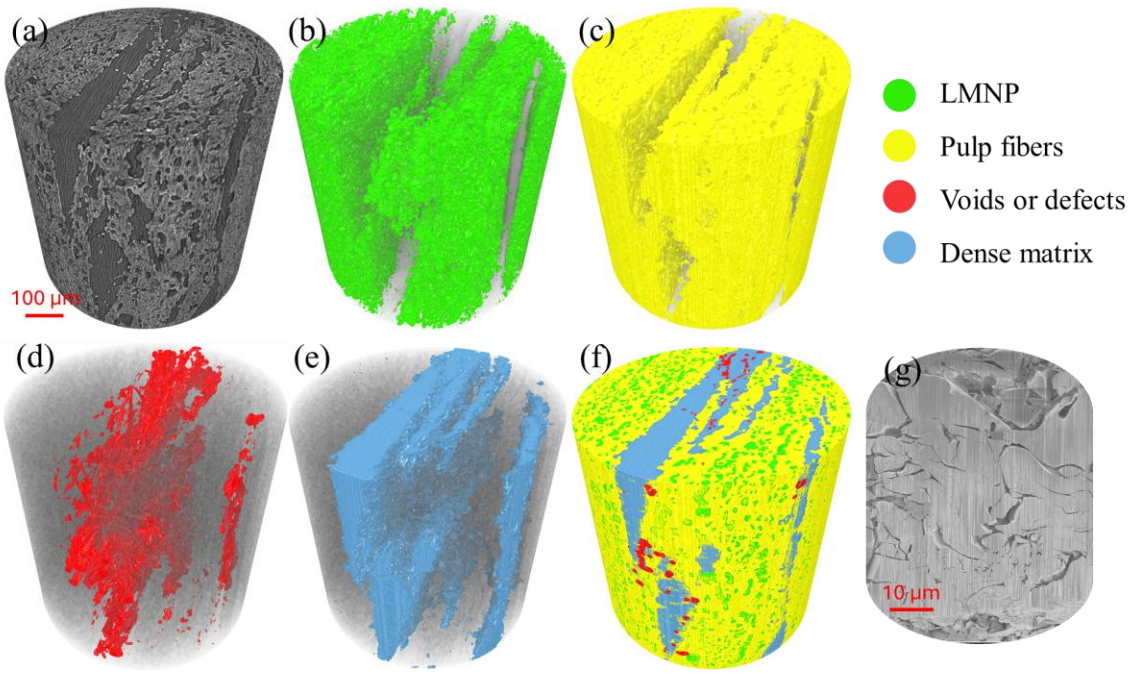

Figure 8.12 X-ray computed tomography (X-CT) 3D morphology and segmented components of LMNP-pulp fiber composite L5-PF5. (a) Overall 3D structure, (b–f) segmentation of different components: lignin micro/nanoparticles (green), pulp fibers (yellow), pores/voids (red), and dense matrix regions (blue). (g) Scanning electron microscopy (SEM) image of the cross-section of L5-PF5 cutting by Focused ion beam (FIB).

The grayscale image (**Figure 8.12a**) illustrates the overall morphology, revealing a well-integrated network of fibers and LMNPs. Segmentation of different components (**Figure 8.12b–f**) highlights distinct material regions. LMNPs (green) are embedded within the fiber network, filling void spaces and coating fiber surfaces, forming a denser structure. The pulp fibers (yellow) demonstrate a tightly packed arrangement, indicating strong fiber entanglement and effective LMNP incorporation. Voids and defects (red) appear minimal, suggesting that LMNPs contribute to reducing microstructural imperfections. Additionally, dense matrix regions (blue) indicate areas where LMNPs reinforce the composite, enhancing mechanical integrity. The cross section of L5-PF5, cut by FIB and shown in **Figure 8.12g**, was found to demonstrate the internal structure more clearly when combined with the X-CT result.

The well-dispersed LMNP distribution is crucial for improving barrier properties, as it reduces porosity and limits fluid penetration pathways. The superior oil and water resistance of LMNP-pulp fiber composites, compared to conventional pulp-based products, can be attributed to several key factors. First, the hydrophobic nature of LMNPs plays a significant role. Lignin's aromatic structure and limited hydroxyl functional groups provide intrinsic hydrophobicity [245, 250], reducing water absorption. The uniform dispersion of LMNPs throughout the composite further enhances this effect, forming a hydrophobic shield that prevents moisture ingress. Second, reduced porosity and improved fiber coating contribute to enhanced barrier performance. X-CT analysis confirms that LMNPs effectively fill inter-fiber gaps and coat cellulose fibers, minimizing voids where liquids could penetrate. This structural densification is a critical factor in limiting the wicking behavior of both water and oil. Lastly, interfacial bonding and enhanced composite stability further improve mechanical strength and liquid resistance. The strong fiber-matrix interactions induced by LMNP incorporation ensure better load distribution and structural cohesion, reinforcing the composite against external stressors.

These findings emphasize the potential of LMNP-pulp fiber composites for high-performance, eco-friendly packaging and tableware, where superior barrier properties and mechanical strength are essential.

8.5 Conclusion

LMNP-pulp fiber composites were successfully developed, demonstrating enhanced mechanical strength and barrier properties. Lignin played multiple functional roles in the composite, serving as a binder, hydrophobic agent, and structural filler, all of which contributed to the overall integrity and performance of the material. The formation mechanism was driven by high-pressure processing at temperatures exceeding lignin's glass transition. Under these conditions, LMNPs adhered to cellulose fibers via electrostatic attraction, leading to a denser composite structure. This mechanism was further confirmed through X-CT analysis and computational simulations, which highlighted the effective interaction between lignin and cellulose at the microstructural level.

The fabricated LMNP–pulp fiber composites exhibited notable improvements in mechanical and barrier properties. At 30 wt.% LMNP loading, Young's modulus reached 2600 MPa—a 73% increase compared to pure pulp fiber composites (1500 MPa). Oil resistance also improved markedly, with oil penetration time extending from a few minutes (0% LMNP) to over 11 hours at 50% loading. Water absorption decreased from 45% to 15%, indicating wet stability. However, the 50% LMNP formulation showed signs of nanoparticle detachment during pressing, suggesting that the retention capacity of the fiber network was exceeded. Moreover, higher LMNP levels (≥30%) introduced noticeable color heterogeneity, which could affect product aesthetics. Given these trade-offs and the cost implications of high LMNP usage, a loading level between 10–30 wt.% appears optimal for balancing mechanical performance, barrier properties, visual uniformity, and economic feasibility.

Further research should optimize LMNP distribution, fine-tune processing conditions, and assess long-term stability under real-world conditions. Expanding applications in food packaging, medical materials, and high-performance biocomposites could enhance commercial viability. Understanding lignin-cellulose interactions will aid in developing sustainable alternatives to petroleum-based plastics, supporting a circular economy.

CHAPTER NINE : CONCLUSIONS AND RECOMMENDATIONS

9.1 Summary

This dissertation explored the development of lignin nanoparticle-based composites for sustainable packaging applications, with a focus on enhancing water and oil resistance while maintaining biodegradability. Through a series of experimental investigations, key advancements were made in optimizing the ultrafine grinding (UFG) process for lignin nanoparticle (LMNP) production, improving energy efficiency, and developing composite structures with enhanced barrier and mechanical properties. The results of these studies underscore the importance of scalable and environmentally friendly material development, particularly in the context of packaging applications where sustainability is increasingly prioritized.

Key findings include:

- **Optimized Lignin Nanoparticle Production:** Process temperature and solid content significantly impact particle size and energy consumption. Higher solid contents (20 wt.%) reduced water and energy usage by 90% compared to conventional low-solid-content processes. The ability to finely control LMNP size and dispersion is critical for achieving consistent material performance, and future refinements in processing conditions may further enhance cost-effectiveness.
- **Water- and Oil-Resistant Composite Development:** Hot-pressed lignin films achieved over 100 minutes of water resistance and 25 minutes of oil resistance under optimized processing conditions (40 g/m² lignin coating, 3 MPa pressure, 160°C, 30 wt.% moisture content). The sandwich-structured LMNP-paper composite maintained barrier properties while improving tensile strength by 50%. This structural approach not only addresses mechanical durability concerns but also paves the way for improved aesthetics and commercial viability in consumer markets.
- **Dry Forming for Eco-Friendly Packaging:** This method eliminated water-intensive processing and significantly reduced drying energy consumption while enhancing mechanical and barrier properties, making it ideal for disposable tableware and food packaging. The elimination of excessive water use aligns with

global efforts to minimize industrial water footprints, presenting a strong case for large-scale adoption.

9.2 Recommendations and future directions

While this research presents a significant step forward in the application of lignin-based composites, several challenges and opportunities remain for future studies. The potential for LMNPs to serve as viable replacements for synthetic packaging materials necessitates further exploration into performance enhancements, economic scalability, and real-world implementation.

- **Enhancing Material Performance:** Improvements in LMNP surface chemistry, such as hydrophobic modifications or crosslinking strategies, could enhance long-term oil resistance. The introduction of chemical functionalization strategies may further broaden the applicability of LMNP composites in more demanding packaging environments. Additionally, thermal stability studies under prolonged heat exposure would provide insight into the feasibility of these materials for food service applications that involve microwaving or oven use.
- **Scalability and Industrial Implementation:** Process optimization for large-scale production while maintaining quality is essential. Cost reduction strategies, such as alternative natural binders, could improve economic feasibility. Collaboration with industry stakeholders will be crucial in identifying production bottlenecks and refining fabrication methods that align with commercial manufacturing processes.
- **Environmental and Lifecycle Assessment:** Comprehensive life-cycle assessments (LCA) and long-term biodegradation studies in various environments (e.g., composting, marine degradation) will help validate the eco-friendly claims of these materials. Understanding the decomposition behavior of LMNP composites in different waste management systems will be essential for regulatory approvals and market adoption.
- **Expanding Applications:** Exploring LMNPs as carriers for active agents (e.g., antimicrobial or oxygen-scavenging compounds) could extend applications beyond disposable tableware to high-performance food packaging. Additionally,

integrating LMNP composites into molded fiber products could expand their usability in diverse industries. The potential for LMNPs to act as structural reinforcements or protective coatings in broader applications, such as biodegradable electronics packaging or sustainable construction materials, should also be investigated.

This research contributes to the growing field of sustainable materials by demonstrating the feasibility of LMNP-based composites as an alternative to conventional plastic-based or PFAS added fiber based food packaging and disposable tableware. The development of bio-based materials that perform comparably to synthetic counterparts while maintaining superior environmental attributes is a key step toward sustainable industrial transformation. Future efforts should focus on further improving performance, reducing costs, and expanding industrial applications to fully harness the benefits of lignin as a sustainable resource. By continuing to refine processing techniques and exploring novel composite structures, LMNP technology has the potential to revolutionize the landscape of biodegradable and renewable material solutions.

LIST OF REFERENCES

1. Haider, T.P., C. Volker, J. Kramm, K. Landfester, and F.R. Wurm, Plastics of the Future? The Impact of Biodegradable Polymers on the Environment and on Society. *Angew Chem Int Ed Engl* **2019**. *58*(1): p. 50-62.
2. Key EPA Actions to Address PFAS. **2024** [cited 2024 20 December 2024]; Available from: https://www.epa.gov/pfas/key-epa-actions-address-pfas#:~:text=In%20January%202024%2C%20the%20EPA%20finalized%20a%20rule%20that%20prevents,and%20review%20by%20the%20EPA.
3. Borrelle, S.B., J. Ringma, K.L. Law, C.C. Monnahan, L. Lebreton, A. McGivern, E. Murphy, J. Jambeck, G.H. Leonard, M.A. Hilleary, M. Eriksen, H.P. Possingham, H.D. Frond, L.R. Gerber, B. Polidoro, A. Tahir, M. Bernard, N. Mallos, M. Barnes, and C.M. Rochman, Predicted growth in plastic waste exceeds efforts to mitigate plastic pollution. *Science* **2020**. *369*(6510): p. 1515-1518.
4. Zhao, X. and F. You, Life Cycle Assessment of Microplastics Reveals Their Greater Environmental Hazards than Mismanaged Polymer Waste Losses. *Environ Sci Technol* **2022**. *56*(16): p. 11780-11797.
5. Debnath, M., R. Sarder, L. Pal, and M.A. Hubbe, Molded pulp products for sustainable packaging: Production rate challenges and product opportunities. *BioResources* **2022**. *17*(2): p. 3810-3870.
6. Singh, A.K., P. Itkor, M. Lee, J. Shin, and Y.S. Lee, Promoting sustainable packaging applications in the circular economy by exploring and advancing molded pulp materials for food products: a review. *Crit Rev Food Sci Nutr* **2022**: p. 1-16.
7. Zhang, Y., C. Duan, S.K. Bokka, Z. He, and Y. Ni, Molded fiber and pulp products as green and sustainable alternatives to plastics: A mini review. *Journal of Bioresources and Bioproducts* **2022**. *7*(1): p. 14-25.
8. North America Molded Pulp Packaging Market Size, Share & Trends Analysis Report By Source (Thick Wall, Transfer, Thermoformed, Processed), By Product, By Application, By Country, And Segment Forecasts, 2023 - 2030. [cited 2025 Feb 11]; Available from: https://www.grandviewresearch.com/industry-analysis/north-america-molded-pulp-packaging-market.

9. Mujtaba, M., J. Lipponen, M. Ojanen, S. Puttonen, and H. Vaittinen, Trends and challenges in the development of bio-based barrier coating materials for paper/cardboard food packaging; a review. *Sci Total Environ* **2022**. *851*(Pt 2): p. 158328.
10. A, H.T., M. Tajvidi, and D. Bousfield, Paper-Based Oil Barrier Packaging using Lignin-Containing Cellulose Nanofibrils. *Molecules* **2020**. *25*(6): p. 1344.
11. Yuan, Z. and Y. Wen, Enhancement of hydrophobicity of nanofibrillated cellulose through grafting of alkyl ketene dimer. *Cellulose* **2018**. *25*(12): p. 6863-6871.
12. Death, C., C. Bell, D. Champness, C. Milne, S. Reichman, and T. Hagen, Per- and polyfluoroalkyl substances (PFAS) in livestock and game species: A review. *Sci Total Environ* **2021**. *774*: p. 144795.
13. TamiL.Lavezzo. The Evolution of PFAS. **2022** [cited 2025 Feb 11]; Available from: https://www.sonomatech.com/node/361?utm.
14. Brunn, H., G. Arnold, W. Körner, G. Rippen, K.G. Steinhäuser, and I. Valentin, PFAS: forever chemicals—persistent, bioaccumulative and mobile. Reviewing the status and the need for their phase out and remediation of contaminated sites. *Environmental Sciences Europe* **2023**. *35*(1): p. 20.
15. Rogers, R.D., C.M. Reh, and P. Breysse, Advancing per- and polyfluoroalkyl substances (PFAS) research: an overview of ATSDR and NCEH activities and recommendations. *J Expo Sci Environ Epidemiol* **2021**. *31*(6): p. 961-971.
16. Burns, P.K. Historic settlement reached to clean up toxic PFAS contamination in South Jersey. **2023** [cited 2025 Feb 11]; Available from: https://whyy.org/articles/solvay-specialty-polymers-historic-settlement-pfas-contamination-south-jersey/.
17. Ramirez Carnero, A., A. Lestido-Cardama, P. Vazquez Loureiro, L. Barbosa-Pereira, A. Rodriguez Bernaldo de Quiros, and R. Sendon, Presence of Perfluoroalkyl and Polyfluoroalkyl Substances (PFAS) in Food Contact Materials (FCM) and Its Migration to Food. *Foods* **2021**. *10*(7): p. 1443.
18. Jones, J., FDA, Industry Actions End Sales of PFAS Used in US Food Packaging. **2024**, U.S. Food & Drug Administration.
19. Lora, J., Chapter 10 - Industrial Commercial Lignins: Sources, Properties and

Applications, in *Monomers, Polymers and Composites from Renewable Resources*, M.N. Belgacem and A. Gandini, Editors. **2008**, Elsevier: Amsterdam. p. 225-241.

20. Yu, O. and K.H. Kim, Lignin to Materials: A Focused Review on Recent Novel Lignin Applications. *Applied Sciences* **2020**. *10*(13): p. 4626.

21. Yu, S., M. Wang, Y. Xie, W. Qian, Y. Bai, and Q. Feng, Lignin self-assembly and auto-adhesion for hydrophobic cellulose/lignin composite film fabrication. *Int J Biol Macromol* **2023**: p. 123598.

22. Schneider, W.D.H., A.J.P. Dillon, and M. Camassola, Lignin nanoparticles enter the scene: A promising versatile green tool for multiple applications. *Biotechnol Adv* **2021**. *47*: p. 107685.

23. Deng, W., X. Hu, K. Wang, F. Wang, Y. Zhai, T. Liu, Z. Yuan, and Y. Wen, Evaluation of the production of lignin-containing cellulose nanofibrils with high whiteness for blocking UV light. *Cellulose* **2024**.

24. Xu, J., W. Liu, J. Zhou, Y. Kong, M. Gong, M. Almajarsh, X. Zhao, and X. Wang, Preparation of lignin-based personal multifunctional protective mask interlayer with antibacterial, anti-UV and iodine trapping effects and exploration of its iodine trapping mechanism. *Industrial Crops and Products* **2023**. *203*.

25. Tarasov, D., M. Leitch, and P. Fatehi, Lignin-carbohydrate complexes: properties, applications, analyses, and methods of extraction: a review. *Biotechnol Biofuels* **2018**. *11*: p. 269.

26. Hussin, M.H., J.N. Appaturi, N.E. Poh, N.H.A. Latif, N. Brosse, I. Ziegler-Devin, H. Vahabi, F.A. Syamani, W. Fatriasari, N.N. Solihat, A. Karimah, A.H. Iswanto, S.H. Sekeri, and M.N.M. Ibrahim, A recent advancement on preparation, characterization and application of nanolignin. *Int J Biol Macromol* **2022**. *200*: p. 303-326.

27. Tian, D., J. Hu, J. Bao, R.P. Chandra, J.N. Saddler, and C. Lu, Lignin valorization: lignin nanoparticles as high-value bio-additive for multifunctional nanocomposites. *Biotechnol Biofuels* **2017**. *10*: p. 192.

28. Ago, M., S. Huan, M. Borghei, J. Raula, E.I. Kauppinen, and O.J. Rojas, High-Throughput Synthesis of Lignin Particles (approximately 30 nm to approximately 2 mum) via Aerosol Flow Reactor: Size Fractionation and Utilization in Pickering

Emulsions. *ACS Appl Mater Interfaces* **2016**. *8*(35): p. 23302-10.

29. Zhou, Z., K. Rajan, N. Labbé, and S. Wang, Significantly reducing energy consumption during nanolignin production via high-solid content grinding. *Industrial Crops and Products* **2024**. *211*: p. 118209.

30. Zhou, Z., K. Rajan, S. Saedi, N. Labbé, M. Li, W. Wang, and S. Wang, A Fully Plant-Based Water- and Oil-Resistant Paper Composite. *ACS Sustainable Chemistry & Engineering* **2024**. *12*(50): p. 18043-18057.

31. Advancing Sustainable Materials Management: 2018 Fact Sheet. Assessing Trends in Materials Generation and Management in the United States, U.S.E.P. Agency, Editor. **2020**, Unite States Environmental Protection Agency: Washington, DC 20460.

32. Li, B., W. Liang, Q.X. Liu, S. Fu, C. Ma, Q. Chen, L. Su, N.J. Craig, and H. Shi, Fish Ingest Microplastics Unintentionally. *Environ Sci Technol* **2021**. *55*(15): p. 10471-10479.

33. Guart, A., F. Bono-Blay, A. Borrell, and S. Lacorte, Migration of plasticizersphthalates, bisphenol A and alkylphenols from plastic containers and evaluation of risk. *Food Additives & Contaminants: Part A* **2011**. *28*(5): p. 676-685.

34. Sirohi, R., J. Prakash Pandey, V. Kumar Gaur, E. Gnansounou, and R. Sindhu, Critical overview of biomass feedstocks as sustainable substrates for the production of polyhydroxybutyrate (PHB). *Bioresour Technol* **2020**. *311*: p. 123536.

35. Rahman, M.Z., M. Rahman, T. Mahbub, M. Ashiquzzaman, S. Sagadevan, and M.E. Hoque, Advanced biopolymers for automobile and aviation engineering applications. *Journal of Polymer Research* **2023**. *30*(3).

36. Murariu, M. and P. Dubois, PLA composites: From production to properties. *Advanced drug delivery reviews* **2016**. *107*: p. 17-46.

37. Ilyas, R., S. Sapuan, M. Harussani, M. Hakimi, M. Haziq, M. Atikah, M. Asyraf, M. Ishak, M. Razman, and N. Nurazzi, Polylactic acid (PLA) biocomposite: Processing, additive manufacturing and advanced applications. *Polymers* **2021**. *13*(8): p. 1326.

38. Gigante, V., I. Canesi, P. Cinelli, M.B. Coltelli, and A. Lazzeri, Rubber toughening of polylactic acid (PLA) with poly (butylene adipate-co-terephthalate)(PBAT): mechanical properties, fracture mechanics and analysis of ductile-

to-brittle behavior while varying temperature and test speed. *European Polymer Journal* **2019**. *115*: p. 125-137.

39. Byun, Y., K. Rodriguez, J.H. Han, and Y.T. Kim, Improved thermal stability of polylactic acid (PLA) composite film via PLA–β-cyclodextrin-inclusion complex systems. *International journal of biological macromolecules* **2015**. *81*: p. 591-598.

40. Reinerte, S., V. Jurkjane, U. Cabulis, and A. Viksna, Identification and evaluation of hazardous pyrolysates in bio-based rigid polyurethane-polyisocyanurate foam smoke. *Polymers* **2021**. *13*(19): p. 3205.

41. Ghasemlou, M., F. Daver, E.P. Ivanova, and B. Adhikari, Polyurethanes from seed oil-based polyols: A review of synthesis, mechanical and thermal properties. *Industrial Crops and Products* **2019**. *142*: p. 111841.

42. Desai, Y., S. Jariwala, and R.K. Gupta, Bio-Based Polyurethanes and Their Applications, in *Polyurethanes: Preparation, Properties, and Applications Volume 2: Advanced Applications*. **2023**, American Chemical Society. p. 1-14.

43. Chen, G.-Q. and X.-R. Jiang, Engineering microorganisms for improving polyhydroxyalkanoate biosynthesis. *Current opinion in biotechnology* **2018**. *53*: p. 20-25.

44. Yeo, J.C.C., J.K. Muiruri, W. Thitsartarn, Z. Li, and C. He, Recent advances in the development of biodegradable PHB-based toughening materials: Approaches, advantages and applications. *Materials Science and Engineering: C* **2018**. *92*: p. 1092-1116.

45. Turco, R., G. Santagata, I. Corrado, C. Pezzella, and M. Di Serio, In vivo and post-synthesis strategies to enhance the properties of PHB-based materials: A review. *Frontiers in Bioengineering and Biotechnology* **2021**. *8*: p. 619266.

46. Yahyapour, R. and Y.Z. Menceloglu, Blending strategies for green packaging: Enhancing polyhydroxybutyrate performance for sustainable solutions. *European Polymer Journal* **2025**. *228*.

47. Soo, X.Y.D., J.K. Muiruri, W.Y. Wu, J.C.C. Yeo, S. Wang, N. Tomczak, W. Thitsartarn, B.H. Tan, P. Wang, and F. Wei, Bio-Polyethylene and Polyethylene Biocomposites: An Alternative toward a Sustainable Future. *Macromolecular Rapid Communications* **2024**: p. 2400064.

48. Barletta, M., C. Aversa, M. Ayyoob, A. Gisario, K. Hamad, M. Mehrpouya, and H. Vahabi, Poly (butylene succinate)(PBS): Materials, processing, and industrial applications. *Progress in Polymer Science* **2022**. *132*: p. 101579.

49. Mochane, M.J., S.I. Magagula, J.S. Sefadi, and T.C. Mokhena, A review on green composites based on natural fiber-reinforced polybutylene succinate (PBS). *Polymers* **2021**. *13*(8): p. 1200.

50. Heinze, T., Cellulose: structure and properties. *Cellulose chemistry and properties: fibers, nanocelluloses and advanced materials* **2016**: p. 1-52.

51. HPS, A.K., C.K. Saurabh, A. Adnan, M.N. Fazita, M. Syakir, Y. Davoudpour, M. Rafatullah, C. Abdullah, M. Haafiz, and R. Dungani, A review on chitosan-cellulose blends and nanocellulose reinforced chitosan biocomposites: Properties and their applications. *Carbohydrate polymers* **2016**. *150*: p. 216-226.

52. Garlapati, V.K., A.K. Chandel, S.P.J. Kumar, S. Sharma, S. Sevda, A.P. Ingle, and D. Pant, Circular economy aspects of lignin: Towards a lignocellulose biorefinery. *Renewable and Sustainable Energy Reviews* **2020**. *130*.

53. Demuner, I., C. F., J., D. L., A. J., and C.M. Jardim, Biorefinery review: Wide-reaching products through kraft lignin. *BioRes* **2019**. *14*(3): p. 7543-7581.

54. Hu, J., Q. Zhang, and D.J. Lee, Kraft lignin biorefinery: A perspective. *Bioresour Technol* **2018**. *247*: p. 1181-1183.

55. Nanda, S., R. Azargohar, A.K. Dalai, and J.A. Kozinski, An assessment on the sustainability of lignocellulosic biomass for biorefining. *Renewable and Sustainable Energy Reviews* **2015**. *50*: p. 925-941.

56. Okolie, J.A., S. Nanda, A.K. Dalai, and J.A. Kozinski, Chemistry and specialty industrial applications of lignocellulosic biomass. *Waste and Biomass Valorization* **2021**. *12*: p. 2145-2169.

57. Petridis, L. and J.C. Smith, Molecular-level driving forces in lignocellulosic biomass deconstruction for bioenergy. *Nature Reviews Chemistry* **2018**. *2*(11): p. 382-389.

58. Moreira, W.M., P.V.V. Moreira, D.F. Dos Santos, M.L. Gimenes, and M.G.A. Vieira, Nanogreen is the new future: the conversion of lignin and lignocellulosic wastes

into nanomaterials. *Environmental Science and Pollution Research* **2023**. *30*(8): p. 19564-19591.

59. Zhang, Z., V. Terrasson, and E. Guénin, Lignin nanoparticles and their nanocomposites. *Nanomaterials* **2021**. *11*(5): p. 1336.

60. Solihat, N.N., L.S. Hua, and W. Fatriasari, Biobased nanoparticles as flame retardant for polymers. *Flame Retardant Nanocomposites* **2024**: p. 321-354.

61. Lin, Y., Q. Zhang, Y. Deng, Q. Wu, X.P. Ye, S. Wang, and G. Fang, Fabricating Graphene and Nanodiamonds from Lignin by Femtosecond Laser Irradiation. *ACS Omega* **2021**. *6*(49): p. 33995-34002.

62. Núñez-Decap, M., C. Friz-Sánchez, C. Opazo-Carlsson, B. Moya-Rojas, and M. Vidal-Vega, A Potential Replacement to Phenol–Formaldehyde-Based Adhesives: A Study of Plywood Panels Manufactured with Bio-Based Wood Protein and Nanolignin Adhesives. *Forests* **2024**. *15*(8): p. 1345.

63. Pylypchuk, I. and M.H. Sipponen, Organic solvent-free production of colloidally stable spherical lignin nanoparticles at high mass concentrations. *Green Chemistry* **2022**.

64. Chauhan, P.S., Lignin nanoparticles: Eco-friendly and versatile tool for new era. *Bioresource Technology Reports* **2020**. *9*: p. 100374.

65. Zhu, J.Y., U.P. Agarwal, P.N. Ciesielski, M.E. Himmel, R.N. Gao, Y.L. Deng, M. Morits, and M. Osterberg, Towards sustainable production and utilization of plant-biomass-based nanomaterials: a review and analysis of recent developments. *Biotechnology for Biofuels* **2021**. *14*(1): p. 114.

66. Barhoum, A., J. Jeevanandam, A. Rastogi, P. Samyn, Y. Boluk, A. Dufresne, M.K. Danquah, and M. Bechelany, Plant celluloses, hemicelluloses, lignins, and volatile oils for the synthesis of nanoparticles and nanostructured materials. *Nanoscale* **2020**. *12*(45): p. 22845-22890.

67. Yeap, S., A.A. Bakar, C. Hassan, and F. Jamaludin, Green Nanocomposites: A Review on Extraction and Applications. *Sustainable Structural Materials*: p. 325-338.

68. Iravani, S. and R.S. Varma, Greener synthesis of lignin nanoparticles and their applications. *Green Chemistry* **2020**. *22*(3): p. 612-636.

69. Garcia Gonzalez, M.N., M. Levi, S. Turri, and G. Griffini, Lignin nanoparticles

by ultrasonication and their incorporation in waterborne polymer nanocomposites. *Journal of Applied Polymer Science* **2017**. *134*(38): p. 45318-45327.

70. Nair, S.S., S. Sharma, Y. Pu, Q. Sun, S. Pan, J.Y. Zhu, Y. Deng, and A.J. Ragauskas, High shear homogenization of lignin to nanolignin and thermal stability of nanolignin-polyvinyl alcohol blends. *ChemSusChem* **2014**. *7*(12): p. 3513-20.

71. Mousavi, S.N., N. Nazarnezhad, G. Asadpour, S.K. Ramamoorthy, and A. Zamani, Ultrafine Friction Grinding of Lignin for Development of Starch Biocomposite Films. *Polymers (Basel)* **2021**. *13*(12): p. 2024.

72. Horseman, T., M. Tajvidi, C.I.K. Diop, and D.J. Gardner, Preparation and property assessment of neat lignocellulose nanofibrils (LCNF) and their composite films. *Cellulose* **2017**. *24*(6): p. 2455-2468.

73. Nair, S.S., J.Y. Zhu, Y. Deng, and A.J. Ragauskas, Characterization of cellulose nanofibrillation by micro grinding. *Journal of Nanoparticle Research* **2014**. *16*(4).

74. Khadraoui, M., R. Khiari, L. Bergaoui, and E. Mauret, Production of lignin-containing cellulose nanofibrils by the combination of different mechanical processes. *Industrial Crops and Products* **2022**. *183*: p. 114991.

75. Huang, D., R. Li, P. Xu, T. Li, R. Deng, S. Chen, and Q. Zhang, The cornerstone of realizing lignin value-addition: Exploiting the native structure and properties of lignin by extraction methods. *Chemical Engineering Journal* **2020**. *402*.

76. Ma, M., L. Dai, J. Xu, Z. Liu, and Y. Ni, A simple and effective approach to fabricate lignin nanoparticles with tunable sizes based on lignin fractionation. *Green Chemistry* **2020**. *22*(6): p. 2011-2017.

77. Wang, X., H. Chen, X. Feng, Q. Zhang, N. Labbé, K. Kim, J. Huang, A.J. Ragauskas, S. Wang, and Y. Zhang, Isolation and characterization of lignocellulosic nanofibers from four kinds of organosolv-fractionated lignocellulosic materials. *Wood Science and Technology* **2020**. *54*(3): p. 503-517.

78. Deng, J., S.-F. Sun, E.-Q. Zhu, J. Yang, H.-Y. Yang, D.-W. Wang, M.-G. Ma, and Z.-J. Shi, Sub-micro and nano-lignin materials: Small size and rapid progress. *Industrial Crops and Products* **2021**. *164*: p. 113412.

79. Gilca, I.A., V.I. Popa, and C. Crestini, Obtaining lignin nanoparticles by

sonication. *Ultrason Sonochem* **2015**. *23*: p. 369-75.

80. Rol, F., N. Belgacem, V. Meyer, M. Petit-Conil, and J. Bras, Production of fire-retardant phosphorylated cellulose fibrils by twin-screw extrusion with low energy consumption. *Cellulose* **2019**. *26*(9): p. 5635-5651.

81. Banvillet, G., C. Grange, D. Curtil, J.-L. Putaux, G. Depres, N. Belgacem, and J. Bras, Cellulose nanofibril production by the combined use of four mechanical fibrillation processes with different destructuration effects. *Cellulose* **2023**. *30*(4): p. 2123-2146.

82. Espinosa, E., F. Rol, J. Bras, and A. Rodríguez, Use of multi-factorial analysis to determine the quality of cellulose nanofibers: effect of nanofibrillation treatment and residual lignin content. *Cellulose* **2020**. *27*(18): p. 10689-10705.

83. Ifuku, S., M. Nogi, M. Yoshioka, M. Morimoto, H. Yano, and H. Saimoto, Fibrillation of dried chitin into 10–20nm nanofibers by a simple grinding method under acidic conditions. *Carbohydrate Polymers* **2010**. *81*(1): p. 134-139.

84. Sanchez-Gutierrez, M., I. Bascon-Villegas, E. Espinosa, E. Carrasco, F. Perez-Rodriguez, and A. Rodriguez, Cellulose Nanofibers from Olive Tree Pruning as Food Packaging Additive of a Biodegradable Film. *Foods* **2021**. *10*(7).

85. Gupta, G.K. and P. Shukla, Lignocellulosic Biomass for the Synthesis of Nanocellulose and Its Eco-Friendly Advanced Applications. *Frontiers in Chemistry* **2020**. *8*.

86. Qin, L., Z. Liu, T. Liu, S. Liu, J. Zhang, J. Wu, and X. Liang, A bioinspired, strong, all-natural, superhydrophobic cellulose-based straw. *Int J Biol Macromol* **2022**. *220*: p. 910-919.

87. Lourencon, T.V., L.G. Greca, D. Tarasov, M. Borrega, T. Tamminen, O.J. Rojas, and M.Y. Balakshin, Lignin-First Integrated Hydrothermal Treatment (HTT) and Synthesis of Low-Cost Biorefinery Particles. *ACS Sustainable Chemistry & Engineering* **2019**. *8*(2): p. 1230-1239.

88. Zhou, Z., K. Rajan, T. Young, N. Labbé, and S. Wang, Effect of processing temperature on nanolignin quality during ultrafine friction grinding. *Industrial Crops and Products* **2023**. *198*: p. 116685.

89. Bhagia, S., J.R. Dunlap, M.Z.A. Khuraishi, R.R. Lowden, W. Muchero, U.K.

Vaidya, Y.Q. Pu, and A.J. Ragauskas, Fabrication of Lignocellulosic Biomass Paper Containing Nanofibrillated Biomasse. *Bioresources* **2021**. *16*(1): p. 209-222.

90. Xu, K., Z. Shi, J. Lyu, Q. Zhang, T. Zhong, G. Du, and S. Wang, Effects of hydrothermal pretreatment on nano-mechanical property of switchgrass cell wall and on energy consumption of isolated lignin-coated cellulose nanofibrils by mechanical grinding. *Industrial Crops and Products* **2020**. *149*: p. 112317.

91. Zhang, Z., W. Liu, B. Lv, T. Ju, and J. Ji, Gas-driven shearing nanonization of lignin particles for efficient reduction of graphene oxide. *Industrial Crops and Products* **2022**. *180*: p. 114665.

92. Assaf, I., Z. Zhang, F. Otaola, M. Leturia, D. Luart, V. Terrasson, and E. Guenin, A continuous flow mode with a scalable tubular reactor for the green preparation of stable alkali lignin nanoparticles assisted by ultrasound. *Int J Biol Macromol* **2023**: p. 125106.

93. Matsakas, L., M. Gerber, L. Yu, U. Rova, and P. Christakopoulos, Preparation of low carbon impact lignin nanoparticles with controllable size by using different strategies for particles recovery. *Industrial Crops and Products* **2020**. *147*: p. 112243.

94. Yaqoob, A.A., S.H. Sekeri, M.B.H. Othman, M.N.M. Ibrahim, and Z.H. Feizi, Thermal degradation and kinetics stability studies of oil palm (Elaeis Guineensis) biomass-derived lignin nanoparticle and its application as an emulsifying agent. *Arabian Journal of Chemistry* **2021**. *14*(6): p. 1878-5352.

95. Boarino, A. and H.A. Klok, Opportunities and Challenges for Lignin Valorization in Food Packaging, Antimicrobial, and Agricultural Applications. *Biomacromolecules* **2023**. *24*(3): p. 1065-1077.

96. Boufi, S., H. Kaddami, and A. Dufresne, Mechanical Performance and Transparency of Nanocellulose Reinforced Polymer Nanocomposites. *Macromolecular Materials and Engineering* **2014**. *299*(5): p. 560-568.

97. Siqueira, G., J. Bras, and A. Dufresne, Cellulosic Bionanocomposites: A Review of Preparation, Properties and Applications. *Polymers* **2010**. *2*(4): p. 728-765.

98. Kargarzadeh, H., J. Huang, N. Lin, I. Ahmad, M. Mariano, A. Dufresne, S. Thomas, and A. Gałęski, Recent developments in nanocellulose-based biodegradable

polymers, thermoplastic polymers, and porous nanocomposites. *Progress in Polymer Science* **2018**. *87*: p. 197-227.

99. Li, Z.-C., W. Li, D.-X. Wang, R. Wang, A.-N. Tang, and D.-M. Kong, Lignin-Based Hydrogen-Bonded Covalent Organic Polymers as Functional "Switches" of Modified Atmosphere Packaging Membranes for Preservation of Perishable Foods. *ACS Sustainable Chemistry & Engineering* **2022**. *10*(33): p. 10803-10815.

100. Didone, M., P. Saxena, E. Brilhuis-Meijer, G. Tosello, G. Bissacco, T.C. Mcaloone, D.C.A. Pigosso, and T.J. Howard, Moulded pulp manufacturing: Overview and prospects for the process technology. *Packaging Technology and Science* **2017**. *30*(6): p. 231-249.

101. Dry Molded Fiber – a new world standard for packaging. [cited 2025 Jan 6]; Available from: https://www.pulpac.com/dry-molded-fiber/#.

102. International, A., Standard Test Method for Rate of Grease Penetration of Flexible Barrier Materials (Rapid Method). **2022**, ASTM International: 100 Barr Harbor Drive, PO Box C700, West Conshohocken, PA 19428-2959. United States. p. 1-3.

103. Liu, C., P. Luan, Q. Li, Z. Cheng, X. Sun, D. Cao, and H. Zhu, Biodegradable, Hygienic, and Compostable Tableware from Hybrid Sugarcane and Bamboo Fibers as Plastic Alternative. *Matter* **2020**. *3*(6): p. 2066-2079.

104. Li, Y., S. Li, and J. Sun, Degradable Poly(vinyl alcohol)-Based Supramolecular Plastics with High Mechanical Strength in a Watery Environment. *Adv Mater* **2021**. *33*(13): p. e2007371.

105. Kwak, H., H. Kim, S.A. Park, M. Lee, M. Jang, S.B. Park, S.Y. Hwang, H.J. Kim, H. Jeon, J.M. Koo, J. Park, and D.X. Oh, Biodegradable, Water-Resistant, Anti-Fizzing, Polyester Nanocellulose Composite Paper Straws. *Adv Sci* **2022**. *10*(1): p. e2205554.

106. Khan, R.J., C.Y. Lau, J. Guan, C.H. Lam, J. Zhao, Y. Ji, H. Wang, J. Xu, D.J. Lee, and S.Y. Leu, Recent advances of lignin valorization techniques toward sustainable aromatics and potential benchmarks to fossil refinery products. *Bioresour Technol* **2022**. *346*: p. 126419.

107. Shu, F., B. Jiang, Y. Yuan, M. Li, W. Wu, Y. Jin, and H. Xiao, Biological Activities and Emerging Roles of Lignin and Lignin-Based Products horizontal line A

Review. *Biomacromolecules* **2021**.

108. Giuliano, A., M.T. Petronea, I.D. Bari, R. Gosselinkb, G. van Ervenb, E. Annevelinkb, K.S. Triantafyllidisc, H. Stichnothed, D. Ladakis, and H. Lange, Sustainable lignin valorization Technical lignin, processes and market development, in *IEA Bioenergy*, L. IEA TASK 42, Editor. **2021**.

109. Jedrzejczak, P., M.N. Collins, T. Jesionowski, and L. Klapiszewski, The role of lignin and lignin-based materials in sustainable construction - A comprehensive review. *Int J Biol Macromol* **2021**. *187*: p. 624-650.

110. Roopan, S.M., An overview of natural renewable bio-polymer lignin towards nano and biotechnological applications. *Int J Biol Macromol* **2017**. *103*: p. 508-514.

111. Mikame, K., Y. Ohashi, Y. Naito, H. Nishimura, M. Katahira, S. Sugawara, K. Koike, and T. Watanabe, Natural Organic Ultraviolet Absorbers from Lignin. *ACS Sustainable Chemistry & Engineering* **2021**. *9*(49): p. 16651-16658.

112. Sadeghifar, H., R. Venditti, J. Jur, R.E. Gorga, and J.J. Pawlak, Cellulose-Lignin Biodegradable and Flexible UV Protection Film. *ACS Sustainable Chemistry & Engineering* **2016**. *5*(1): p. 625-631.

113. Zhang, S., S.-N. Li, Q. Wu, Q. Li, J. Huang, W. Li, W. Zhang, and S. Wang, Phosphorus containing group and lignin toward intrinsically flame retardant cellulose nanofibril-based film with enhanced mechanical properties. *Composites Part B: Engineering* **2021**. *212*.

114. Lin, Y., Q. Zhang, Y. Deng, K. Shen, K. Xu, Y. Yu, S. Wang, and G. Fang, Fabricating Nanodiamonds from Biomass by Direct Laser Writing under Ambient Conditions. *ACS Sustainable Chemistry & Engineering* **2021**. *9*(8): p. 3112-3123.

115. Singh, S.K., K. Ostendorf, M. Euring, and K. Zhang, Environmentally sustainable, high-performance lignin-derived universal adhesive. *Green Chemistry* **2022**. *24*(6): p. 2624-2635.

116. Parvathy, S. As, J.S. Jayan, A. Raman, and A. Saritha, Lignin based nano-composites: Synthesis and applications. *Process Safety and Environmental Protection* **2021**. *145*: p. 395-410.

117. Chen, Y., K. Zheng, L. Niu, Y. Zhang, Y. Liu, C. Wang, and F. Chu, Highly

mechanical properties nanocomposite hydrogels with biorenewable lignin nanoparticles. *Int J Biol Macromol* **2019**. *128*: p. 414-420.

118. Yang, Y., J. Xu, J. Zhou, and X. Wang, Preparation, characterization and formation mechanism of size-controlled lignin nanoparticles. *Int J Biol Macromol* **2022**. *217*: p. 312-320.

119. Pylypchuk, I.V., A. Riazanova, M.E. Lindström, and O. Sevastyanova, Structural and molecular-weight-dependency in the formation of lignin nanoparticles from fractionated soft- and hardwood lignins. *Green Chemistry* **2021**. *23*(8): p. 3061-3072.

120. Silva, G.G.D., M. Couturier, J.-G. Berrin, A. Buléon, and X. Rouau, Effects of grinding processes on enzymatic degradation of wheat straw. *Bioresour Technol* **2012**. *103*(1): p. 192-200.

121. Hennart, S.L.A., W.J. Wildeboer, P. van Hee, and G.M.H. Meesters, Stability of particle suspensions after fine grinding. *Powder Technology* **2010**. *199*(3): p. 226-231.

122. Jiang, Y., Z. Wang, L. Zhou, S. Jiang, X. Liu, H. Zhao, Q. Huang, L. Wang, G. Chen, and S. Wang, Highly efficient and selective modification of lignin towards optically designable and multifunctional lignocellulose nanopaper for green light-management applications. *Int J Biol Macromol* **2022**. *206*: p. 264-276.

123. Jin, H., H. Shi, W. Jia, Y. Sun, X. Sheng, Y. Guo, H. Li, and H. Sun, Green solvents-based molecular weight controllable fractionation process for industrial alkali lignin at room temperature. *Int J Biol Macromol* **2022**. *207*: p. 531-540.

124. Gordobil, O., R. Delucis, I. Egüés, and J. Labidi, Kraft lignin as filler in PLA to improve ductility and thermal properties. *Industrial Crops and Products* **2015**. *72*: p. 46-53.

125. Dai, Z., X.J. Shi, H. Liu, H.M. Li, Y. Han, and J.H. Zhou, High-strength lignin-based carbon fibers via a low-energy method. *Rsc Advances* **2018**. *8*(3): p. 1218-1224.

126. Ago, M., J.E. Jakes, and O.J. Rojas, Thermomechanical properties of lignin-based electrospun nanofibers and films reinforced with cellulose nanocrystals: a dynamic mechanical and nanoindentation study. *ACS Appl Mater Interfaces* **2013**. *5*(22): p. 11768-76.

127. Serpa Guerra, A.M., C. Gomez Hoyos, J.A. Velasquez-Cock, L. Velez Penagos,

P. Ganan Rojo, L. Velez Acosta, M.A. Pereira, and R. Zuluaga, Effect of ultra-fine friction grinding on the physical and chemical properties of curcuma (Curcuma longa L.) suspensions. *J Food Sci* **2020**. *85*(1): p. 132-142.

128. Nakata, A.F.L., M. Hyde, H. Hyodo, and Murata, A probabilistic approach to sand particle crushing in the triaxial test. **1999**. *49*(5): p. 567-583.

129. Kikumoto, M., D.M. Wood, and A. Russell, Particle Crushing and Deformation Behaviour. *Soils and Foundations* **2010**. *50*(4): p. 547-563.

130. Vural, D., C. Gainaru, H. O'Neill, Y. Pu, M.D. Smith, J.M. Parks, S.V. Pingali, E. Mamontov, B.H. Davison, A.P. Sokolov, A.J. Ragauskas, J.C. Smith, and L. Petridis, Impact of hydration and temperature history on the structure and dynamics of lignin. *Green Chemistry* **2018**. *20*(7): p. 1602-1611.

131. Naduparambath, S., V.J. T, S. V, P.S. M, A.K. Balan, and P. E, Isolation and characterisation of cellulose nanocrystals from sago seed shells. *Carbohydr Polym* **2018**. *180*: p. 13-20.

132. Mattinen, M.L., G. Riviere, A. Henn, R.W.N. Nugroho, T. Leskinen, O. Nivala, J.J. Valle-Delgado, M.A. Kostiainen, and M. Osterberg, Colloidal Lignin Particles as Adhesives for Soft Materials. *Nanomaterials (Basel)* **2018**. *8*(12).

133. Wang, J., Y. Qian, L. Li, and X. Qiu, Atomic Force Microscopy and Molecular Dynamics Simulations for Study of Lignin Solution Self-Assembly Mechanisms in Organic-Aqueous Solvent Mixtures. *ChemSusChem* **2020**. *13*(17): p. 4420-4427.

134. Lievonen, M., J.J. Valle-Delgado, M.-L. Mattinen, E.-L. Hult, K. Lintinen, M.A. Kostiainen, A. Paananen, G.R. Szilvay, H. Setälä, and M. Österberg, A simple process for lignin nanoparticle preparation. *Green Chemistry* **2016**. *18*(5): p. 1416-1422.

135. Pizzi, A., J.M. Leban, F. Kanazawa, M. Properzi, and F. Pichelin, Wood dowel bonding by high-speed rotation welding. *Journal of Adhesion Science and Technology* **2004**. *18*(11): p. 1263-1278.

136. Ganne-Chédeville, C., M. Properzi, J.-M. Leban, A. Pizzi, and F. Pichelin, Wood Welding Chemical and Physical Changes According to the Welding Time. *Journal ofAdhesion Science and Technology* **2008**. *22*: p. 761-773.

137. Lizundia, E., I. Armentano, F. Luzi, F. Bertoglio, E. Restivo, L. Visai, L. Torre,

and D. Puglia, Synergic Effect of Nanolignin and Metal Oxide Nanoparticles into Poly(L-lactide) Bionanocomposites: Material Properties, Antioxidant Activity, and Antibacterial Performance. *Acs Applied Bio Materials* **2020**. *3*(8): p. 5263-5274.

138. Cusola, O., O.J. Rojas, and M.B. Roncero, Lignin Particles for Multifunctional Membranes, Antioxidative Microfiltration, Patterning, and 3D Structuring. *Acs Applied Materials & Interfaces* **2019**. *11*(48): p. 45226-45236.

139. Sutton, J.T., K. Rajan, D.P. Harper, and S.C. Chmely, Lignin-Containing Photoactive Resins for 3D Printing by Stereolithography. *ACS Appl Mater Interfaces* **2018**. *10*(42): p. 36456-36463.

140. Gendron, J., I. Stambouli, C. Bruel, Y. Boumghar, and D. Montplaisir, Characterization of different types of lignin and their potential use in green adhesives. *Industrial Crops and Products* **2022**. *182*.

141. Lee, J.H., T.M. Kim, I.G. Choi, and J.W. Choi, Phenolic Hydroxyl Groups in the Lignin Polymer Affect the Formation of Lignin Nanoparticles. *Nanomaterials (Basel)* **2021**. *11*(7).

142. Wen, J.-L., S.-L. Sun, T.-Q. Yuan, and R.-C. Sun, Structural elucidation of whole lignin from Eucalyptus based on preswelling and enzymatic hydrolysis. *Green Chemistry* **2015**. *17*(3): p. 1589-1596.

143. Wang, J., K. Rajan, A. Annamraju, S.C. Chmely, S.V. Pingali, D.J. Carrier, and N. Labbé, A Sequential Autohydrolysis-Ionic Liquid Fractionation Process for High Quality Lignin Production. *Energy & Fuels* **2021**. *35*(3): p. 2293-2302.

144. De Santi, A., S. Monti, G. Barcaro, Z. Zhang, K. Barta, and P.J. Deuss, New Mechanistic Insights into the Lignin beta-O-4 Linkage Acidolysis with Ethylene Glycol Stabilization Aided by Multilevel Computational Chemistry. *ACS Sustain Chem Eng* **2021**. *9*(5): p. 2388-2399.

145. Chen, K., S.Y. Wang, Y.G. Qi, H. Guo, Y.Z. Guo, and H.M. Li, State-of-the-Art: Applications and Industrialization of Lignin Micro/Nano Particles. *Chemsuschem* **2021**. *14*(5): p. 1284-1294.

146. Huang, J., S. Lyu, Z. Chen, S. Wang, and F. Fu, A facile method for fabricating robust cellulose nanocrystal/SiO2 superhydrophobic coatings. *J Colloid Interface Sci*

2019. *536*: p. 349-362.

147. Toledano, A., L. Serrano, A. Garcia, I. Mondragon, and J. Labidi, Comparative study of lignin fractionation by ultrafiltration and selective precipitation. *Chemical Engineering Journal* **2010**. *157*(1): p. 93-99.

148. Li, Z., Y. Ge, and L. Wan, Fabrication of a green porous lignin-based sphere for the removal of lead ions from aqueous media. *J Hazard Mater* **2015**. *285*: p. 77-83.

149. Gao, K., J. Liu, X. Li, H. Gojzewski, X. Sui, and G.J. Vancso, Lignin Nanoparticles as Highly Efficient, Recyclable Emulsifiers for Enhanced Oil Recovery. *ACS Sustainable Chemistry & Engineering* **2022**. *10*(29): p. 9334–9344.

150. Zhou, X., E. Liu, J. Li, F. Chen, Y. Zhang, K. Chen, and D. Qi, Facile Synthesis of Rodlike TiO2/Lignin Nanostructures as Multifunctional Emulsifiers for High Internal Phase Emulsions. *ACS Applied Nano Materials* **2023**.

151. Yu, H., B. Wang, Y. Wang, E. Xu, R. Wang, S. Wu, W. Wu, B. Ji, X. Feng, H. Xu, Y. Zhong, and Z. Mao, Lignin Nanoparticles with High Phenolic Content as Efficient Antioxidant and Sun-Blocker for Food and Cosmetics. *ACS Sustainable Chemistry & Engineering* **2023**. *11*(10): p. 4082-4092.

152. Huang, J., Y. Wan, M. Wang, J. Yang, F. Sun, A. Abdulkhani, X. Liu, H. Nawaz, F. Xu, and X. Zhang, Lignin nanorods reinforced nanocomposite hydrogels with UV-shielding, anti-freezing and anti-drying applications. *Industrial Crops and Products* **2022**. *187*: p. 115324.

153. Zhang, D.X., R. Wang, C. Ren, Y. Wang, B.X. Li, W. Mu, F. Liu, and Y. Hou, One-Step Construct Responsive Lignin/Polysaccharide/Fe Nano Loading System Driven by Digestive Enzymes of Lepidopteran for Precise Delivery of Pesticides. *ACS Appl Mater Interfaces* **2022**. *14*(36): p. 41337−47.

154. Beaucamp, A., M. Culebras, and M.N. Collins, Sustainable mesoporous carbon nanostructures derived from lignin for early detection of glucose. *Green Chemistry* **2021**. *23*(15): p. 5696-5705.

155. Qu, W., P. Hu, J. Liu, H. Jin, and K. Wang, Lignin-based carbon fiber: A renewable and low-cost substitute towards featured fiber-shaped pseudocapacitor electrodes. *Journal of Cleaner Production* **2022**. *343*.

156. Shavandi, A., S. Hosseini, O.V. Okoro, L. Nie, F.E. Babadi, and F. Melchels, 3D Bioprinting of Lignocellulosic Biomaterials. *Advanced Healthcare Materials* **2020**. *9*(24): p. 2001472.
157. Verma, S., S.A.R. Hashmi, M. Mili, V. Hada, N. Prashant, A. Naik, S.K.S. Rathore, and A.K. Srivastava, Extraction and applications of lignin from bamboo: a critical review. *European Journal of Wood and Wood Products* **2021**. *79*(6): p. 1341-1357.
158. S, S., A.M. Shabbirahmed, D. Haldar, A.K. Patel, and R.R. Singhania, Influence of reaction conditions on synthesis and applications of lignin nanoparticles derived from agricultural wastes. *Environmental Technology & Innovation* **2023**. *31*.
159. Yadav, V.K., N. Gupta, P. Kumar, M.G. Dashti, V. Tirth, S.H. Khan, K.K. Yadav, S. Islam, N. Choudhary, A. Algahtani, S.P. Bera, D.H. Kim, and B.H. Jeon, Recent Advances in Synthesis and Degradation of Lignin and Lignin Nanoparticles and Their Emerging Applications in Nanotechnology. *Materials (Basel)* **2022**. *15*(3).
160. Do, N.H., H.H. Pham, T.M. Le, J. Lauwaert, L. Diels, A. Verberckmoes, N.H.N. Do, V.T. Tran, and P.K. Le, The novel method to reduce the silica content in lignin recovered from black liquor originating from rice straw. *Sci Rep* **2020**. *10*(1): p. 21263.
161. Xiong, F., Y. Han, S. Wang, G. Li, T. Qin, Y. Chen, and F. Chu, Preparation and formation mechanism of size-controlled lignin nanospheres by self-assembly. *Industrial Crops and Products* **2017**. *100*: p. 146-152.
162. Xiong, F., Y. Han, S. Wang, G. Li, T. Qin, Y. Chen, and F. Chu, Preparation and Formation Mechanism of Renewable Lignin Hollow Nanospheres with a Single Hole by Self-Assembly. *ACS Sustainable Chemistry & Engineering* **2017**. *5*(3): p. 2273-2281.
163. Mastrolitti, S., E. Borsella, A. Giuliano, T. Petrone, I.D. Bari, R. Gosselink, G.v. Erven, E. Annevelink, K.S. Triantafyllidis, and H. Stichnothe. Sustainable lignin valorization Technical lignin, processes and market development. in *Task 42 Webinar on Sustainable Lignin Valorisation*. **2021**. Zoom: IEA Bioenergy.
164. Rol, F., B. Karakashov, O. Nechyporchuk, M. Terrien, V. Meyer, A. Dufresne, M.N. Belgacem, and J. Bras, Pilot-Scale Twin Screw Extrusion and Chemical Pretreatment as an Energy-Efficient Method for the Production of Nanofibrillated

Cellulose at High Solid Content. *ACS Sustainable Chemistry & Engineering* **2017**. *5*(8): p. 6524-6531.

165. benBonjour, O., H. Nederstedt, M.V. Arcos-Hernandez, S. Laanesoo, L. Vares, and P. Jannasch, Lignin-Inspired Polymers with High Glass Transition Temperature and Solvent Resistance from 4-Hydroxybenzonitrile, Vanillonitrile, and Syringonitrile Methacrylates. *ACS Sustain Chem Eng* **2021**. *9*(50): p. 16874-16880.

166. Li, W., N. Sun, B. Stoner, X. Jiang, X. Lu, and R.D. Rogers, Rapid dissolution of lignocellulosic biomass in ionic liquids using temperatures above the glass transition of lignin. *Green Chemistry* **2011**. *13*(8): p. 2038–2047.

167. Vural, D., J.C. Smith, and L. Petridis, Dynamics of the lignin glass transition. *Phys Chem Chem Phys* **2018**. *20*(31): p. 20504-20512.

168. Irvine, G.M., The significance of the glass transition of lignin in thermomechanical pulping. *Wood Science and Technology* **1985**. *19*: p. 139-149.

169. Gallego-Garcia, M., A.D. Moreno, P. Manzanares, M.J. Negro, and A. Duque, Recent advances on physical technologies for the pretreatment of food waste and lignocellulosic residues. *Bioresour Technol* **2023**. *369*: p. 128397.

170. Luo, J.Q., Y.Q. Su, J.H. Chen, X.H. Wang, and J.G. Liu, Pretreatment of lignin-containing cellulose micro/nano-fibrils (LCMNF) from corncob residues. *Cellulose* **2021**. *28*(8): p. 4671-4684.

171. Österberg, M., M.H. Sipponen, B.D. Mattos, and O.J. Rojas, Spherical lignin particles: a review on their sustainability and applications. *Green Chemistry* **2020**. *22*(9): p. 2712-2733.

172. Yang, L. and H. Yin, Parametric study of particle sedimentation by dissipative particle dynamics simulation. *Physical Review E* **2014**. *90*(3): p. 033311.

173. MacLeod, M., H.P.H. Arp, M.B. Tekman4, and A. Jahnke, The global threat from plastic pollution. *Science* **2021**. *373*: p. 61-65.

174. García-Gil, Á., M.D. Molina-Ramírez, R.A. García-Muñoz, R. Marasini, L. Buck, K.G. McGuigan, and J. Marugán, Weathering of plastic SODIS containers and the impact of ageing on their lifetime and disinfection efficacy. *Chemical Engineering Journal* **2022**. *435*: p. 134881.

175. Guan, Q.F., H.B. Yang, Y.X. Zhao, Z.M. Han, Z.C. Ling, K.P. Yang, C.H. Yin, and S.H. Yu, Microplastics release from victuals packaging materials during daily usage. *EcoMat* **2021**. *3*(3): p. e12107.
176. Filiciotto, L. and G. Rothenberg, Biodegradable Plastics: Standards, Policies, and Impacts. *ChemSusChem* **2021**. *14*(1): p. 56-72.
177. Lefroy, K.S., B.S. Murray, and M.E. Ries, Effect of Oil on Cellulose Dissolution in the Ionic Liquid 1-Butyl-3-methyl Imidazolium Acetate. *ACS Omega* **2022**. *7*(42): p. 37532-37545.
178. Wang, X., Q. Xia, S. Jing, C. Li, Q. Chen, B. Chen, Z. Pang, B. Jiang, W. Gan, G. Chen, M. Cui, L. Hu, and T. Li, Strong, Hydrostable, and Degradable Straws Based on Cellulose-Lignin Reinforced Composites. *Small* **2021**. *17*(18): p. e2008011.
179. Scheringer, M., J.H. Johansson, M.E. Salter, B. Sha, and I.T. Cousins, Stories of Global Chemical Pollution: Will We Ever Understand Environmental Persistence? *Environ Sci Technol* **2022**. *56*(24): p. 17498-17501.
180. Li, T., C. Chen, A.H. Brozena, J.Y. Zhu, L. Xu, C. Driemeier, J. Dai, O.J. Rojas, A. Isogai, L. Wagberg, and L. Hu, Developing fibrillated cellulose as a sustainable technological material. *Nature* **2021**. *590*(7844): p. 47-56.
181. Proestos, C. and T. Varzakas, Aromatic Plants: Antioxidant Capacity and Polyphenol Characterisation. *Foods* **2017**. *6*(4): p. 28.
182. Wang, Y., J. Hou, Y. Huang, and Y. Fu, Structure-controlled lignin complex for PLA composites with outstanding antibacterial, fluorescent and photothermal conversion properties. *Int J Biol Macromol* **2022**. *194*: p. 1002-1009.
183. Xiang, H.J., A.L. Zhong, L. Xiao, T.R. Deng, T.G. Hu, H. Wang, and P. Wen, Fabrication of alkali lignin-based emulsion electrospun nanofibers for the nanoencapsulation of beta-carotene and the enhanced antioxidant property. *Int J Biol Macromol* **2022**. *218*: p. 739-750.
184. Sirvio, J.A., M.Y. Ismail, K.T. Zhang, M.V. Tejesvi, and A. Ammala, Transparent lignin-containing wood nanofiber films with UV-blocking, oxygen barrier, and anti-microbial properties. *Journal of Materials Chemistry A* **2020**. *8*(16): p. 7935-7946.
185. Najahi, A., Q. Tarres, M. Delgado-Aguilar, J.L. Putaux, and S. Boufi, High-

Lignin-Containing Cellulose Nanofibrils from Date Palm Waste Produced by Hydrothermal Treatment in the Presence of Maleic Acid. *Biomacromolecules* **2023**.

186. Feng, X., Z. Yang, S. Chmely, Q. Wang, S. Wang, and Y. Xie, Lignin-coated cellulose nanocrystal filled methacrylate composites prepared via 3D stereolithography printing: Mechanical reinforcement and thermal stabilization. *Carbohydr Polym* **2017**. *169*: p. 272-281.

187. Solala, I., M.C. Iglesias, and M.S. Peresin, On the potential of lignin-containing cellulose nanofibrils (LCNFs): a review on properties and applications. *Cellulose* **2020**. *27*(4): p. 1853-1877.

188. Rojo, E., M.S. Peresin, W.W. Sampson, I.C. Hoeger, J. Vartiainen, J. Laine, and O.J. Rojas, Comprehensive elucidation of the effect of residual lignin on the physical, barrier, mechanical and surface properties of nanocellulose films. *Green Chemistry* **2015**. *17*(3): p. 1853-1866.

189. Li, W., S.F. Wang, W. Wang, C.R. Qin, and M. Wu, Facile preparation of reactive hydrophobic cellulose nanofibril film for reducing water vapor permeability (WVP) in packaging applications. *Cellulose* **2019**. *26*(5): p. 3271-3284.

190. Wang, W., C.R. Qin, W. Li, Z.H. Li, and J. Li, Design of antibacterial cellulose nanofibril film by the incorporation of guanidine-attached lignin nanoparticles. *Cellulose* **2022**. *29*(6): p. 3439-3451.

191. Li, Z., M. Rabnawaz, M.G. Sarwar, B. Khan, A. Krishna Nair, N. Sirinakbumrung, and D.P. Kamdem, A closed-loop and sustainable approach for the fabrication of plastic-free oil- and water-resistant paper products. *Green Chemistry* **2019**. *21*(20): p. 5691-5700.

192. Bayer, I.S., Superhydrophobic Coatings from Ecofriendly Materials and Processes: A Review. *Advanced Materials Interfaces* **2020**. *7*(13).

193. Cai, H., F. Du, L. Li, B. Li, J. Li, and H. Shi, A practical approach based on FT-IR spectroscopy for identification of semi-synthetic and natural celluloses in microplastic investigation. *Sci Total Environ* **2019**. *669*: p. 692-701.

194. Xu, K., Q. Li, L. Xie, Z. Shi, G. Su, D. Harper, Z. Tang, J. Zhou, G. Du, and S. Wang, Novel flexible, strong, thermal-stable, and high-barrier switchgrass-based lignin-

containing cellulose nanofibrils/chitosan biocomposites for food packaging. *Industrial Crops and Products* **2022**. *179*.

195. Youssef, B., A. Soumia, E. Mounir, C. Omar, L. Abdelaziz, E. Mehdi, and Z. Mohamed, Preparation and Properties of Bionanocomposite Films Reinforced with Nanocellulose Isolated from Moroccan Alfa Fibres. *Autex Research Journal* **2015**. *15*(3): p. 164-172.

196. Rynkowska, E., K. Fatyeyeva, S. Marais, J. Kujawa, and W. Kujawski, Chemically and Thermally Crosslinked PVA-Based Membranes: Effect on Swelling and Transport Behavior. *Polymers (Basel)* **2019**. *11*(11): p. 1799.

197. Mizan, M.M.H., P.M. Gurave, M. Rastgar, A. Rahimpour, R.K. Srivastava, and M. Sadrzadeh, "Biomass to Membrane": Sulfonated Kraft Lignin/PCL Superhydrophilic Electrospun Membrane for Gravity-Driven Oil-in-Water Emulsion Separation. *ACS Appl Mater Interfaces* **2023**. *15*(35): p. 41961-41976.

198. Fu, J., S. Wang, C. He, Z. Lu, J. Huang, and Z. Chen, Facilitated fabrication of high strength silica aerogels using cellulose nanofibrils as scaffold. *Carbohydr Polym* **2016**. *147*: p. 89-96.

199. Barbe, S., M. Berger, R. Engstler, A. Dieste, L. Clavijo, E. Favvas, and A. Sapalidis, One-step preparation of bilayered films from kraft lignin and cellulose acetate to mimic tree bark. *European Journal of Wood and Wood Products* **2020**. *78*(4): p. 831-834.

200. Geyer, R., J.R. Jambeck, and K.L. Law, Production, use, and fate of all plastics ever made. *Science Advances* **2017**. *3*(7): p. e1700782.

201. Jiang, B., C. Chen, Z. Liang, S. He, Y. Kuang, J. Song, R. Mi, G. Chen, M. Jiao, and L. Hu, Lignin as a Wood-Inspired Binder Enabled Strong, Water Stable, and Biodegradable Paper for Plastic Replacement. *Advanced Functional Materials* **2019**. *30*(4).

202. Qin, Z.H., J.H. Mou, C.Y.H. Chao, S.S. Chopra, W. Daoud, S.Y. Leu, Z. Ning, C.Y. Tso, C.K. Chan, S. Tang, Z.J. Hathi, M.A. Haque, X. Wang, and C.S.K. Lin, Biotechnology of Plastic Waste Degradation, Recycling, and Valorization: Current Advances and Future Perspectives. *ChemSusChem* **2021**. *14*(19): p. 4103-4114.

203. Chamas, A., H. Moon, J. Zheng, Y. Qiu, T. Tabassum, J.H. Jang, M. Abu-Omar, S.L. Scott, and S. Suh, Degradation Rates of Plastics in the Environment. *ACS Sustainable Chemistry & Engineering* **2020**. *8*(9): p. 3494-3511.
204. Ghosh, K. and B.H. Jones, Roadmap to Biodegradable Plastics—Current State and Research Needs. *ACS Sustainable Chemistry & Engineering* **2021**. *9*(18): p. 6170-6187.
205. Lambert, S. and M. Wagner, Environmental performance of bio-based and biodegradable plastics: the road ahead. *Chem Soc Rev* **2017**. *46*(22): p. 6855-6871.
206. Bagheri, A.R., C. Laforsch, A. Greiner, and S. Agarwal, Fate of So-Called Biodegradable Polymers in Seawater and Freshwater. *Glob Chall* **2017**. *1*(4): p. 1700048.
207. Zhao, X., K. Cornish, and Y. Vodovotz, Narrowing the Gap for Bioplastic Use in Food Packaging: An Update. *Environ Sci Technol* **2020**. *54*(8): p. 4712-4732.
208. Li, D.H., Z.M. Han, Q. He, K.P. Yang, W.B. Sun, H.C. Liu, Y.X. Zhao, Z.X. Liu, C.N. Zong, H.B. Yang, Q.F. Guan, and S.H. Yu, Ultrastrong, Thermally Stable, and Food-Safe Seaweed-Based Structural Material for Tableware. *Adv Mater* **2023**. *35*(1): p. e2208098.
209. Luan, P., J. Li, S. He, Y. Kuang, L. Mo, and T. Song, Investigation of deposit problem during sugarcane bagasse pulp molded tableware production. *Journal of Cleaner Production* **2019**. *237*: p. 117856.
210. Wang, H., F. Xiong, Y. Tan, J. Yang, Y. Qing, F. Chu, and Y. Wu, Preparation and Formation Mechanism of Covalent–Noncovalent Forces Stabilizing Lignin Nanospheres and Their Application in Superhydrophobic and Carbon Materials. *ACS Sustainable Chemistry & Engineering* **2021**. *9*(10): p. 3811-3820.
211. Ma, B., F. Xiong, H. Wang, Y. Qing, F. Chu, and Y. Wu, Tailorable and scalable production of eco-friendly lignin micro-nanospheres and their application in functional superhydrophobic coating. *Chemical Engineering Journal* **2023**: p. 141309.
212. Su, W., Z. Yang, H. Wang, J. Fang, C. Li, G. Lyu, and H. Li, Synergistic Effect of Sodium Alginate and Lignin on the Properties of Biodegradable Poly(vinyl alcohol) Mulch Films. *ACS Sustainable Chemistry & Engineering* **2022**. *10*(36): p. 11800–11814.
213. Wang, H.-M., T.-Q. Yuan, G.-Y. Song, and R.-C. Sun, Advanced and versatile

lignin-derived biodegradable composite film materials toward a sustainable world. *Green Chemistry* **2021**. *23*(11): p. 3790-3817.

214. Roostazadeh, R., T. Behzad, and K. Karimi, Isolation and characterization of lignin-rich particles as byproducts of bioethanol production from wheat straw to reinforce starch composite films. *Industrial Crops and Products* **2022**. *186*: p. 115175.

215. Feng, Y., J. Yu, D. Sun, W. Ren, C. Shao, and R. Sun, Solvent-induced in-situ self-assembly lignin nanoparticles to reinforce conductive nanocomposite organogels as anti-freezing and anti-dehydration flexible strain sensors. *Chemical Engineering Journal* **2022**. *433*.

216. Choe, S., S. You, K. Park, Y. Kim, J. Park, Y. Cho, J. Seo, H. Yang, and J. Myung, Boric acid-crosslinked poly(vinyl alcohol): biodegradable, biocompatible, robust, and high-barrier paper coating. *Green Chemistry* **2024**. *26*(14): p. 8230-8241.

217. Rojas, K., D. Canales, N. Amigo, L. Montoille, A. Cament, L.M. Rivas, O. Gil-Castell, P. Reyes, M.T. Ulloa, A. Ribes-Greus, and P.A. Zapata, Effective antimicrobial materials based on low-density polyethylene (LDPE) with zinc oxide (ZnO) nanoparticles. *Composites Part B: Engineering* **2019**. *172*: p. 173-178.

218. Oun, A.A., S. Shankar, and J.W. Rhim, Multifunctional nanocellulose/metal and metal oxide nanoparticle hybrid nanomaterials. *Critical Reviews in Food Science and Nutrition* **2020**. *60*(3): p. 435-460.

219. Guan, M.Y., H.N. Zhong, Z.W. Wang, W.W. Yu, and C.Y. Hu, Chemical contaminants from food contact materials and articles made from or containing wood and bamboo - a review. *Food Addit Contam Part A Chem Anal Control Expo Risk Assess* **2023**. *40*(3): p. 434-453.

220. Zhang, X., X. He, D. Pan, L. Shi, Y. Wu, Y. Yang, Y. Zhu, Y. Wang, H. Wang, L. Pu, S. He, L. Meng, and J. Li, Effects of thermal exposure to disposable plastic tableware on human gut microbiota and metabolites: A quasi-experimental study. *J Hazard Mater* **2024**. *462*: p. 132800.

221. Grechko, J.S., S. Brosché, and Valeriya, Forever chemicals in single-use food packaging and tableware from 17 countries. **2023**, IPEN. p. 1-57.

222. Hannon, J.C., J. Kerry, M. Cruz-Romero, M. Morris, and E. Cummins, Advances

and challenges for the use of engineered nanoparticles in food contact materials. *Trends in Food Science & Technology* **2015**. *43*(1): p. 43-62.

223. Alamri, M.S., A.A.A. Qasem, A.A. Mohamed, S. Hussain, M.A. Ibraheem, G. Shamlan, H.A. Alqah, and A.S. Qasha, Food packaging's materials: A food safety perspective. *Saudi J Biol Sci* **2021**. *28*(8): p. 4490-4499.

224. Parit, M., H. Du, X. Zhang, and Z. Jiang, Flexible, Transparent, UV-Protecting, Water-Resistant Nanocomposite Films Based on Polyvinyl Alcohol and Kraft Lignin-Grafted Cellulose Nanofibers. *ACS Applied Polymer Materials* **2022**. *4*(5): p. 3587-3597.

225. Franca, T., D. Goncalves, and C. Cena, ATR-FTIR spectroscopy combined with machine learning for classification of PVA/PVP blends in low concentration. *Vibrational Spectroscopy* **2022**. *120*.

226. Cuiffo, M.A., J. Snyder, A.M. Elliott, N. Romero, S. Kannan, and G.P. Halada, Impact of the Fused Deposition (FDM) Printing Process on Polylactic Acid (PLA) Chemistry and Structure. *Applied Sciences* **2017**. *7*(6).

227. Ma, L., Y. Zhang, Y. Meng, P. Anusonti-Inthra, and S. Wang, Preparing cellulose nanocrystal/acrylonitrile-butadiene-styrene nanocomposites using the master-batch method. *Carbohydr Polym* **2015**. *125*: p. 352-9.

228. Xiang, S., L. Feng, X. Bian, G. Li, and X. Chen, Evaluation of PLA content in PLA/PBAT blends using TGA. *Polymer Testing* **2020**. *81*: p. 106211.

229. Yang, W., H. Ding, G. Qi, C. Li, P. Xu, T. Zheng, X. Zhu, J.M. Kenny, D. Puglia, and P. Ma, Highly transparent PVA/nanolignin composite films with excellent UV shielding, antibacterial and antioxidant performance. *Reactive and Functional Polymers* **2021**. *162*: p. 104873.

230. Hubbe, M.A., A. Pizzi, H. Zhang, and R. Halis, Critical Links Governing Performance of Self-binding and Natural Binders for Hot-pressed Reconstituted Lignocellulosic Board without Added Formaldehyde: A Review. *BioResources* **2018**. *13*(1): p. 2049-2115.

231. Zhang, G., C. Tian, J. Shi, X. Zhang, J. Liu, T. Tan, and L. Zhang, Mechanically Robust, Self-Repairable, Shape Memory and Recyclable Ionomeric Elastomer Composites with Renewable Lignin via Interfacial Metal-Ligand Interactions. *ACS Appl*

Mater Interfaces **2022**. *14*(33): p. 38216-38227.

232. Ji, M., J. Li, F. Li, X. Wang, J. Man, J. Li, C. Zhang, and S. Peng, A biodegradable chitosan-based composite film reinforced by ramie fibre and lignin for food packaging. *Carbohydr Polym* **2022**. *281*: p. 119078.

233. Li, P., C. Yang, D. Yi, S. Li, M. Wang, H. Wang, Y. Jin, and W. Wu, Preparation of spherical porous carbon from lignin-derived phenolic resin and its application in supercapacitor electrodes. *Int J Biol Macromol* **2023**. *252*: p. 126271.

234. Zhang, B., S. Fang, and J. Ke, High efficient adsorption of W(VI) with a novel lignin-based biosorbent functionalized with Zn(2+) and polyamine. *Int J Biol Macromol* **2023**. *250*: p. 126083.

235. Song, D., L.-W. Ma, B. Pang, R. An, J.-H. Nie, Y.-R. Guo, and S. Li, An Active Bio-Based Food Packaging Material of ZnO@Plant Polyphenols/Cellulose/Polyvinyl Alcohol: DESIGN, Characterization and Application. *International Journal of Molecular Sciences* **2023**. *24*(2): p. 1577.

236. Ramos-Corona, A., R. Rangel, J. Espino, J. Lara, R. Nuñez, P. Bartolo-Pérez, and J.J. Alvarado-Gil, High-yield of Lignin degradation under N-ZnO/Graphene oxide compounds. *Catalysis Today* **2022**. *392-393*: p. 81-92.

237. Hussain, M.Z., G.S. Pawar, Z. Huang, A.A. Tahir, R.A. Fischer, Y. Zhu, and Y. Xia, Porous ZnO/Carbon nanocomposites derived from metal organic frameworks for highly efficient photocatalytic applications: A correlational study. *Carbon* **2019**. *146*: p. 348-363.

238. Wang, G.X., D. Huang, J.H. Ji, C. Volker, and F.R. Wurm, Seawater-Degradable Polymers-Fighting the Marine Plastic Pollution. *Adv Sci (Weinh)* **2020**. *8*(1): p. 2001121.

239. Semple, K.E., C. Zhou, O.J. Rojas, W.N. Nkeuwa, and C. Dai, Moulded pulp fibers for disposable food packaging: A state-of-the-art review. *Food Packaging and Shelf Life* **2022**. *33*.

240. Final national strategy to prevent plastic pollution. **2024**, The US Environmental Protection Agency (EPA).

241. Ginebreda, A., D. Guillén, D. Barceló, and R.M. Darbra, Additives in the Paper Industry, in *Global Risk-Based Management of Chemical Additives I: Production, Usage*

and Environmental Occurrence, B. Bilitewski, R.M. Darbra, and D. Barceló, Editors. **2012**, Springer Berlin Heidelberg: Berlin, Heidelberg. p. 11-34.

242. Larsson, O.L., Linus, METHOD FOR MANUFACTURING A CELLULOSE PRODUCT, CELLULOSE PRODUCT FORMING APPARATUS AND CELLULOSE PRODUCT. **2024**, Pulpac AB: AUSTRALIAN. p. 35.

243. Aydemir, D. and D.J. Gardner, Biopolymer blends of polyhydroxybutyrate and polylactic acid reinforced with cellulose nanofibrils. *Carbohydr Polym* **2020**. *250*: p. 116867.

244. Mohammadalipour, M., T. Behzad, S. Karbasi, M.B. Khorzoghi, and Z. Mohammadalipour, Osteogenic potential of PHB-lignin/cellulose nanofiber electrospun scaffold as a novel bone regeneration construct. *Int J Biol Macromol* **2023**: p. 126076.

245. Guo, H., Y. Zhao, J.S. Chang, and D.J. Lee, Lignin to value-added products: Research updates and prospects. *Bioresour Technol* **2023**: p. 129294.

246. Blánquez, A., A.M. Borrero-López, G. Domínguez, C. Valencia, J.M. Molina-Guijarro, M.E. Eugenio, D. Ibarra, and M. Hernández, Solid-State Fermentation withStreptomycesas an Ecofriendly Route to Tune Lignin Properties and Its Use as a Binder in Adhesive Formulation. *ACS Sustainable Chemistry & Engineering* **2022**. *10*(31): p. 10403-10416.

247. Dong, T., W. Chen, C. Cai, F. Bai, Z. Zhou, J. Wang, and X. Li, Water-stable, strong, biodegradable lignocellulose straws replacement for plastic straws. *Chemical Engineering Journal* **2023**. *451*.

248. (TAPPI), T.A.o.t.P.a.P.I., Grease Resistance Test for Paper and Paperboard. **2022**: Atlanta, GA.

249. Richter, A.P., B. Bharti, H.B. Armstrong, J.S. Brown, D. Plemmons, V.N. Paunov, S.D. Stoyanov, and O.D. Velev, Synthesis and Characterization of Biodegradable Lignin Nanoparticles with Tunable Surface Properties. *Langmuir* **2016**. *32*(25): p. 6468-77.

250. Mankar, A.R., A. Pandey, A. Modak, and K.K. Pant, Pretreatment of lignocellulosic biomass: A review on recent advances. *Bioresour Technol* **2021**. *334*: p. 125235.

VITA

Zhongjin Zhou was born Taizhou, Jiangsu province, China. He graduated with a B.S. in Process Equipment and Control Engineering in 2017 from Changzhou University (China) and a M.S. in Chemical Engineering in 2020 from University of Chinese Academy of Sciences (China). In 2021, He pursued started his PhD study at the School of Natural Resources in University of Tennessee, Knoxville (Knoxville, TN) and joined Dr. Siqun Wang's research group. His doctoral research focused on the lignin nanoparticles' manufacturing and its application in water and oil proof composites.